Glucose metabolism in idiopathic pulmonary fibrosis

A thesis submitted to University College London in partial fulfilment of the requirements of the

MD(res) degree

Ilan Azuelos 2019

Centre for Inflammation and Tissue Repair

University College London

Division of Medicine

Gower Street

LONDON

WC1E 6BT

Declaration

I, Ilan Azuelos, confirm that the work presented in this thesis is my own. Where information has been derived from other sources, I confirm that this has been indicated in the thesis.

Signature…..……………………………………………………..……..….

Acknowledgements

First, I would like to thank my supervisor Prof. Rachel C. Chambers who, thanks to her vast scientific knowledge, rigour and integrity, provided me with the tools necessary to complete this thesis. She has been of immense help in guiding me through this research journey, offering constant advice and being always accessible when necessary. I would also like to thank Dr Paul Mercer for providing me with great ideas and suggestions during our numerous laboratory meetings.

Of course, none of this work would have been possible without the support and help from all the members of the Centre for Inflammation and Tissue Repair of UCL, London. First and foremost, I am immensely grateful to Dr Brintha Selvarajah who has been a colleague, partner and friend during this work. I would also like to thank Dr Ellen Forty who has introduced me to many of the techniques that were required for the successful completion of this thesis.

I take this opportunity to also acknowledge Dr Jess Eley and Dr Hannah Woodcock who have given me the chance to sail through this research journey by providing me with continuous support.

Last but not least, I would like to thank Gino Brunori who has accompanied me during the long and fruitful journey of the mitochondrial stress test protocol using the SeaHorse XF96e assay. Much of this work would not have been possible without him.

Abstract

Idiopathic pulmonary fibrosis (IPF) is a life-threatening interstitial lung disease of unknown aetiology characterized by progressive scarring of the lung parenchyma. Histologically, the hallmark of the disease is the presence of interspersed fibroblastic foci in the lung, composed of contractile myofibroblasts synthesizing a dense collagen-rich matrix. Transforming growth factor-β1 (TGFβ1) has been recognized as a key cytokine in the pathophysiology of IPF and other fibrotic disorders. Highly proliferative cells, such as cancer cells, reprogram their glucose metabolism through the activation of the PI3K-AKT-mTOR axis towards enhanced glycolysis, a process known as aerobic glycolysis. In view of the high biosynthetic nature of myofibroblasts, this thesis aimed to (1) describe the changes in glucose metabolism that occur during the process of TGFβ1-induced fibroblast to myofibroblast differentiation, (2) examine whether these changes are regulated by the PI3K-AKT-mTOR axis, and (3) examine the relationship between glucose uptake and fibrogenesis in an experimental model of lung fibrosis.

For the *in vitro* experiments, the metabolic profile of primary human lung fibroblasts was assessed by examining cellular glucose uptake, glycolytic flux and mitochondrial respiration. Furthermore, using highly selective and potent pharmacological inhibitors, the role of the PI3K-AKT-mTOR pathway in promoting changes in glucose metabolism during fibroblast differentiation was examined. For the *in vivo* experiments, position emission tomography-computed tomography scanning and autoradiography were performed in the murine bleomycin model of lung injury and fibrosis following administration of radioactive ^{18}F-labeled fluoro-2-deoxyglucose.

Taken together, the data presented in this thesis demonstrate that the metabolic phenotype of fibroblasts changes during TGFβ1-induced fibroblast differentiation and is regulated by mTOR, in a PI3K-AKT-independent manner. This metabolic switch may further explain the observation of increased glucose uptake in the fibrotic lesions in the bleomycin model of lung fibrosis. These findings support the notion that pharmacological targeting of glucose metabolism and/or the mTOR kinase may be beneficial in preventing myofibroblast differentiation in IPF.

Impact statement

Idiopathic pulmonary fibrosis (IPF) is a rare but life-threatening disease that has increased in incidence over the last decades. It is characterized by the uncontrolled deposition of scar tissue in the lungs, without any clear cause or precipitant. It has previously been recognized that the key effector cells of this process are the myofibroblasts. These are specialized cells that have differentiated from quiescent fibroblasts, thought to be located in the lungs or circulating in the blood. Upon stimulation by cytokines, such as transforming growth factor-β1 (TGFβ1), fibroblasts transform into collagen-producing myofibroblasts, leading to scar tissue deposition in the lungs.

This thesis examines the metabolic changes that occur during fibroblast to myofibroblast differentiation and has led to the discovery that the process of fibroblast differentiation is accompanied by increases in glucose uptake, glucose consumption and mitochondrial energy production. In addition to being published and accessible to the world, these findings have tremendous potential clinical applications, as glucose metabolism may now become a target for future drug development for this disease.

In addition, the mechanism by which glucose metabolism is enhanced during fibroblast to myofibroblast differentiation was assessed. Specifically, I looked at the PI3K-AKT-mTOR signalling pathway, a pathway previously shown to (i) be active in fibrotic lungs and (ii) play a role in modulating glucose metabolism in other conditions such as cancer. This work describes how mTOR is critical in enabling fibroblast glucose metabolism to be enhanced while PI3K and AKT are dispensable, and therefore raises the possibility that targeting mTOR may offer an approach to block the progression of fibrosis in IPF.

Finally, these findings were investigated in an experimental mouse model of IPF. This work required much optimisation and involved the injection of radioactive [^{18}F]FDG (a radiolabeled glucose analogue) into mice after subjecting them to lung injury by the pro-fibrotic agent bleomycin. As a result of this work, the link between glucose metabolism and fibrosis can now be examined *in vivo,* and allow investigators worldwide to develop novel therapeutic agents that will hopefully help slow down and reverse this disorder.

The work has led to conference presentations across the globe and has allowed researchers to discuss the link between the process of lung fibrosis and changes in cellular metabolism in many

different fields. This work has been published in open-access format and is therefore widely accessible.

Table of Contents

List of Tables and List of Figures

1. Introduction

1.1. What is Idiopathic Pulmonary Fibrosis?

In 1975, Dr Averill Liebow, a pathologist in California, USA described the various types of diseases that may occur in the supporting tissues of the lungs ('lung interstitium') rather than in the alveoli ('lung airspace')(Liebow, 1975). He brought along the notion of classifying these various *interstitial* lung diseases (ILDs) according to their histological pattern and the clinical context. Over the following decades and following various updates in classification (American Thoracic Society and European Respiratory Society, 2002; Travis et al., 2013), it became evident that idiopathic pulmonary fibrosis (IPF) was among the most common and lethal of the ILDs (Duchemann et al., 2017).

The major global respiratory societies have defined IPF as "a specific form of chronic, progressive fibrosing interstitial pneumonia of unknown cause." (Raghu et al., 2018). Although familial forms affecting younger people exist, it is a disease generally considered to affect the older population, with patients presenting typically in their sixth and seventh decades of life. The disease is thought to affect about 0.5-27.9/100 000 patients with an incidence of 0.22-8.8/100 000 new cases per year (Kaunisto et al., 2013). However, in older adults such as among Medicare beneficiaries in the United States aged 65 years and older, the prevalence was 494.5 cases per 100 000 people and the incidence was 94 cases per 100 000 person-years (Raghu et al., 2014). Furthermore, a global systematic review of 34 studies reported that the incidence of IPF worldwide has been increasing over time (Hutchinson et al., 2015). In the UK for instance, the incidence rate increased by 35% from 2000 to 2008, with an overall incidence rate increasing to 7.44 per 100,000 person-years (Navaratnam et al., 2011). Although the individual clinical course can be very variable and very difficult to predict, current best estimates suggest a median survival of only 3-5 years from diagnosis (Ley et al., 2011). This translates in IPF being the cause of about 5000 deaths per year in the UK, a number sadly higher to many cancers such as ovarian cancer, lymphoma, leukaemia, mesothelioma or renal carcinoma (Navaratnam et al., 2011; Vancheri et al., 2010). For yet unclear reasons, the prevalence and incidence of IPF are both higher in men than in women (Esposito et al., 2015).

Patients affected by IPF classically describe progressive breathlessness on exertion and a lingering

11

dry cough, and chest auscultation typically reveals velcro-sounding crackles. Physiologic evaluation shows evidence of restrictive lung disease on pulmonary function testing and honeycombing on high-resolution computed tomography (HRCT) of the lungs. The natural history is of a rapid and progressive decline in lung function culminating in respiratory failure and death.

The aetiology of IPF is by definition unknown, and thus the diagnosis of IPF requires the exclusion of known injurious mechanisms of the lungs causing other forms of interstitial lung diseases, such as those associated with connective tissue diseases, pneumotoxic drugs or environmental/occupational exposures. Nevertheless, risk factors for developing the disease have been identified and include gender (male-predominant), age (classically after age 50), smoking history, and certain comorbid illnesses such as cardiovascular disease, diabetes mellitus and gastroesophageal reflux disease (GERD).

1.2. Pathophysiology of IPF

The current paradigm of the pathogenesis of IPF is that recurrent damage to the alveolar epithelium in a susceptible individual drives an abnormal wound-healing response that results in fibrosis rather than repair (Ahluwalia et al., 2014). The development and progression of pulmonary fibrosis is therefore thought to depend on 3 principal factors: (i) genetic predisposition to the disease, (ii) repeated pulmonary injury (of unknown cause but made worse with smoking, environmental dust exposure, viral infections, GERD) and (iii) 'time' to explain why pulmonary fibrosis occurs more frequently in older adults (King et al., 2016). Ultimately, these 3 combined factors lead to perpetual injury to the alveolar epithelium, which is followed by a defective mechanism of wound healing and tissue regeneration. This is characterized by abnormal reepithelization and repair as well as increases in fibrogenic mediators produced by inflammatory and epithelial cells. This fibrogenic milieu leads to activation, migration, recruitment and proliferation of the normally sparse fibroblasts in the healthy lung (Hamid et al., 2005), and their differentiation into activated myofibroblasts.

Myofibroblasts are cells that are normally produced upon tissue injury for wound healing (Sandbo and Dulin, 2011). They have long been known to produce and remodel granulation tissue by producing extracellular matrix components and ultimately facilitating contraction and closure of the wound (Powell et al., 1999; Ryan et al., 1974). In addition to promoting wound repair, they also participate in the stromal reaction of tumours, where they have been shown to play an important role in remodelling the normal tissue matrix, leading to both the promotion and/or retardation of tumour invasion (Kobayashi et al., 2019; Kunz-Schughart and Knuechel, 2002). The presence and persistence of myofibroblasts in organs, however, can be the cause of a variety of disorders characterized by exuberant and non-resolving progressive fibrosis. These include renal, liver, skin fibrosis and, most pertinent to this thesis, IPF.

Myofibroblasts produce copious amounts of extracellular matrix (ECM) proteins (Fernandez and Eickelberg, 2012). In IPF, the deposition of collagens type I, type III and fibronectin predominates (Burgess et al., 2016) and occurs near the air-tissue interface, leading to the impaired gas exchange that culminates into the respiratory failure seen in afflicted patients (Kuhn et al., 1989). This collagen-rich ECM itself has been shown to promote fibroblast activation and migration, therefore perpetuating the development of pulmonary fibrosis (Asano et al., 2017; Parker et al., 2014).

In addition to producing large amounts of ECM, myofibroblasts have the characteristic feature of expressing α-smooth muscle actin (α-SMA), leading to the formation of actin stress fibres (Cutroneo et al., 2007). Actin stress fibres are composed of bundles of polymerized actin filaments, which are linked to components of the extracellular matrix via transmembrane molecules called integrins (Hynes, 2002). Although actin has 6 isoforms that can all participate in the formation of the stress fibres, α-smooth muscle actin (α-SMA) expression is strongly induced *de novo* in fibroblasts under pro-fibrotic stimulation. This results in the rapid incorporation of α-SMA into actin stress fibres, resulting in the ability for contractile force generation and eventual wound closure (Chaponnier and Gabbiani, 2004; Serini and Gabbiani, 1999). For those reasons, myofibroblasts are considered *the key effector cells* in the disease (Eickelberg and Laurent, 2010) and targeting fibroblast activation has been considered an important therapeutic option in IPF (Scotton and Chambers, 2007) and will be the focus of this thesis.

In the lung, the histologic outcome of this process is the presence of a large number of mesenchymal cells and large amounts of collagen-rich extracellular matrix. The histopathologic pattern associated with the clinical diagnosis of IPF has been coined UIP (usual interstitial pneumonia), although a variety of other disorders (eg. drug-toxicity, pneumoconiosis, chronic hypersensitivity pneumonitis) can also cause a pattern of UIP on lung biopsy. By definition, UIP is characterized by heterogeneous parenchymal abnormalities mainly affecting the peripheral subpleural areas of the lungs, with alternating areas of normal lung. The parenchymal abnormalities include the disorganized deposition of a collagen-rich extracellular matrix, distortion of the normal pulmonary architecture and subpleural cystic airspaces (<10 mm diameter) called honeycomb cysts. The level of inflammation is mild and patchy. Fibroblastic foci are the hallmark lesions in UIP and are characterized by clusters of myofibroblasts with overlying abnormal hyperplastic epithelium that lies in continuity with the established fibrosis. These areas are considered to be the active lesion in IPF and in line with this, the burden of fibrotic foci found in lung biopsy samples inversely correlates with patient survival (King et al., 2001).
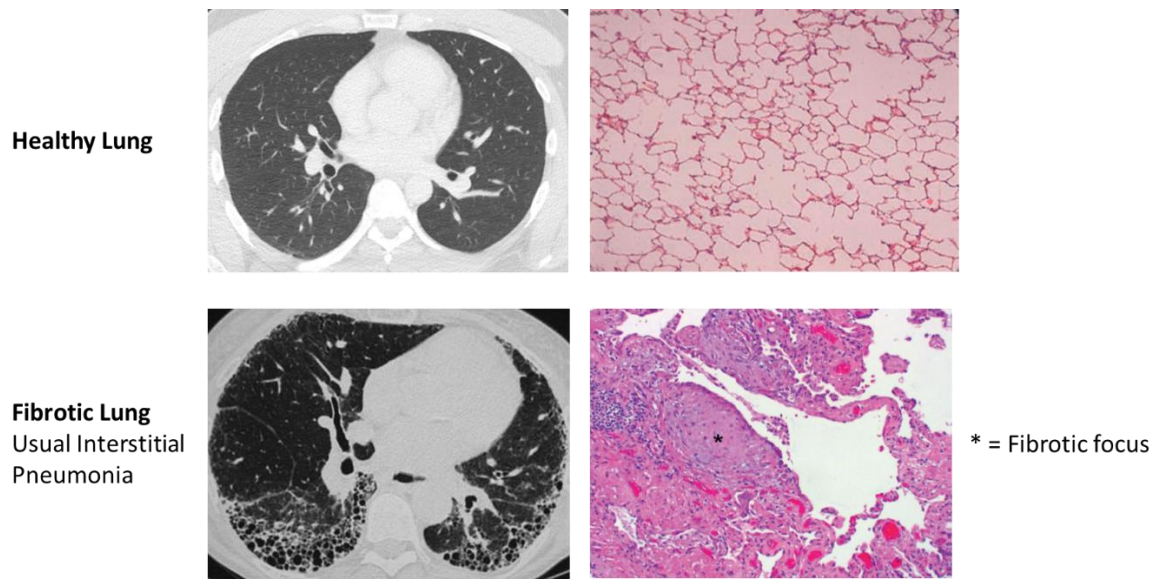
Figure 1-1. Representative images of a normal healthy lung and fibrotic lung

Left-sided images show a typical HRCT slice of a lung from a healthy and IPF-affected individual. Right-sided images show typical histopathology of healthy and IPF lung. Images obtained from anonymized clinical cases and from the American Thoracic Society (Raghu et al., 2011).

Since the precise triggers that promote epithelial injury are still elusive, the current research focus and strategy have been to modify the fibrotic response itself. So far, therapies that influence fibroblast growth and matrix deposition are very limited. The only anti-fibrotic agents currently used to treat patients with IPF are pirfenidone and nintedanib. While the cellular mechanism of action of pirfenidone remains largely unknown, nintedanib is a tyrosine kinase receptor inhibitor that targets the platelet-derived growth factor receptor (PDGF-R), the FGF receptor (FGF-R) and the vascular endothelial growth factor receptor (VEGF-R). So far, these drugs have been shown to slow the decline in lung function but not to improve survival, symptoms or quality of life convincingly (King et al., 2014; Richeldi et al., 2014). Thus, the need for new and novel diagnostic and/or therapeutic targets for pulmonary fibrosis is exceedingly high.

1.3. Role of Transforming-Growth Factor β in IPF

The differentiation of fibroblasts into ECM-producing myofibroblasts can occur under the direction a variety of cytokines and growth factors, but notably transforming growth factorβ (TGFβ). The TGFβ superfamily of ligands includes over 30 members in humans which are essential for numerous biological functions such as fetal development, tumour suppression and regulation of the immune response (Chambers et al., 2003; Dickson et al., 1995; Kubiczkova et al., 2012). They include 3 different TGFβ gene products (TGFβ1, TGFβ2 and TGFβ3), of which TGFβ1 is the isoform most implicated in the development of IPF (Ask et al., 2008; Massagué, 2008; Xaubet et al., 2003). In fact, TGFβ1 is the most potent and established stimulator of myofibroblast differentiation (Sandbo and Dulin, 2011).

The fibrogenic effects of TGFβ1 include the differentiation and survival of myofibroblasts during fibrosis (Desmoulière et al., 1993), the secretion of extracellular matrix proteins (Cutroneo et al., 2007; McAnulty et al., 1991; Raghow et al., 1987), the modulation of matrix turnover (Eickelberg et al., 1999; Overall et al., 1989) and the proliferation of fibroblasts via other profibrotic cytokines, such as platelet-derived growth factor (PDGF), connective tissue growth factor (CTGF) and fibroblast growth factor -2 (FGF-2) (Goldsmith et al., 1991; Grotendorst et al., 1996; Leask et al., 2003; Soma and Grotendorst, 1989). In addition, TGFβ1 also stimulates the expression of several pro-inflammatory and fibrogenic cytokines, such as TNFα, PDGF, IL-1β, or IL-13, thereby further enhancing and perpetuating the fibrotic response.

The fibrogenic effects of TGFβ1 eventually lead to the differentiation of myofibroblasts from resident lung fibroblasts (Hinz et al., 2012), but can also enhance growth of bone-marrow-derived fibrocytes (Galligan and Fish, 2013; Reilkoff et al., 2011) and promote epithelial and endothelial cells to undergo mesenchymal-like changes (Ho et al., 2015; Kim et al., 2006b; Zeisberg and Kalluri, 2004). Once committed to terminal differentiation, myofibroblasts must then be removed by apoptosis for the restoration of normal tissue homeostasis, a critical process that fails in IPF (Desmoulière et al., 1995).

The importance of TGFβ1 in IPF is exemplified by the fact that TGFβ1 levels are significantly increased in bronchoalveolar lavage fluid of patients with IPF (Salez et al., 1998), and that TGFβ1 expression is upregulated in alveolar macrophages and mesenchymal cells in lung sections from patients with IPF (Khalil et al., 1991). Furthermore, over-expression of active TGFβ1 in animal models

via intratracheal administration of TGFβ1-expressing adenovirus induces pulmonary fibrosis (Sime et al., 1997), while small inhibitors of the TGFβ1 receptor reduce fibrosis in murine models of fibrosis (Bonniaud et al., 2005; Higashiyama et al., 2007). For these reasons, global inhibition of TGFβ1 would be a very attractive therapeutic option but unfortunately causes many adverse effects because of its key homeostatic functions, making it an undesirable therapeutic target. In fact, complete knockout of TGFβ1 in animals results in extensive inflammatory infiltrates in the lung (Kulkarni et al., 1993) and animals with heterozygous deletion of TGFβ1 display increased susceptibility to lung malignancy (Tang et al., 1998). It has therefore been tempting to try to better understand the mechanisms regulating, and required, for TGFβ1-induced fibroblast differentiation.

1.3.1. TGFβ1 signalling: canonical and non-canonical pathways

TGFβ1 is synthesized as a precursor molecule and is secreted by many cell types in the lung, including activated alveolar epithelial cells, alveolar macrophages, neutrophils, endothelial cells and fibroblasts themselves. It then interacts in the extracellular matrix with the latency-associated peptide/latent TGFβ–binding protein, maintaining it in an inactive state. Dissociation of the latent complex by proteolytic cleavage or conformational change allows the active ligand to be presented to its receptor (Sarrazy et al., 2014; Travis and Sheppard, 2014). This can be induced by matrix metalloproteinases (Dancer et al., 2011), lowering in pH (Nocera and Chu, 1995), exposure to reactive oxygen species (Bargagli et al., 2009), changes in tissue stiffness (Hinz, 2009), and binding to integrins (Margadant and Sonnenberg, 2010).

TGFβ1 family ligands signal by assembling a hetero-tetrameric serine-threonine receptor complex comprising of two type I ('signal propagating') and two type II ('activator') receptor components. Upon ligand binding, type II receptors phosphorylate the cytoplasmic domain of the type I receptors which then propagate the signal (Heldin and Moustakas, 2016). Although seven type I receptors and five type II receptors exist in humans, TGFβ1 signals via the type I receptor TGFβR1 (also known as ALK5 orTβRI). Phosphorylation switches a region in the type I receptor from a site that binds 12 kDa FK506-binding protein, which silences kinase activity, into a site that binds substrate SMAD (Suppressor of Mothers against Decapentaplegic) proteins for their phosphorylation (Huse et al., 2001).

Receptor activation during canonical TGFβ1 signalling leads to the regulation of gene expression by

receptor-mediated activation of SMAD transcription factors. The receptor complex recruits Smad2 and 3, which are phosphorylated by the active TGβR1. These SMADs form a complex with the co-SMAD, SMAD4, and translocate to the nucleus where they recognize specific SMAD binding elements in the enhancer or promoter regions of target genes (Derynck and Zhang, 2003; LEASK and ABRAHAM, 2004).
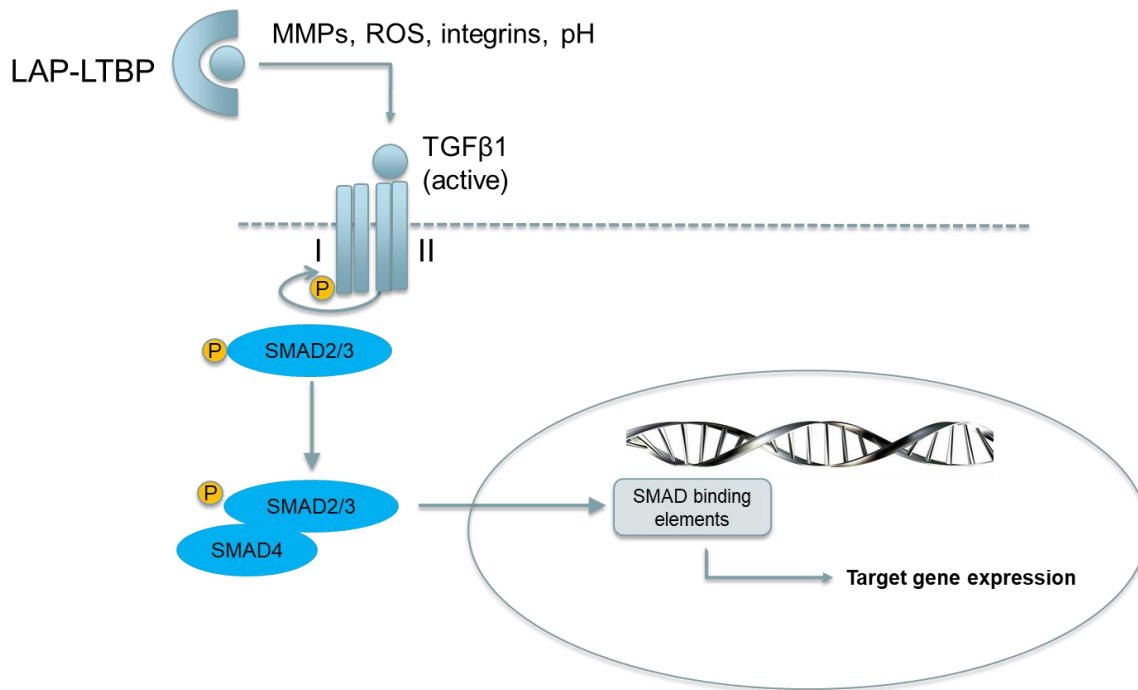
Figure 1-2. Schematic representation of the TGFβ1 canonical signalling pathway.

LAP-LTBP: Latency-associated peptide/latent TGFβ–binding protein; MMPs: Matrix metalloproteinases; ROS: Reactive oxygen species

Although TGFβ1 signals mainly via the SMAD pathway, TGFβ1 can also activate other pathways that are collectively referred to as 'non-canonical' TGFβ1 signalling and complement SMAD action (Massagué, 2012; Zhang, 2009). These include the mitogen-activated protein kinase (MAPK) pathways, including the extracellular signal-regulated kinases, c-Jun amino-terminal kinase, p38 MAPK, as well as the IκB kinase, Rho family GTPases, and phosphatidylinositol-3 kinase (Zhang, 2017). The exact mechanisms by which TGFβ1 activates the non-canonical pathways is still an area of active research and will not be the focus of this thesis. However, over the last decade, the role of the PI3K-AKT-mTOR axis on IPF has emerged as being particularly important, and for that reason, the rest of this thesis will focus on the role of the PI3K-AKT-mTOR pathway in mediating TGFβ1-induced fibroblast differentiation.

1.4. Overview of the PI3K-AKT-mTOR axis

The PI3K-AKT-mTOR pathway is involved in many key biological processes, including cell survival, proliferation, and metabolism (Fruman and Rommel, 2014; Vanhaesebroeck et al., 2010).

PI3 kinases phosphorylate the 3-OH group of the inositol ring of phosphatidylinositol (PtdIns) lipid substrates, generating lipid mediators. Class 1 PI3 kinases, the most extensively studied, are heterodimers comprising a regulatory and a catalytic subunit. They are classically activated by receptor tyrosine kinases, but can also be activated by G-protein coupled receptor signalling or by Ras via the Ras-binding domain in the p110 catalytic subunit (Guillermet-Guibert et al., 2008).

Once activated, they use phosphatidylinositol-4,5-bisphosphate (PtdIns(4,5)P2) as their substrate and generate phosphatidylinositol-3,4,5-bisphosphate (PtdIns(3,4,5)P3, 'PIP3') at the cell membrane. Subsequently, PIP3 recruits and activates proteins containing the lipid-binding pleckstrin homology (PH) domain. One of these proteins is AKT, a serine-threonine kinase. Upon binding of the PH domain of AKT with PIP3, AKT undergoes a conformational change exposing its phosphorylation sites. This allows 3-phosphoinositide-dependent protein kinase-1 (PDK1) and the mechanistic target of rapamycin complex 2 (mTORC2) to phosphorylate AKT at Thr308 and Ser473 respectively, leading to its full activation (Alessi et al., 1997; Sarbassov et al., 2005). AKT, once fully activated, plays a key role in many key cellular functions. These include cell survival, cell proliferation, cell growth, and cell metabolism, with many of these effects occurring through its activation of mTORC1.

Since its formal identification in the mid-1990s, mTOR has been extensively studied and is now established to play a key role in in the coordination of cell growth, protein synthesis and cell metabolism (Saxton and Sabatini, 2017). mTOR is a serine-threonine protein kinase in the PI3K-related kinase (PIKK) family that forms the catalytic subunit of two distinct protein complexes, known as mTOR Complex 1 (mTORC1) and 2 (mTORC2). Each complex is defined by its core components, with mTORC1 consisting of mTOR, mammalian lethal with Sec13 protein 8 (mLST8), a regulatory-associated protein of mTOR (RAPTOR), DEP-domain-containing mTOR interacting protein (DEPTOR) and proline-rich AKT substrate 40kDa (PRAS40) proteins. mTORC2 consists of mTOR, mLST8, Rictor (rapamycin-insensitive companion of mTOR), DEPTOR, mSin1 and Protor1/2.

mTORC1 is by far the most studied and better understood of the two mTOR complexes. In

physiological conditions, mTORC1 is activated upon replete cellular conditions and promotes an anabolic cellular state. In this context, mTORC1 is sensitive to a variety of growth-factors, high levels of amino acids (in particular leucine) and high intracellular energy (low AMP/ATP ratio). Mechanistically, the tuberous sclerosis complex (TSC) plays a central role in integrating these signals. TSC is a heterodimer (TSC1 and TSC2 subunits) acting as a GTPase-activating protein towards the small GTPase RHEB (Ras homologous Enriched in Brain), inactivating RHEB and thereby inhibiting mTORC1 activity. Inhibition of TSC2, which leads to mTORC1 activation, can occur via its phosphorylation by AKT (Haar et al., 2007). Conversely, a reduction in cellular energy (high AMP/ATP ratio, glucose deprivation) activates the stress-responsive metabolic regulator AMPK, which inhibits mTORC1 both indirectly, through phosphorylation and activation of TSC2, as well as directly, through the phosphorylation of Raptor (Gwinn et al., 2008; Inoki et al., 2003; Shaw et al., 2004). Other inputs, such as hypoxia and DNA damage can also modulate mTORC1 activity. One key feature of mTORC1 is its partial sensitivity to rapamycin, a molecule that complexes with the intracellular receptor FK506-binding protein of 12 kDa (FKB12), weakening the interaction between mTOR and Raptor (Kim et al., 2002).

The downstream effects of mTORC1 are numerous and critical for cellular homeostasis. They include anabolic pathways such as mRNA translation, ribosome biogenesis, inhibition of autophagy and regulation of metabolism. In contrast, mTORC2 has been much less studied and is less well understood. It plays important roles in cell proliferation, survival and cytoskeletal assembly, mainly by phosphorylating the protein kinases PKA, AKT and PKC. Its regulation is also likely to be affected by growth factors, such as insulin and PI3K signalling, via feedback loops (Saxton and Sabatini, 2017). Although mTORC2 is generally considered to be insensitive to rapamycin, prolonged treatment with rapamycin can deplete free mTOR and prevent de novo assembly of mTORC2, reducing mTORC2 levels in certain cell types (Sarbassov et al., 2006).
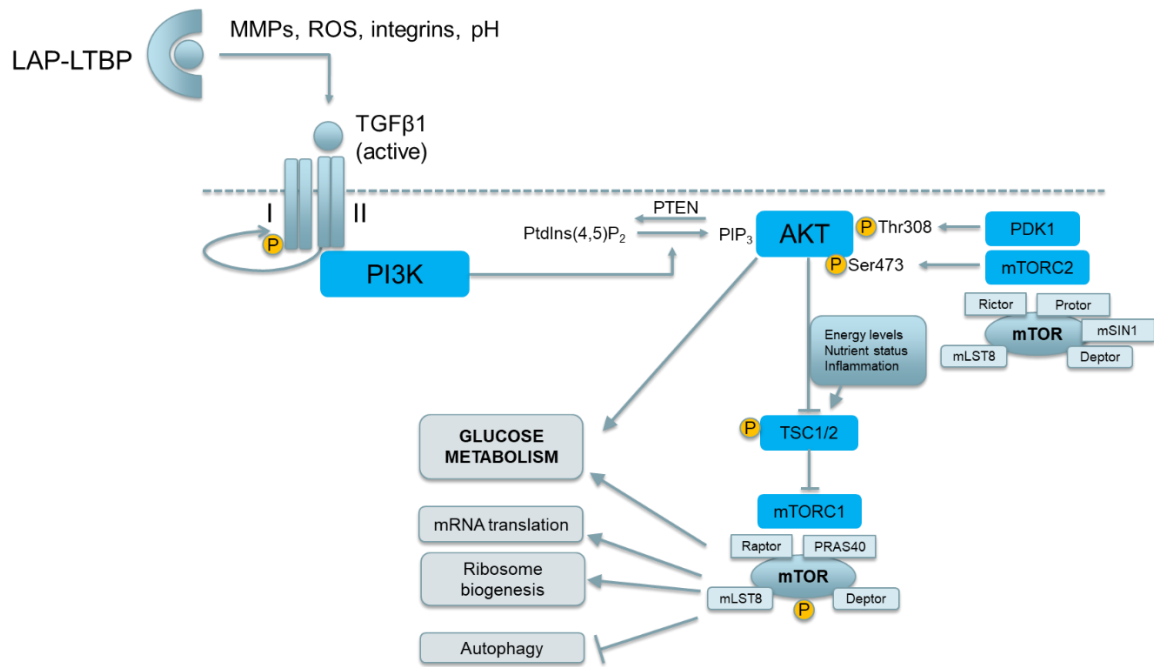
Figure 1-3. Schematic representation of the PI3K-AKT-mTOR axis.

LAP-LTBP: Latency-associated peptide/latent TGFβ–binding protein; MMPs: Matrix metalloproteinases; ROS: Reactive oxygen species; PI3K: Phosphatidylinositol-3 kinase; mTOR: mechanistic target of rapamycin; mLST8: mammalian lethal with Sec13 protein 8; Raptor: regulatory-associated protein of mTOR; Deptor: DEP-domain-containing mTOR interacting protein; PRAS40: proline-rich AKT substrate 40kDa (PRAS40) proteins; Rictor: rapamycin-insensitive companion of mTOR.

1.4.1. Role of PI3K-AKT-mTOR axis in IPF

A growing number of reports in the literature from our laboratory and others have established an important link between the PI3K-AKT-mTOR axis and fibrogenesis.

First, specific isoforms of the PI3K catalytic subunit were shown to be more greatly expressed in IPF-derived fibroblast cell lines relative to non-IPF controls and were found to play an important role in TGFβ1-induced fibroblast proliferation and differentiation (Conte et al., 2011, 2013). Furthermore, while mTOR plays a role in fibroblast proliferation (Syed et al., 2012), both complexes are needed to mediate the TGFβ1 fibrogenic responses (Chang et al., 2014; Rahimi et al., 2009). In addition, reports have also emerged that epithelial-mesenchymal transition (EMT) is disrupted following inhibition of PI3K-AKT-mTOR, although the exact mechanism by which mTOR signalling directly modulates EMT is not clear (Cheng and Hao, 2016; Lamouille and Derynck, 2011; Lamouille et al., 2012; Lin et al., 2014). Histologic analysis of lung tissue from IPF patients has also demonstrated increased mTOR expression, which is correlated with the degree of fibrosis and pulmonary function (Park et al., 2014). Furthermore, mTOR inhibition was found to inhibit collagen I expression in mesenchymal cells derived from fibrotic human lung allografts (Walker et al., 2016), as well as to mitigate the development of fibrosis in an experimental animal model of lung injury and fibrosis (Chang et al., 2014; Gui et al., 2015).

Our laboratory showed that the PI3K pathway is activated in IPF fibrotic foci and that the compound GSK2126458, a potent inhibitor of PI3K and mTOR, inhibits fibroblast proliferation and TGFβ1-induced collagen deposition (Mercer et al., 2016). More recently, our laboratory published an in-depth report detailing the mechanism by which TGFβ1-activation of the PI3K-AKT-mTOR axis regulates collagen synthesis (Woodcock et al., 2019). Woodcock et al. elegantly demonstrated that although TGFβ1-stimulation induced downstream PI3K signalling in lung fibroblasts, specific pharmacological inhibition of PI3K or of AKT had no effect on TGFβ1-induced collagen synthesis. In contrast, mTOR inhibition had a profound impact on TGFβ1-induced collagen synthesis, with evidence suggesting that mTOR acts, at least in part, by influencing COL1A1 mRNA levels. Further work using fibrogenic cells from different organs (hepatic stellate cells, dermal fibroblasts, lung fibroblasts, cancer-associated fibroblasts) and using ex-vivo IPF lung tissue then identified mTORC1 as the key signalling node involved in mediating the fibrogenic effects of TGFβ1.

The PI3K-AKT-mTOR pathway is involved in many key biological processes and it is therefore not

surprising that dysregulation of this pathway is associated with several disease processes, notably cancer (Abraham and O'Neill, 2014; Millis et al., 2016). In fact, progressive understanding in the pathogenesis of IPF has led investigators to recognize that IPF shares similarities with cancer on multiple levels, suggesting that the identification of shared pathways may lead to new prognostic or therapeutic tools for IPF. Such similarities include the lack of clear aetiology in both conditions and risk factors that include advancing age and smoking. Both conditions are thought to occur in the presence of a predisposing genetic background, have a poor response to medical treatment and carry a poor prognosis. On a cellular level, some have argued that IPF may be a neo-proliferative disorder of the lung, akin to cancer. Indeed, both cancer and IPF share similar epigenetic changes, delayed apoptosis, altered response to regulatory signals, abnormal expression of microRNAs (miRNAs), reduced cell-to-cell communication and activation of specific signalling pathways (Chambers and Mercer, 2015; Vancheri, 2013).

One characteristic feature of cancer cells is their unique way of metabolizing nutrients, a field that has been intensely studied and termed *cancer metabolism*. Interestingly, the PI3K-AKT-mTOR signalling pathway is hyperactive in many malignancies (Kaira et al., 2014; Soga, 2013; Sun et al., 2011; Zha et al., 2011) and acts as the key driver for the metabolic changes that occur in cancer (Haissaguerre et al., 2014; Laplante and Sabatini, 2013; Morita et al., 2015; Robey and Hay, 2009; Shimobayashi and Hall, 2014). The following section will summarize what is known about the PI3K-AKT-mTOR axis effects on glucose metabolism and illustrate the need to examine this process in the context of IPF.

1.5. Overview of glucose metabolism

Cancer metabolism has become a field of huge interest with a vast number of research projects aiming to use this characteristic feature of cancer for the development of novel therapeutic agents. The following chapter will summarize the glycolytic pathway and mitochondrial respiration and conclude by describing the characteristic features of cancer metabolism.

1.5.1. Overview of glycolysis

Glycolysis is a well-conserved pathway among living organisms which has likely evolved well before oxygen was present on earth (Chandel, 2015). The glycolytic pathway starts with glucose uptake into the cells via glucose transporters, then comprises 10 enzymatic steps that take place in the cytosol and generates 2 molecules of ATP per metabolized glucose molecule without any requirement for oxygen. The overall glycolytic reaction can be summarized as:

$$Glucose + 2[NAD]^+ + 2[ADP] + 2P_i \rightarrow 2[Pyruvate] + 2[NADH] + 2[H^+] + 2[H_2O] + 2[ATP]$$
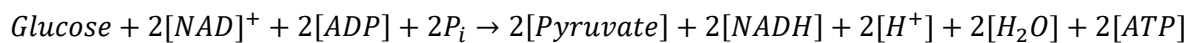
In view of its large size and polar nature, glucose molecules cannot freely cross the lipid membrane of cells by simple diffusion. Instead, glucose enters cells via sodium-glucose linked transporters (SGLTs) and facilitated diffusion glucose transporters (GLUTs) (Navale and Paranjape, 2016). SGLTs rely on the sodium concentration gradient across the cell membrane acting as a source of chemical potential to transport glucose and are mainly expressed in the gut and renal tubular cells. In contrast, GLUTs transport glucose across the plasma membrane by means of a facilitated diffusion mechanism, with 14 GLUTs currently identified. Of those, GLUT1 is of particular importance since it is expressed in all cell types, and its level of expression correlates with the degree of invasion and metastatic potential in cancer (Adekola et al., 2012).

Once into the cytosol, three of the glycolytic steps are considered regulatory and essentially irreversible. The first and likely most important regulatory step in the glycolytic pathway is catalysed by a family of enzymes called hexokinases, that phosphorylate glucose to produce glucose-6-

phosphate (G6P). These enzymes are inhibited by G6P, ensuring feedback control of this reaction and therefore guaranteeing that glucose is not committed to glycolysis. This first committed glycolytic step also keeps the intracellular glucose level low, which in essence "traps" glucose inside the cell as the cells lack G6P transporters. Although there are 4 main hexokinases (HK1-4) expressed in normal cells, HK2 is expressed at high levels in embryonic tissue and cancer cells.

The second committing step of glycolysis is at the level of phosphofructokinase 1 (PFK1), an enzyme that catalyses the conversion of fructose 6-Phosphate (F6P) into fructose 1,6-bisphosphate (F1,6BP) (Chandel, 2015). High levels of ATP allosterically inhibits this reaction to ensure a reduction in the flux of glycolysis under energy-replete conditions. In addition, the enzyme PFK2, which converts the same substrate F6P into F2,6BP plays an important role in regulating the glycolytic pathway as F2,6BP decreases the inhibitory effects of ATP on PFK1, allowing an increase in glycolytic flux. Four different isozymes of PFK2 exist with PFKFB3 (encoded by the gene *PFKFB3*) being highly expressed and playing an important in cancer (Shi et al., 2017).

The third committing step of glycolysis is catalysed by the enzyme pyruvate kinase (PK) which metabolises phosphoenolpyruvate (PEP) into pyruvate (Chandel, 2015). This reaction is also inhibited by the tricarboxylic acid cycle (TCA) metabolites citrate and acetyl co-A, ensuring feedback inhibition of the pathway. Importantly, a reduction of PK activity leads to the accumulation of upstream glycolytic intermediates and their diversion into branching pathways, such as the pentose phosphate pathway and the serine biosynthesis pathway, leading to the generation of nucleotides, lipids and amino acids that may be required for cell growth and proliferation.

Overall, the glycolytic pathway leads to the conversion of a single molecule of glucose into 2 molecules of pyruvate. In the presence of oxygen, pyruvate generally enters mitochondria - while in the absence of oxygen, pyruvate is reduced into lactate (*anaerobic glycolysis*) via lactate dehydrogenases (LDH).

Glucose

Hexokinase

Glucose 6-phosphate

Phosphoglucose isomerase

Phosphofructokinase-2

Fructose 6-phosphate → Fructose 2,6-bisphosphate

Phosphofructokinase-1

Fructose 1,6-bisphosphate

Aldolase

Glyceraldehyde 3-phosphate ↔ Dihydroxyacetone phosphate

Glyceraldehyde 3-phosphate dehydrogenase

1, 3-bisphosphoglycerate

Phosphoglycerate kinase

3-phosphoglycerate

Phosphoglycerate mutase

2-phosphoglycerate

2x

Enolase

Phosphoenolpyruate

Pyruvate kinase

Lactate dehydrogenase

Pyruvate → Lactate

Figure 1-4. Schematic representation of the glycolytic pathway.

Glucose entry into the cell undergoes metabolism in the cytosol as depicted. Please refer to text for further details of the enzymatic steps.

1.5.2. Overview of mitochondrial respiration

Mitochondria are oval-shaped organelles that are present in all eukaryotic cells. The current leading hypothesis suggests that around 2 billion years ago, a biological relationship between 2 prokaryotes developed, in which both were mutually dependent for nutritional requirements. This 'endosymbiotic theory' supposes that one of these prokaryotes became the primordial mitochondria and have become an essential component for cellular health.

Mitochondria are double-membrane organelles containing an inner and outer membrane separated by the intermembrane space. The space within the inner membrane is called the mitochondrial matrix. Although the nuclear DNA encodes most of the proteins present in mitochondria, mitochondria have their own DNA (mtDNA), which is maternally inherited, and which encodes 37 genes including 13 critical for oxidative phosphorylation. For that reason, mitochondrial mass can

be estimated, for instance, by the levels of mitochondrial proteins or levels of mtDNA. Mitochondria can generate energy in the form of ATP from various sources, including glycolysis-derived pyruvate, as well as amino acids and fatty acids, through the process of oxidative phosphorylation (OXPHOS).

During OXPHOS, the 2-carbon molecule acetyl co-A (generated from fatty acid oxidation or glycolysis-derived pyruvate) undergoes a series of chemical reactions in the mitochondrial matrix through the tricarboxylic acid (TCA) cycle, leading to the generation of NADH and FADH2. These molecules feed into the electron transport chain (ETC) located on the inner mitochondrial membrane where their electrons are passed through complexes and eventually to oxygen, forming H_2O. Through this process, H^+ molecules are extruded from the matrix to the intermembrane space, generating a proton gradient across the inner mitochondrial membrane. It is the enzyme ATP synthase (complex V) that allows re-entry of H^+ back into the matrix, generating enough energy to phosphorylate ADP into ATP. This process is coupled to the use of oxygen, hence the process referred to as *oxidative phosphorylation* (Chandel, 2015).

During OXPHOS, the amount of energy released by oxidative phosphorylation is much higher than with simple glycolysis. Indeed, glycolysis generates 2 ATP molecules (and 2 NADH) while OXPHOS generates a total of 30-36 ATP molecules, depending on the efficiency of the mitochondrial ETC.
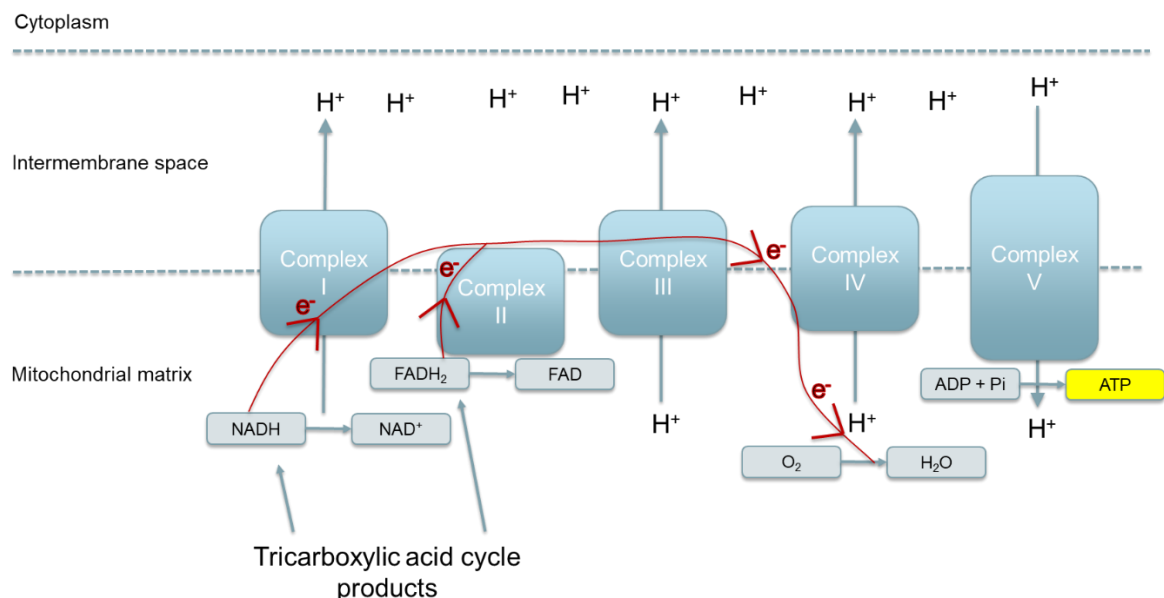
Figure 1-5. Schematic representation of the mitochondrial electron transport chain.

Electrons from products of the tricarboxylic acid cycle (NADH and FADH$_2$) are transferred to oxygen, which is

reduced to water. During this process, a proton gradient across the inner mitochondrial membrane is generated. Dissipation of this gradient allows the production of energy as ATP. Please refer to text for further details.

1.5.3. Aerobic glycolysis

Aerobic glycolysis also referred to as the "Warburg effect", represents the predominant use by cells to undergo glycolysis and to produce lactate, despite the presence of adequate oxygen for mitochondrial respiration (Devic, 2016).

This concept, also referred to as *metabolic reprogramming*, originates from the work of the Nobel laureate Otto Warburg in the 1920s. He initially recognized that cancer tissues consume glucose at much higher rates than healthy tissues, with up to 66% of the consumed glucose converted into lactate (Otto Warburg et al., 1923). These experiments were performed in the presence of oxygen; for that reason, his initial thought was that cancer cells had mitochondrial defects that impair oxidative phosphorylation, thus forcing them to rely on glycolysis for energy production (WARBURG, 1956). However, further work revealed that oxygen consumption is intact in cancer cells (Moreno-Sánchez et al., 2007; Weinhouse, 1976) and that cancer cells benefit from metabolic reprogramming for improved survival and to allow for cell proliferation.

Indeed, the huge increase in glucose uptake that characterizes the Warburg effect leads to the generation of large amounts of glycolytic intermediates which can be metabolized into nucleotides, lipids and amino acids. The massive increase in glycolysis, therefore, provides these cells with the building blocks required to produce the key elements for new cell formation. In short, this "reprogrammed" metabolism helps perpetuate cell growth and survival, features that are characteristic of proliferating cancer cells. Therefore, even though one glucose molecule produces only two molecules of ATP via glycolysis which is far less efficient in producing energy than through OXPHOS (up to 36 ATPs per glucose molecule), tumours that use glycolysis for their energy supply may have a growth advantage over tumours that mainly use OXPHOS. Importantly, in order for glycolysis to remain in high-flux during this process, proliferating cells require a constant supply of NAD^+, which can be obtained either slowly via the mitochondrial electron transport chain or much more rapidly via the conversion of pyruvate into lactate.

To summarize, the hallmark of cancer cell metabolism is an impressive increase in glucose uptake, a very high rate of glycolysis and large amounts of lactate being produced, despite the presence of oxygen (Hirschey et al., 2015).
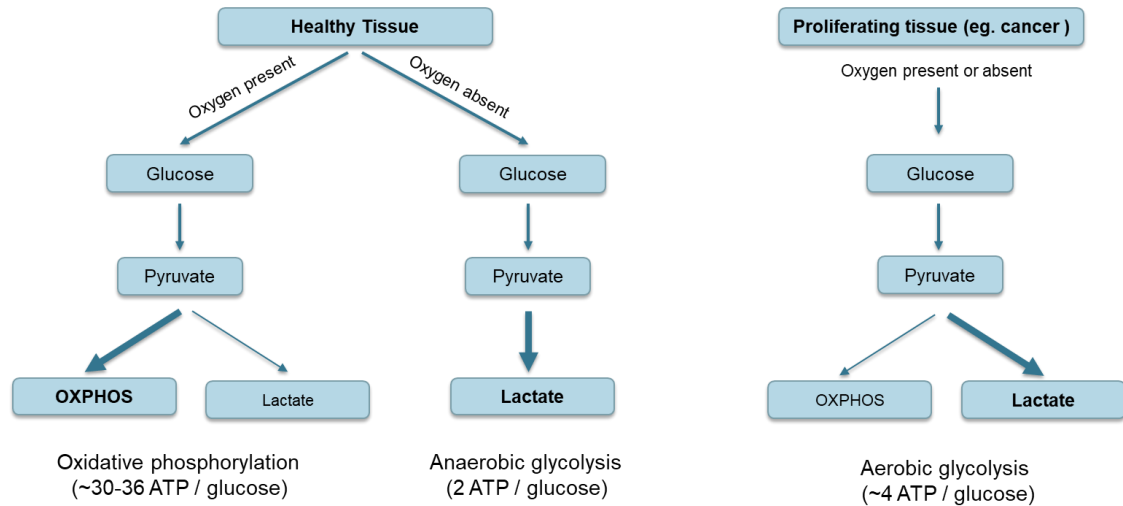
Figure 1-6. Schematic representation of aerobic glycolysis.

In healthy tissues, pyruvate preferentially undergoes OXPHOS (oxidative phosphorylation) when oxygen is available. However, in proliferating tissue such as cancer, pyruvate is preferentially converted into lactate despite the presence of oxygen, a process termed 'aerobic glycolysis'. Image reproduced from (Vander Heiden et al., 2009).

1.5.4. Metabolic reprogramming in non-cancer cells

In addition to cancer cells, many other human cell types have been shown to undergo the Warburg effect, with the bulk of the literature describing these changes in proliferating embryonic and immune cells (Vander Heiden et al., 2001; Hirschey et al., 2015; Lunt and Vander Heiden, 2011).

First, rapidly proliferating embryonic cells rely heavily on glycolysis, regardless of oxygen availability, and highly express GLUT1, GLUT3, HK, and PFKFB3 (Ito and Suda, 2014; Leese and Barton, 1984; Pantaleon and Kaye, 1998; Varum et al., 2011). As these cells progress towards differentiation and as their proliferative state abates, mitochondrial respiration starts to take over the enhanced glycolytic flux (Shyh-Chang et al., 2013).

Similarly, stimulated effector T-cells induce the expression of GLUT1 and glycolytic enzymes in order to increase glucose uptake and glycolysis (Gerriets and Rathmell, 2012; Macintyre et al., 2014; Palmer et al., 2015). Interestingly, some of these changes are regulated by AKT (Jacobs et al., 2008). In addition, activated 'pro-inflammatory' macrophages also upregulate glycolysis in response to tissue injury or infection to cope with increased production of host defence factors, enhanced phagocytosis, and antigen presentation (O'Neill and Hardie, 2013). These changes are also accompanied by an increase in GLUT1 expression as well as an increase in the expression of HK and PFKFB3. In contrast, 'anti-inflammatory' macrophages show increased mitochondrial respiration and reduced glycolysis (O'Neill et al., 2016). Importantly, studies have shown that changes in glycolytic flux in some immune cells can have an impact on cell phenotype and function (Buck et al., 2015, 2017; Everts et al., 2014; Neill and Pearce, 2016; O'Neill et al., 2016). For instance, a shift towards glycolysis (and away from OXPHOS) has been shown to make macrophages "proinflammatory" (Jha et al., 2015; O'Neill and Hardie, 2013), leading to enhanced production of IL-1β, a pro-inflammatory cytokine (Tannahill et al., 2013). Similarly, enhanced glycolysis is also required for T cells to assume their pro-inflammatory function (Buck et al., 2015).

The proliferation of endothelial cells is a marked feature of angiogenesis. During this process, endothelial cells were shown to also exhibit the Warburg effect. Again, these changes were associated with large induction in the expression of *PFKFB3*, with evidence that silencing this gene limited vessel sprouting (De Bock et al., 2013).

1.6. How does the PI3K-AKT-mTOR axis induce metabolic reprogramming?

Over the last decades, multiple studies have established the PI3K-AKT-mTOR signalling pathway as the critical regulator of metabolic reprogramming in cancer (Cramer and Editors, 2016; Hirschey et al., 2015; Robey and Hay, 2009). This signalling axis acts via both transcriptional and post-translational mechanisms.

On the transcriptional level, several transcription factors are regulated by this axis and play important roles in modulating glucose uptake, glycolysis and OXPHOS. First, the hypoxia-inducible factor (HIF) family of transcription factors, consisting of the 3 members HIF1, HIF2, and HIF3, upregulates the expression of genes that facilitate adaptation to the hypoxic environment by promoting the diversion of glucose metabolism away from OXPHOS and towards glycolysis and lactate production. Each HIF consists of an oxygen-dependent α subunit and a constitutively expressed β subunit. The active heterodimer is stabilized under hypoxic conditions (Brahimi-Horn et al., 2007). Independent of the oxygen tension in cells, the PI3K-AKT-mTOR signalling can also upregulate HIF1 by increasing its level and activity (Bárdos and Ashcroft, 2004; Blancher et al., 2001; Zhong et al., 2000; Zundel et al., 2000). This occurs via both transcriptional activation and increased translation of HIF1α by mTORC1 through the 5'-untranslated region of HIF1α mRNA (Laughner et al., 2001; Thomas et al., 2006). Increased HIF1 activity leads to an increase in glucose uptake and glycolysis (Bhaskar et al., 2009; Buller et al., 2008; Dodd et al., 2015; Düvel et al., 2010) via the HIF-1-mediated increase in GLUT expression, notably GLUT1 and GLUT3. In addition, HIF-1 activation upregulates levels of hexokinase in tumour cells (Semenza, 2010), the first regulatory and committing step of the glycolytic pathway. HIF-1 also induces the transcription of pyruvate dehydrogenase kinase 1 (PDK1), an enzyme that inhibits pyruvate dehydrogenase activity, leading to the reduced conversion of pyruvate into acetyl CoA, and thus resulting in decreased flow to the TCA cycle (Kim et al., 2006a). In order to regenerate NAD^+ normally recycled by oxidative phosphorylation, HIF1a also upregulates the enzyme lactate dehydrogenase A (LDHA), which converts pyruvate into lactate, another hallmark of aerobic glycolysis (Semenza et al., 1996).

Second, the forkhead box O (FoxO) transcription factor family is also regulated via AKT. It consists of FoxO1, FoxO3, FoxO4, and FoxO6, which have multiple effects on cell metabolism (Tzivion et al., 2011). The FoxO transcription factors result in the decreased expression of several glycolytic genes,

including glucokinase (GCK), GPI, aldolase B (ALDOB), ENO1, and pyruvate kinase 1 (PK1) (Zhang et al., 2006). By inhibiting FoxO, AKT relieves the suppression of glycolytic gene expression.

Third, c-Myc is another important transcription factor that can regulate a number of physiological cellular processes, including cell growth, proliferation, apoptosis, and energy metabolism (Eilers and Eisenman, 2008). c-Myc is encoded by the MYC oncogene and its activation has been noted in multiple cancer cell lines and involves the transcriptional upregulation of GLUT1 (Osthus et al., 2000) and multiple glycolytic genes, such as glucose phosphate isomerase (GPI), PFK1, glyceraldehyde 3-phosphate dehydrogenase (GAPDH), triosephosphate isomerase (TPI), phosphoglycerate kinase 1 (PGK1), and enolase (ENO1) (Kim et al., 2004; Osthus et al., 2000). Its activity is also regulated by AKT, notably through glycogen synthase kinase-3b (GSK-3b), which is directly phosphorylated and inhibited by AKT. Once inhibited by AKT, GSK-3b prevents c-Myc degradation (Gregory et al., 2003; Welcker et al., 2004). Finally, in addition to glucose metabolism, mTOR also increases lipid synthesis through transcription factors, (such as SREBP) controlling genes involved in fatty acid and cholesterol, as well as ion channel transport (García-Martínez and Alessi, 2008).

At the post-translational level, the PI3K-AKT-mTOR axis promotes glucose uptake by increasing glucose transporter trafficking and the activity of certain glycolytic enzymes. First, the translocation of the glucose transporter GLUT4 to the plasma membrane is PI3K-AKT mediated (Cong et al., 1997; Huang and Czech, 2007; Kohn et al., 1996; Okada et al., 1994). In the lung, however, expression of the GLUT4 isoform is very low relative to the ubiquitous GLUT1 transporter. There is some evidence, albeit much less than for GLUT4, that PI3K-AKT signalling can regulate GLUT1 trafficking to the plasma membrane (Bentley et al., 2003; Olsen et al., 2014; Rathmell et al., 2003). With regards to glycolytic enzymes, AKT activation has been reported to increase the activity of HK (Mathupala et al., 2006; Wolf et al., 2011) and to promote its association with mitochondria. This association is thought to provide mitochondrial-generated ATP, which is required for the conversion of glucose to G6P by HK (Majewski et al., 2004). Finally, both AKT and mTOR can phosphorylate PFK2, thereby generating fructose 2,6-bisphosphate, a potent allosteric activator of the rate-limiting enzyme PFK1 (Deprez et al., 1997).

In summary, the PI3K-AKT-mTOR axis promotes aerobic glycolysis with most of the studies reported in cancer cells. As described above, these metabolic changes are thought to allow cancer cells to use all these glucose-derived carbons as building blocks for the formation of nucleotides, amino acids and lipids, allowing for efficient cell proliferation.

1.7. Clinical applications of aerobic glycolysis

Since the 1970s, the characteristic metabolic feature of cancer cells of increased glucose uptake has been used clinically for diagnostic and staging applications in the oncology field through the use of the [18F]FDG-PET ([18F]-labeled fluoro-2-deoxyglucose positron emission tomography) scanning modality.

[18F]FDG-PET scanning is a noninvasive imaging technique widely used clinically for tumour imaging and has been shown to improve the diagnosis and subsequent treatment of cancers. It involves the intravenous administration of [18F]FDG, a glucose analogue containing a radioactive fluorine-18 atom with a half-life of 110 minutes. [18F]FDG is transported across cell membranes by glucose transporters and is enzymatically phosphorylated to [18F]FDG-6-phosphate, which cannot further undergo glycolysis. This molecule essentially becomes *trapped* intracellularly, in contrast to the natural glucose-6-phosphate which can be metabolized further down the glycolytic pathway. Following intravenous [18F]FDG administration, patients then undergo PET scanning, a noninvasive imaging technique that detects the gamma rays from positron-emitting isotopes. When the positron-emitting radiotracer is administered to patients, the nucleus emits a positron which travels a short distance (up to a few millimetres), to meet an electron in tissue, resulting in the annihilation of the two particles. This annihilation event produces a pair of 511-KeV photons that are emitted in opposite directions (Zhu et al., 2011). The resulting gamma rays are the signals detected by the PET system and converted to images. Based on its half-life, [18F] is the most practical isotope for clinical practice, which is why more than 90% of oncologic PET imaging is performed using [18F]FDG. Due to the excessive glycolytic rate found in cancer tissues, the uptake of [18F]FDG is substantially increased in most types of cancers. Unfortunately, the spatial resolution of PET is not comparable to high-resolution computed tomography (HRCT) or magnetic resonance imaging (MRI), which can provide detailed anatomical information. Therefore, the fused anatomical images from HRCT and functional images from PET are now routinely used in clinical practise, where the fusion is achieved by advanced software methods. The increase in [18F]FDG-PET activity in cancer is in fact correlated with an increase in glucose transporters and in glycolytic enzyme activity (Kaira et al., 2014; Li et al., 2010; Patching, 2015). In view of the importance of PI3K-AKT-mTOR signalling on cellular glucose uptake, it is therefore not surprising that [18F]FDG-PET has also been used clinically to monitor the response

to chemotherapeutic drugs that target the PI3K-AKT-mTOR pathway (Engelman et al., 2008; Juvekar et al., 2012; Rodon et al., 2013).

Initial studies published about 10 years ago reported that patients with histologically proven IPF had a 'positive' [^{18}F]FDG-PET scan and suggested that this modality may be used as a marker for the evaluation of IPF (Meissner et al., 2006). Unfortunately, PET-CT at that time was unable to differentiate IPF from other interstitial lung diseases (Nusair et al., 2007). A more comprehensive study (Groves et al., 2009) was performed a few years later and correlated parenchymal abnormalities in the IPF lung with maximal [^{18}F]FDG uptake, measured as standardized uptake value (SUV). Areas of highest SUV corresponded to areas of fibrosis in the lungs (e.g. honeycombing, reticulations). Remarkably, the extent of [^{18}F]FDG uptake correlated with important physiological parameters of the lungs, such as the forced vital capacity and transfer factor. A follow-up study from the same group reported that repeat [^{18}F]FDG-PET scanning over a 1-week interval offers excellent reproducibility of the results (Win et al., 2012).

The ability to predict the clinical outcome and progression of IPF is of critical importance for both patients and clinicians. The suggestion that metabolic activity in IPF lungs could predict outcomes has also been studied recently (Justet et al., 2017). In this study, markers of metabolic activity by PET-CT were correlated with physiologic lung impairment and were independent predictors of mortality. Furthermore, in a more recent study, 113 patients with IPF underwent [^{18}F]FDG-PET scanning. The maximal pulmonary uptake relative to the background activity (target-to-background ratio) was quantified and found to predict mortality (Win et al., 2018).

1.8. Experimental models of lung fibrosis

Although various models exist (Tashiro et al., 2017), the bleomycin model of lung fibrosis is the most commonly applied experimental model of IPF. In 2017, a panel of experts expressed their views on the preclinical assessment of potential therapies for pulmonary fibrosis. This workshop was published by the American Thoracic Society and describes the murine intratracheal bleomycin model as "the best-characterized animal model available for preclinical testing" (Jenkins et al., 2017).

Bleomycin is a chemotherapeutic antibiotic used in clinical practice to treat a variety of malignancies but was found to have profibrotic effects with patients developing pulmonary fibrosis after its administration. Following oropharyngeal administration of bleomycin, an early period of lung injury develops. This acute injury and *inflammatory phase* occurs over the first week following bleomycin administration and is characterized by epithelial injury and vascular leak which leads to the influx of inflammatory cells, activation and elaboration of a multitude of inflammatory mediators including the upregulation of pro-inflammatory cytokines, and chemokines (Liu et al., 2017; Moore et al., 2013). The initial mechanism of bleomycin-lung injury is thought to be due to single and double-strand DNA breaks, leading to cell-cycle arrest and apoptosis. Although the enzyme bleomycin hydrolase inactivates bleomycin, levels of this enzyme are low in the lungs, which explains the susceptibility of this organ to bleomycin administration.

Following DNA damage, large amounts of ROS are produced, leading to epithelial injury, infiltration of inflammatory cells, and ultimately to fibroblast activation, extracellular matrix deposition, and development of fibrosis (Cai et al., 2013; Degryse et al., 2010; Naik and Moore, 2010; Sueblinvong et al., 2012; Tashiro et al., 2017). Subsequently, a transition phase from inflammation to active fibrosis occurs (around day 7-14 post instillation of bleomycin) with a gradual replacement of the inflammatory response with the emergence of myofibroblasts and interstitial collagen deposition. Eventually, the *fibrotic stage* develops and is characterized by intra-alveolar and septal fibrosis, expansion of the myofibroblast population and increased deposition of extracellular matrix. As bleomycin is inhaled in this model, much of the fibrotic lung areas develop around the airways, a pattern described as peribronchial. Lung collagen synthesis usually peaks around 28 days following bleomycin administration (Scotton and Chambers, 2010). Although some have reported that the fibrotic lesions resolve after day 21–28 (Lawson et al., 2005), the fibrotic stage is thought to last for

as long as 6 months following bleomycin administration (Jenkins et al., 2017; Scotton et al., 2013).

Although well characterized and very commonly used, the bleomycin model of lung fibrosis has been heavily criticized for not being representative of IPF, for the following reasons (BORZONE et al., 2001; Liu et al., 2017; Scotton and Chambers, 2010). First, the characteristic histology of IPF is of UIP (usual interstitial pneumonia), a pattern that is characterized by (i) dense fibrosis with architectural distortion (i.e., destructive scarring and/or honeycombing) with a (ii) predominant subpleural and/or paraseptal distribution of fibrosis, (iii) patchy involvement of lung parenchyma by fibrosis, and with the presence of (iv) fibroblast foci. This pattern is *not* observed in the lungs of mice exposed to bleomycin, which causes a more central, bronchocentric pattern of injury with fibroblastic foci and hyperplastic AECII being absent in the single-dose model of bleomycin (Scotton and Chambers, 2010). Furthermore, the bleomycin model develops relatively rapidly (over 21-28 days), while IPF lesions are thought to develop over years. IPF lesions characteristically progress while bleomycin-induced lung injury stabilizes with spontaneous resolution described by some groups over time (BORZONE et al., 2001; Della Latta et al., 2015). Finally, the extent of inflammatory cell infiltrates is much more pronounced in the bleomycin model than in IPF lungs although chronic inflammation diminishes during the fibrotic stage (Scotton et al., 2013). For all these reasons, the model is certainly not optimal but is easy to perform, cost-effective, rapid, reproducible and already well-described.

Nevertheless, the bleomycin mouse model does share important features with IPF lungs. These include epithelial cell injury, basement membrane damage, interstitial fibrosis with dense collagen deposition as well as molecular and genomic signatures (eg. TGFβ1 activation) resembling those encountered in IPF (Bauer et al., 2015; Munger et al., 1999). The importance of this model is exemplified by the fact that the only 2 drugs approved for IPF (pirfenidone and nintedanib) used this model for its preclinical development (Grimminger et al., 2015; King and Nathan, 2015; Wollin et al., 2015). Therefore, despite its imperfections as a model of human chronic progressive lung disease, the bleomycin model has been quite useful in providing mechanistic insight and for drug discovery (Liu et al., 2017).

1.9. Hypothesis and aims

IPF is a life-threatening interstitial lung disease characterized by progressive scarring of the lung parenchyma. The disease is characterized by the proliferation of fibroblasts and the excessive deposition of a collagen-rich matrix. TGFβ1 has been recognized as a key cytokine in the pathophysiology of IPF and other fibrotic disorders by promoting the differentiation of fibroblasts into myofibroblasts. Highly proliferative cells, such as cancer cells, reprogram their glucose metabolism through the activation of the PI3K-AKT-mTOR axis towards enhanced glycolysis, a process known as aerobic glycolysis. In view of the high biosynthetic nature of myofibroblasts, this thesis examines the **hypothesis that TGFβ1-induced fibroblast to myofibroblast differentiation involves metabolic reprogramming towards aerobic glycolysis, that these metabolic changes are regulated by the PI3K-AKT-mTOR axis, and that changes in glucose metabolism can be assessed in a murine model of lung injury and fibrosis.**

To address this hypothesis, this thesis has the following 3 aims:

Aim 1. Describe the changes in glucose metabolism that occur during the process of TGFβ1-induced fibroblast to myofibroblast differentiation.

Primary human lung fibroblasts (pHLFs) will be stimulated with TGFβ1 and the metabolic profile of these cells will be examined by measuring mRNA and protein levels of glucose transporters and glycolytic enzymes. In addition, glycolytic flux will be assessed using NMR (nuclear magnetic resonance) spectroscopy. Finally, further metabolomic analysis will be performed to measure cellular oxygen consumption and extracellular acidification rates using the SeaHorse XF96e platform.

Aim 2. Determine whether the PI3K-AKT-mTOR axis regulates the changes in glucose metabolism that occur during the process of TGFβ1-induced fibroblast to myofibroblast differentiation.

Using highly selective and potent pharmacological inhibitors, the role of the PI3K-AKT-mTOR pathway in promoting changes in glucose uptake, glycolytic flux, expression of glucose transporters and mitochondrial respiration will be examined.

Aim 3. Examine *in vivo* glucose uptake in the lungs using the bleomycin model of lung fibrosis

Using the well-established mouse model of bleomycin-induced lung injury, glucose uptake in the

lung will be assessed by administering [^{18}F]FDG and then localizing its lung uptake using PET-CT scanning and autoradiography.

2. Methods

2.1. Materials

All chemicals were of analytical grade and obtained from Sigma Aldrich (UK) unless otherwise stated. All water used for the preparation of buffers was distilled and deionised using a Millipore Water Purification System (Milipore R010 followed by Milli-Q Plus, Milipore Ltd, UK). All sterile tissue culture media, sterile tissue culture grade trypsin/EDTA, antibiotics (penicillin/streptomycin) and fetal calf serum (FCS) were purchased from Thermo Fisher Scientific (UK). Bovine serum albumin was obtained from Merck Millipore (UK). Sterile tissue culture flasks, plates and disposable pipettes were obtained from Nunc (Denmark). Sterile polypropylene centrifuge tubes were obtained from Falcon (New Jersey, USA). Transforming growth factor β1 (TGFβ1) was purchased from R&D Biosystems (UK) and was reconstituted in 4mM HCl/ 0.1% BSA (w/v) to 10μg/ml and stored in aliquots at -20°C.

2.2. Primary human fibroblast cell lines

Primary human lung fibroblasts (pHLFs) were grown from explant as previously described (Keerthisingam et al., 2001), and were all derived from a single lung donor. The experiments performed in this thesis were independently replicated using these cells.

Human tissues were sourced ethically, and their research use was in accord with the terms of informed consents. Institutional research ethics committee approvals for this work was obtained from the UCL Research Ethics Committee (12/EM/0058).

2.3. Primary cell culture

All fibroblasts used for experimental work described in this thesis were obtained from a single healthy lung donor and were maintained using standard cell culture techniques. To avoid exposing cells to super-physiological high glucose and glutamine concentrations in standard DMEM, pHLFs

(passage 4-8) were cultured in glucose and glutamine-free DMEM (Thermo Fischer A14430) that was supplemented with 10% FCS (v/v), 5mM glucose, 0.7mM glutamine and 1% Penicillin/Streptomycin (referred throughout the thesis as "growth medium"). All fibroblast lines tested negative for mycoplasma.

Cells were incubated in a humidified atmosphere containing 10% CO_2. The medium was removed and the cell monolayer was incubated with 5ml of 0.05% trypsin-EDTA at 37°C until cell detachment was observed. Trypsin was neutralised with DMEM containing 10% FCS and the cell suspension was centrifuged for 5 minutes at 300g at room temperature using a bench centrifuge (MSE Mistral 3000, UK). The supernatant was discarded and cell pellet split at 1:4 ratio before being resuspended in 10% FCS DMEM and transferred to new T175 flasks.

For experiments, the fibroblast monolayer was trypsinised and the cell pellet prepared as above. The supernatant was discarded and the cell pellet brought into a single cell suspension with 10ml DMEM containing 10%FCS (v/v) by gentle mixing. An aliquot of the suspension was used to determine the cell count (Scepter 2.0 Handheld Automatic Cell Counter, Millipore). For each experiment, the cell density was adjusted with DMEM/10% FCS (v/v) to reach a concentration of 1×10^5/ml, unless otherwise stated. Cells were grown to confluence and serum-starved for 12-24 hours prior to experimentation. Before each experiment, the serum-free medium was removed and replaced with fresh serum-free DMEM, with or without cytokines or inhibitors for a selected length of time.

2.4. Pharmacological Inhibitors

All pharmacological kinase inhibitors were obtained from GlaxoSmithKline, with pIC50 values shown in Table 1. pIC50 values correspond to the inverse log of the IC50 (half maximal inhibitory concentration). Compounds were reconstituted in sterile 100% DMSO to a stock concentration of 10mM and stored at room temperature, protected from light.

Compound	PI3K				mTORC1/2	AKT1
	α	β	γ	δ		
GSK2864918A	7.4	7.1	7.1	7.7	<4.3	
AZD8055	5.6	4.7	5.3	5.9	>9.1	
MK2206	4.5	4.8	4.5	4.7	<4.3	8.3
GSK2119126	<45	<4.5	<4.5	<4.5	<4.3	8.6

Table 1. pIC50 in recombinant assays (GlaxoSmithKline data).

2.5. Macromolecular crowding assay

Collagen biosynthesis in a 96-well format was measured by a high-content imaging-based molecular crowding assay modified from a previously described method (Chen et al., 2009). pHLFs were seeded in a black-walled 96-well plate (Corning, USA) in 10% FCS DMEM (v/v) on day 1. On day 2, the medium was changed to DMEM containing 0.4% FCS (v/v). Macromolecular crowding medium was prepared by diluting ascorbic acid (final concentration 17µg/ml) in 0.4% FCS DMEM containing Ficoll 70 (37.5 mg/ml) and Ficoll 400 (25mg/ml) (Sigma Aldrich, UK) as molecular crowding agents. The medium was filter-sterilised with a 0.2µM filter (Thermo Fisher Scientific, UK). The medium on the wells was discarded to waste and replaced with 100µl of crowding medium. Inhibitor concentrations were prepared by serially diluting 100% DMSO 10mM stock solution in crowding medium before application to the cells. The final DMSO concentration was 0.1% in all wells, including that of vehicle controls. Cells were incubated at 37°C in 10% CO2 prior to stimulation with TGFβ1 (1ng/ml) for 72 hours. pHLFs were fixed in ice-cold methanol (VWR, UK), permeabilised with 0.1% (v/v) Triton-X-100 in PBS (Sigma Aldrich, UK) and stained with primary antibody specific for human collagen I or α-SMA overnight at 4°C. Plates were washed three times with 0.05% (v/v) Tween-20 in PBS, followed by the addition of fluorescent secondary antibody (Alex Fluor488) and DAPI to counterstain the nuclei for cell count. Plates were incubated for 1 hour at room temperature followed by three final washes with 0.05% (v/v) Tween-20 in PBS. 200µl PBS was added to each well and the plates were stored at 4°C before imaging. The fluorescent signal was measured on the

ImageQuant high content system at 20x magnification. Quantitative image analysis was performed using a custom algorithm within the object analysis module which detects and quantifies changes in intensity of fluorescent signals. Mean fluorescent intensity per well was calculated with 4 reads per well, adjusted for cell count. Data were expressed as the mean+/-SEM intensity of 4 technical replicates minus mean background intensity.

2.6. Nuclear magnetic resonance spectrometry

Extracellular glucose and lactate levels were measured in cell supernatants by ^{1}H-NMR. To do so, 900ul of cell culture supernatant was collected after the indicated time points, as described in Figure 2-1.
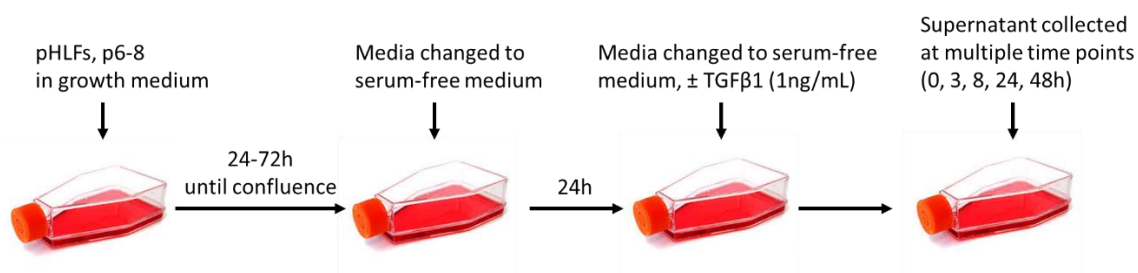
Figure 2-1. Schematic diagram of the cell culture methods for NMR acquisition.
These methods were performed to obtain the data obtained in Figure 3-4, Figure 3-5, Figure 3-6 and Figure 3-7. Full experimental details can be found in the 'Methods' section of this thesis.

The samples were then spun at 13200rpm and 4°C for 10 minutes to remove any potential cell debris. The supernatant was then supplemented with 100µl of 10mM trimethylsilylpropanoic acid (TSP) in D2O in order to obtain a solution containing 1mM of TSP and 10% D2O. These samples were then stored at 4°C for up to 72 hours. Using a 500MHz Bruker machine, the samples were then run using a water-Suppression using pre-saturation pulses (ZGPR) technique after 128 scans. The resulting spectra were obtained and analyzed using ACD labs software. For measurement of individual metabolites, the integrals of the 1.3 ppm and 5.2 ppm peaks, corresponding respectively to lactate and glucose, were measured and corrected for the 0ppm integral reference peak created by the internal reference standard (TSP).

2.7. Real-time quantitative polymerized chain reaction analysis of gene expression

Fibroblasts for RNA extraction were seeded into 6-well plates as previously described and samples collected at specified time-points following treatment as described in Figure 2-2.
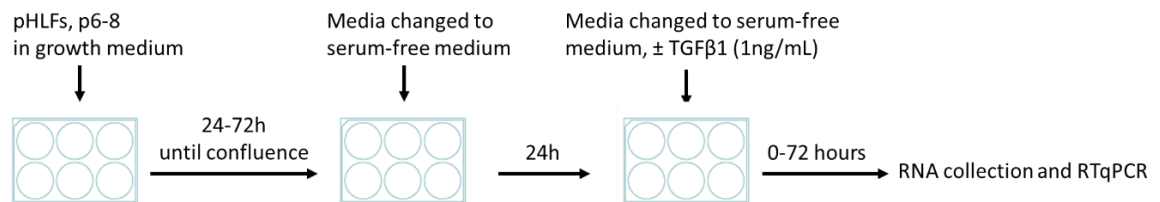
Figure 2-2. Schematic diagram of the cell culture methods for RNA collection and RT-PCR.

pHLFs: Primary human lung fibroblasts

To minimise RNA degradation, all equipment and surfaces were cleaned thoroughly with RNaseZap and filter pipette tips were used throughout. Qiagen RNeasy Mini kit was used to extract RNA. Supernatants were removed from tissue culture plates prior to the addition of 350µl /well of Buffer RLT (Qiagen). Cell lysates were then passed through a filter pipette tip several times, transferred to 1.5ml microcentrifuge tubes and frozen at -80°C if RNA was not immediately extracted. If frozen, samples were thawed on ice and then placed at room temperature for 5 minutes before being centrifuged at 13200rpm and 4°C for 2 minutes to remove any lysate from the lid of the tube. To each sample 350µl of 70%, ethanol was added. The tubes were mixed thoroughly for 5-10 seconds using a vortex. 700µl of the sample was placed in an RNeasy Mini spin column and centrifuged for 15s at >8000 x g. The flow-through was discarded and 700µl of Buffer RW1 (Qiagen) was added to the spin column and centrifuged again. Flowthrough was discarded and 500µl Buffer RPE (Qiagen) was added to the column and recentrifuged. Flow-through was again discarded and the above step repeated. 30-50µl RNase-free water was added directly to the spin column and centrifuged to elute RNA.

Contaminating genomic DNA was removed using the Precision DNase kit (Primer Design). RNA concentration and protein contamination were quantified on a Nanodrop spectrophotometer (Thermo Fisher Scientific) by measuring the A260 and A260/280 ratios respectively. The A260/280 ratio was used as a guide as the purity of the RNA sample; ratios between 1.7 and 2.0 were considered acceptable.

cDNA was prepared by reverse transcription using qScript cDNA Supermix kit (Quanta Biosciences, USA). Up to 1µg of RNA sample was added to 4µl of qScript cDNA Supermix (5X reaction buffer containing optimized concentrations of MgCl2, dNTPs (dATP, dCTP, dGTP, dTTP), recombinant RNase inhibitor protein, qScript reverse transcriptase, random primers and oligo (dT) primers). A final volume of 20µl was achieved by the addition of nuclease-free water. Samples were incubated for 5 minutes at 25°C, 30 minutes at 42°C and 5 minutes at 85°C.

Quantitative real-time polymerase chain reaction (qRT-PCR) was performed using the Power SYBR® Green PCR Master Mix (ThermoFisher Scientific, UK). 2µl of cDNA and forward and reverse primers were added at a final concentration of 800nM. Samples were run as duplicates on the Mastercycler EP Realplex (Eppendorf, Germany). Cycling conditions: 95°C for 10 minutes for SYBR green activation, 95°C for 15 seconds and 60°C for 1 minute for 40 cycles. The specificity of the products obtained by PCR was confirmed by melting curve analysis, demonstrating a single melting curve indicative of a single PCR product.

Primer efficiency was assessed by determining the Ct (cycle threshold) values for qRT-PCR reactions using a series of 1:2 dilutions of template cDNA. Ct values were defined as the earliest point of the linear region of the logarithmic amplification plot reaching a threshold level of detection. Concentrations of samples were plotted against Ct values, and the slope of the plot determined, to calculate the efficiency of the primers. Primers with >95% efficiency were used, Ct values of genes of interest were determined from the linear region of the logarithmic amplification plot and normalized by subtraction of the geometric mean of the Ct values for two housekeeping genes: ATP synthase 5B (ATP5B) and β2 macroglobulin (β2M), identified by GeNorm analysis as the most stable housekeeping genes for this study. This generated the ΔCt value. Relative expression was calculated using the $2^{-\Delta Ct}$ approach. Statistical analysis was performed using $2^{-\Delta Ct}$ values.

COL1A1 (F)	ATGTAGGCCACGCTGTTCTT
COL1A1 (R)	GAGAGCATGACCGATGGATT
ACTA2 (F)	AATCCTGTGAAGCAGCTCCAG
ACTA2 (R)	TTACAGAGCCCAGAGCCATTG
SLC2A1 (F)	5'-ACTGTCGTGTCGCTGTTTGT-3'
SLC2A1 (R)	5'-GATGGCCACGATGCTCAGAT-3'
HKII (F)	GGTGGAGTGGAGATGCACAA
HKII (R)	GAGGATGCTCTCGTCCAGG
PFKFB3 (F)	5'-AAAAGTGTTCAACGTCGGGG-3'
PFKFB3 (R)	5'-CATGGCTTCCTCATTGTCGG-3'
LDHA (F)	5'-GGAGATTCCAGTGTGCCTGT-3'
LDHA (R)	5'-GTCCAATAGCCCAGGATGTG-3'

Table 2. Primer sequence used for RTqPCR experiments

2.8. Western blotting

Primary human lung fibroblasts were lysed in 100µl of ice-cold lysis buffer (Phosphosafe extraction reagent (Novagen) supplemented with Protease Inhibitor (Complete mini, Roche). Lysates were scraped and collected into labelled Eppendorf tubes on ice and stored at -20°C. Protein concentrations were measured using BCA protein assay (Pierce, USA), as per the manufacturer's instructions. Briefly, the assay was performed by adding 100µl of freshly prepared BCA reagent to 10µl of each sample or standard (assayed in duplicate) in a 96-well plate. The plate was agitated on a plate shaker for 30 seconds and then incubated at 37°C for 20 min prior to reading the absorbance at 562nm on a Titertek Multiscan MCC/340 plate reader (Labsystems, Finland).

Equal amounts of protein were diluted in sample buffer (Bolt LDS sample buffer 4x, Life

Technologies) and reducing agent (Bolt Sample reducing agent 10x, Life Technologies) prior to a 10-minute incubation at 80°C. Samples were loaded on to a pre-cast 4-12% Bis-Tris Plus gel (Life Technologies) with a 10-250kDA protein ladder (PageRuler Plus Prestained Protein Ladder). Electrophoresis was performed at 165V for 30 minutes. Proteins were transferred onto a nitrocellulose membrane using the iBlot dry transfer system (Life Technologies). The quality of protein transfer was assessed by briefly staining the membrane with 2% Ponceau Red solution (Sigma). Membranes were incubated with blocking buffer (5% milk or 5% BSA in TBS-0.1%Tween) for one hour at room temperature. The membranes were incubated in primary antibody at 4°C overnight. Membranes were washed in TBS-0.1%Tween and incubated for 2 hours at room temperature with specific horseradish peroxidase (HRP)-linked secondary antibody. The membrane was washed in TBS-0.1%Tween and then developed by enhanced chemiluminescence (ECL) according to the manufacturer's instructions (Amersham). Immunoreactive bands were visualized and quantified using ImageQuant TL v8.1 software (GE Healthcare). For loading controls, membranes were stripped, re-blocked and re-probed with a further primary antibody.

2.9. SeaHorse assay

The Seahorse Bioscience XF96e extracellular flux analyzer (Agilent) was used to measure oxygen consumption rate (OCR) and extracellular acidification rate (ECAR). Briefly, primary human fibroblasts were seeded in XF96e microplates at 10 000 cells per well and incubated for 3 days in growth media. The media was then replaced with serum-free (FBS 0.4%) media for 24 hours. The next day, cells were stimulated with (or without) TGFβ1 at 1ng/mL, in the presence or absence of pharmacological inhibitors of the PI3K-AKT-mTOR axis as described in detail in the results section. At the desired time point, the media in each well was replaced with 175uL of SeaHorse assay media (Agilent) prewarmed to 37°C and supplemented with 5mM of glucose, 0.7 mM of glutamine and 1mM of pyruvate.

In order to perform the mitochondrial stress test protocol, the XF sensor cartridge had its port A loaded with 25uL of oligomycin at 20ug/mL (for a final concentration in well of 2.5ug.mL), port B with 25uL of FCCP at 9uM (for a final concentration in well of 1000nM), port C with 25uL of Antimycin A at 10uM and rotenone at 10uM (for a final concentration in well of 1uM for Antimycin A and 1uM for rotenone) and port D with 25uL of assay media. Measurements of OCR and ECAR

could then be performed after equilibration in assay medium (lacking supplemental CO2) for about 45 minutes. The assay protocol then involved 3 measurements of OCR and ECAR with an interval of 3 minutes before each measurement before and after the injection of each port. The resulting values were then analyzed using the Seahorse XF Mito Stress Test Report Generator offered by Agilent which automatically calculates the Seahorse XF Cell Mito Stress Test parameters to obtain the basal respiration, ATP production, proton leak, maximal respiration, spare respiratory capacity, and non-mitochondrial respiration, as shown in Figure 2-3.
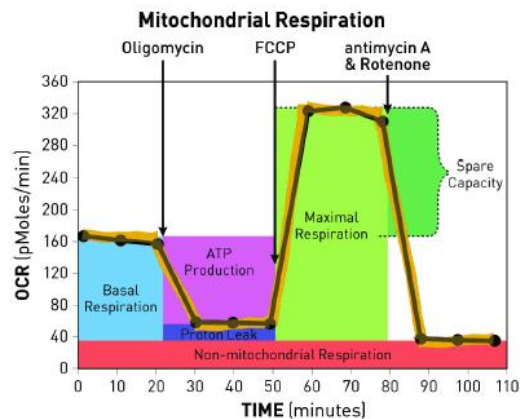
Figure 2-3. Schematic representation of the mitochondrial stress test protocol

Figure copied from the manufacturer's website, describing the fundamental parameters of mitochondrial function (https://www.agilent.com/en/products/cell-analysis/mitochondrial-respiration-xf-cell-mito-stress-test)

2.10. Cell count measurement for the SeaHorse assay

Cell count was measured after each SeaHorse assay protocol. To do so, media was removed from each well upon assay completion and placed in a -80C freezer. On the day of the assay, the plate was thawed and 200uL of lysis buffer was added as to the manufacturer's instruction (Thermo Fischer, C7026). Fluorescence was then measured at 480nm-520nm as a surrogate of cell count.

2.11. [^{18}F]FDG experiment

Four (4) C57/BL male mice between 10-12 weeks of age (Charles River Laboratories, UK) were initially administered bleomycin (Bleo-kyowa, Kyowa Hakko Ltd, Slough, UK; 1mg/kg or sterile 0.9% saline) by oropharyngeal instillation under light isoflurane anaesthesia. [^{18}F]FDG was provided by PETNET Solutions, Northwood Middlesex, UK. Mice were fasted the night prior to the day of the experiment. That day, they were injected intravenously (lateral tail vein) with 13.0 ± 1.9 MBq (mean ± SEM) of [^{18}F]FDG and kept under isoflurane anaesthesia for 1 hour after injection to maximise tracer uptake in the lungs. After 1 hour the mice underwent PET-CT scanning. Following imaging, the animals were then sacrificed by exsanguination, the lungs were insufflated with H_2O/OCT (1:1 v/v) at a constant pressure of 20cm H_2O. Lung samples were then embedded in OCT compound and frozen in isopentane on dry ice. Frozen lung sections (5 μm) were cut in the transaxial plane with a cryostat (Bright 5030). From a mid-lung region onwards every 7th frozen lung section was selected for autoradiography, for 3 sections per lung, the remaining sections were stored at -80°C. In the bleomycin perfused group, following exsanguination the right ventricle was perfused with 3-5 ml sterile PBS until the lungs appeared white indicating blood was flushed out of the pulmonary circulation, after which lungs were then insufflated with dH_2O/OCT (1:1 v/v) as described above.

2.12. Autoradiography

Internal standards used for activity calibration were prepared by serial dilution of the [^{18}F]FDG solution. Lung sections and internal standards absorbed on filter paper were left to air-dry and subsequently exposed to a phosphor screen (BAS-IP MS; GE Healthcare) overnight. Phosphorimaging was performed on a Typhoon Trio scanner (GE Healthcare) on 3 sections per mouse. Image analysis was performed using the software Image J (version 1.48). Quantification of ^{18}F activity was based on a calibration curve from internal standards using the Rodbard regression model ($R^2 > 0.998$). The signal intensity of internal standards and lung slices was obtained from a region of interest encompassing the whole standard or lung slice on greyscale images. Activity in each lung slice was decay corrected to the injection time and normalised to the injected activity (MBq). To account for lung slice size variation, activity was expressed as the activity per cm^2 lung slice surface area (‰ID/cm^2). Images were then pseudo-coloured to provide ease of contrast for

comparison to adjacent histological slices.

2.13. Histology

Cryo-frozen 5 μm mouse lung sections immediately adjacent to sections used for autoradiography were stained for hematoxylin and eosin (H&E) or modified trichrome (Martius Scarlet Blue [MSB]) with collagen staining blue, fibrin in red and erythrocytes in yellow.

2.14. Statistical analysis of data

All data are expressed as means ± SEM unless otherwise stated. All experiments were repeated on three separate occasions unless otherwise stated. Statistical differences between two groups were analysed using a standard two-tailed t-test (assuming unpaired data sets and unequal variances). When more than two groups were compared, either one-way or 2-way ANOVA was used with posthoc application using the Bonferroni method. The α level was set at 0.05 for all tests (GraphPad Prism).

3. Results

3.1. Experimental optimization of TGFβ1 concentration

The initial experiments were aimed at determining the optimal concentration of TGFβ1 required to promote a significant increase in collagen I deposition by fibroblasts. In order to do so, a concentration-response curve was performed using a macromolecular crowding assay (see Methods 2.5). As shown in Figure 3-1, the lowest TGFβ1 concentration that significantly increased collagen I deposition was of 1ng/mL. Based on these results, all future experiments were performed using a TGFβ1 concentration of 1ng/mL.
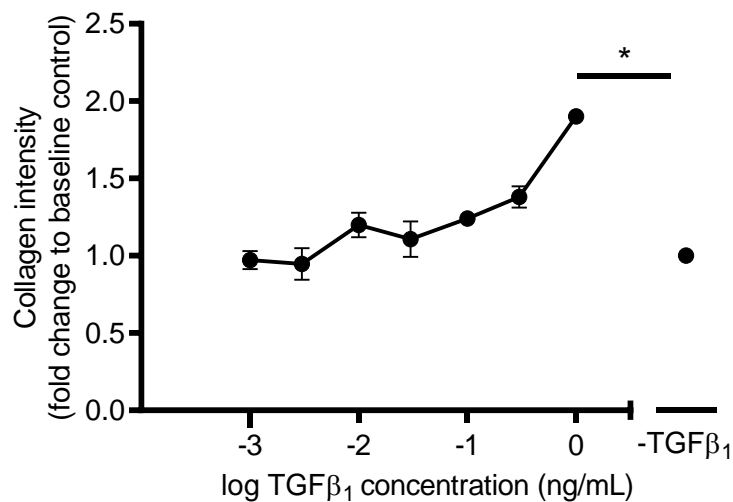
Figure 3-1. Concentration-response curve of TGFβ1 on collagen I deposition.

Primary human lung fibroblasts were grown in serum-free conditions for 24 hours prior to stimulation with TGFβ1 at increasing concentrations as depicted above. After 72 hours of incubation in a macromolecular crowding assay, collagen I deposition was assessed by immunofluorescence microscopy and corrected for cell count (mean ± SEM, n=4 replicates). Difference between groups was evaluated with 1-way ANOVA, using Tukey correction for multiple comparisons *p<0.05.

Using a concentration of 1ng/mL, the activation by TGFβ1 of downstream SMAD signalling was then examined by assessing the phosphorylation of pSMAD3 over time by immunoblotting. TGFβ1

stimulation caused rapid phosphorylation of SMAD3, with peak phosphorylation occurring as early as 1 hour after stimulation (Figure 3-2).
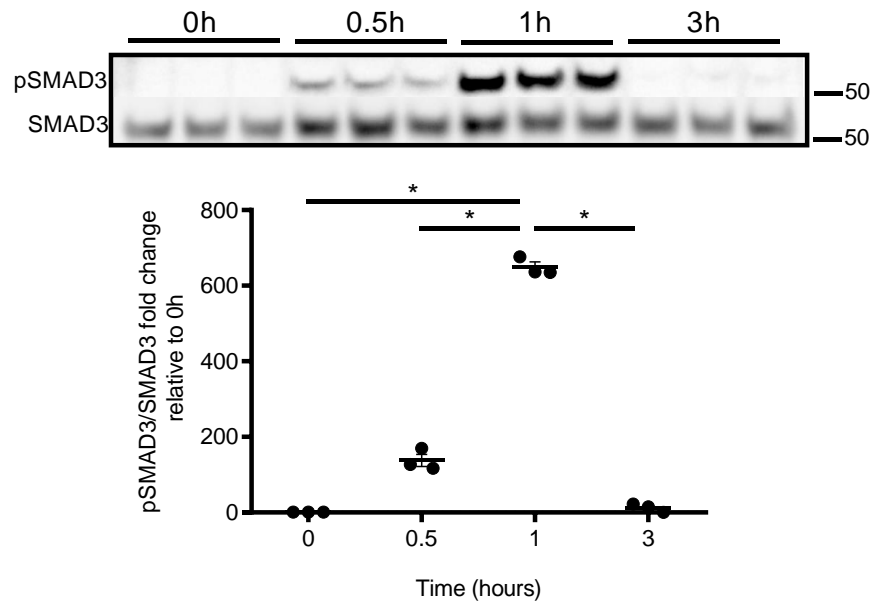
Figure 3-2. Effect of TGFβ1 on SMAD3 phosphorylation over time.

Primary human lung fibroblasts were grown in serum-free conditions for 24 hours prior to stimulation with TGFβ1 (1ng/ml) or media control. Cells were lysed, followed by immunoblot with anti-pSMAD3 and SMAD3 antibodies on the same membrane. Data shown represent the densitometry of pSMAD3/ SMAD3 (mean, n=3 replicates). Difference between groups was evaluated with one-way ANOVA with Tukey correction for multiple comparisons. *p<0.05.

3.2. Effect of TGFβ1 stimulation on collagen I and α-SMA mRNA levels

TGFβ1 is a critical profibrotic cytokine that promotes fibroblast to myofibroblast differentiation, as defined by increased expression of α-SMA and formation of α-SMA positive stress fibres. It also promotes the secretion of ECM proteins, notably collagen I.

The following experiment was aimed at determining the time course of the effect of TGFβ1 on the induction of the genes encoding α-SMA (*ACTA2*) and collagen I (*COL1A1*). To this end, primary human lung fibroblasts were stimulated with TGFβ1 (1ng/ml) and mRNA levels of *COL1A1* and *ACTA2* were assessed over a 72-hour time course by qRT-PCR, as described in Figure 2-2.

Figure 3-3 reveals that the mRNA levels of *ACTA2* significantly increased after 12 hours of TGFβ1 stimulation and peaked at 24 hours. For *COL1A1*, mRNA levels were also significantly increased 12 hours after TGFβ1 stimulation with a peak at 32 hours. TGFβ1 stimulation led to a 6-fold increase in *COL1A1* mRNA levels ($p<0.05$) and a 50-fold increase in *ACTA2* mRNA levels ($p<0.05$) relative to unstimulated cells at the 24-hour time point.
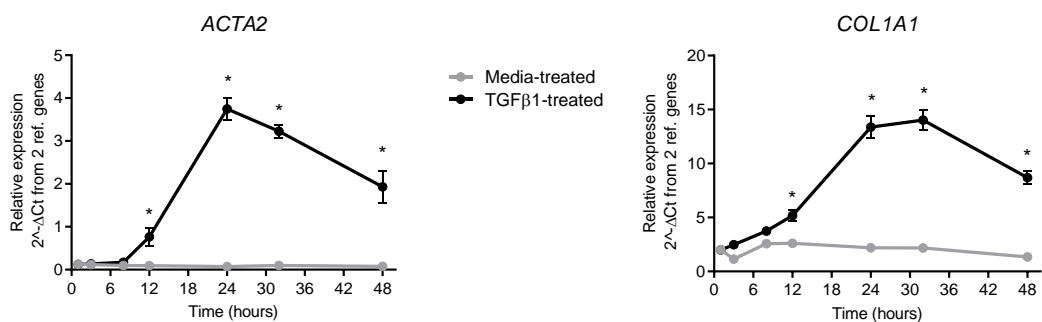
Figure 3-3. Effect of TGFβ1 on *ACTA2* and *COL1A1* mRNA levels.
Primary human lung fibroblasts were grown in serum-free conditions for 24 hours prior to stimulation with TGFβ1 (1ng/ml) or media control, as depicted in Figure 2-2. RNA was isolated at specified time points. Data shown represent the mRNA levels of *ACTA2* and *COL1A1* relative to the geometric mean of *ATP5B* and *β2M* housekeeping genes (mean ± SEM, n=3 replicates). Difference between groups was evaluated with two-way ANOVA with Tukey correction for multiple comparisons. *$p<0.05$.

These results indicate that after 24 hours of TGFβ1 stimulation, fibroblasts have differentiated into myofibroblasts, as evidenced by large increases in both *ACTA2* and *COL1A1* mRNA levels. For that reason and for practical purposes, the bulk of the next set of experiments was performed after 24 hours of TGFβ1 stimulation, unless otherwise noted.

3.3. Effect of TGFβ1 stimulation on glycolytic flux

To determine whether the metabolism of glucose in fibroblasts is altered upon TGFβ1 stimulation, the rate at which glucose is metabolized into lactate in the presence (or absence) of TGFβ1 stimulation was examined. This rate, also described as glycolytic flux, was estimated based on the measured changes in the extracellular levels of glucose and lactate molecules over time. Although a variety of metabolomic methods have been used to determine glycolytic flux, I chose to use proton nuclear magnetic resonance spectroscopy (^{1}H-NMR) for its cost, reproducibility and access (Emwas, 2015).

Supernatants from multiple time points were collected after fibroblasts were exposed to media in the presence or absence of TGFβ1 (1ng/mL), as depicted in Figure 2-1. These supernatants were then spun and carefully prepared for 1H-NMR, as described in detail in the Methods section (2.6) of this thesis. The 5.2ppm and 1.3ppm peaks of the spectra were selected to represent glucose and lactate, respectively. Although the glucose spectrum contains multiple peaks (HMDB, 2010), the 5.2ppm peak was chosen based on its distance from the peaks of water and other metabolites present in the sample. Similarly, although lactate contains 2 main peaks (HMDB, 2010), the 1.3ppm peak was chosen due to its easier distinction from other metabolite peaks. The integral (area under the curve) of the 5.2 ppm and 1.3ppm peaks were measured and divided by the integral of TSP (0ppm), used as an internal standard. Representative spectra of 2 samples after 24hours of control media or TGFβ1-treatment are depicted in Figure 3-4.

Media-treated   TGFβ1-treated
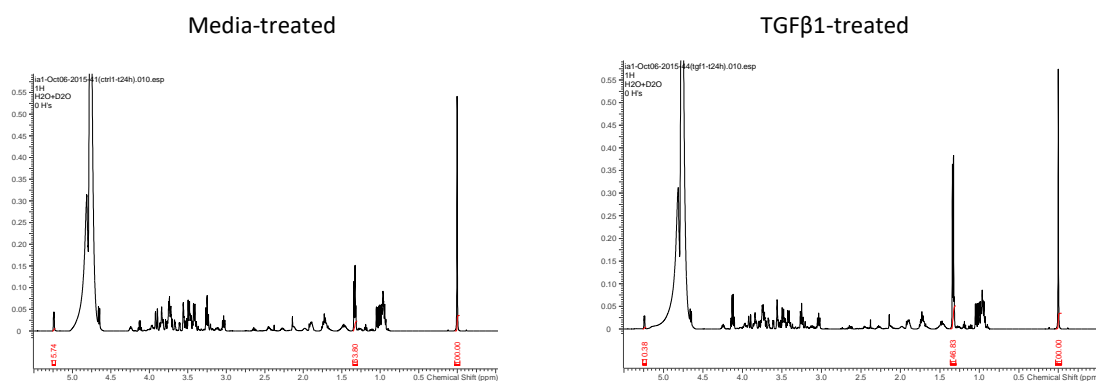
Figure 3-4. Representative ¹H-NMR spectra of cell supernatants.

Cell supernatants were collected and run on 500MHz NMR spectrometer. Spectra obtained were then analyzed and interpreted using ACDlabs software. The area under the curves (AUC) of the peaks at 5.2ppm, 1.3ppm and 0ppm were measured. In these samples, supernatants of TGFβ1-stimulated cells had an AUC of 146.83 vs 63.80 for media-treated cells at the 1.3ppm peak, and an AUC of 10.38 vs 15.74 at the 5.2ppm peak, after standardized with the AUC of the 0ppm peak (standard).

Using this method, the rate of decline in glucose levels was found to be significantly increased upon TGFβ1 stimulation when compared to control cells (Figure 3-5). Similarly, extracellular lactate levels rose significantly over time in both TGFβ1-treated and media-treated samples, although the lactate levels rose more rapidly in TGFβ1-stimulated samples (Figure 3-6). At the 8-hour time point, the levels of lactate were significantly increased relative to those of media-treated cells. The lactate: glucose ratio was also calculated as it was felt to best illustrate overall glycolytic flux (Figure 3-7).

Extracellular glucose

Media-treated
TGFβ1-treated

$Y = -0.2143 * X + 20.57$

$Y = -0.4292 * X + 20.39$
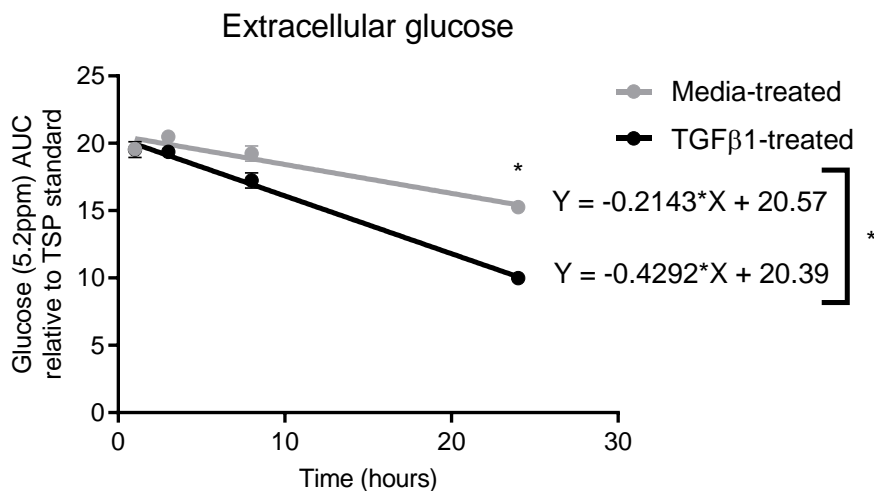
**Figure 3-5. Effect of TGFβ1-stimulation on extracellular levels of glucose.**

Primary human lung fibroblasts were grown in serum-free conditions for 24 hours prior to stimulation with TGFβ1 (1ng/ml) or media control. Cell supernatants were then collected at the time points indicated and run on a 500MHz NMR spectrometer. Data shown represent the AUC of the 5.2 ppm glucose peak after standardization to the 0ppm TSP peak (mean ± SEM, n=3 replicates). Difference between groups was evaluated with two-way ANOVA with Tukey correction for multiple comparisons. In addition, a linear regression equation was calculated for each condition, with the difference between the slopes found to be significant. *p<0.05.

Extracellular lactate

Media-treated
TGFβ1-treated

$Y = 5.681 * X + 19.67$

$Y = 1.668 * X + 27.55$
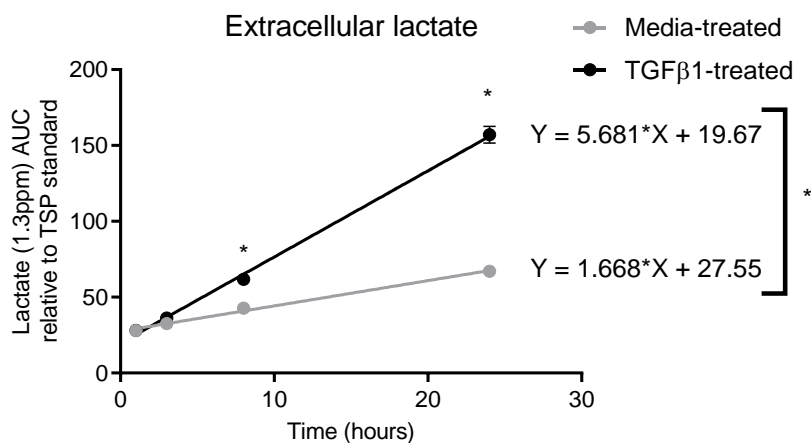
Figure 3-6. Effect of TGFβ1-stimulation on extracellular levels of lactate.

Primary human lung fibroblasts were grown in serum-free conditions for 24 hours prior to stimulation with TGFβ1 (1ng/ml) or media control. Cell supernatants were then collected at the time points indicated and run on a 500MHz NMR spectrometer. Data shown represent the AUC of the 1.3ppm lactate peak after

56

standardization to the 0ppm TSP peak (mean ± SEM, n=3 replicates). Difference between groups was evaluated with two-way ANOVA with Tukey correction for multiple comparisons. In addition, a linear regression equation was calculated for each condition, with the difference between the slopes found to be significant. *p<0.05.
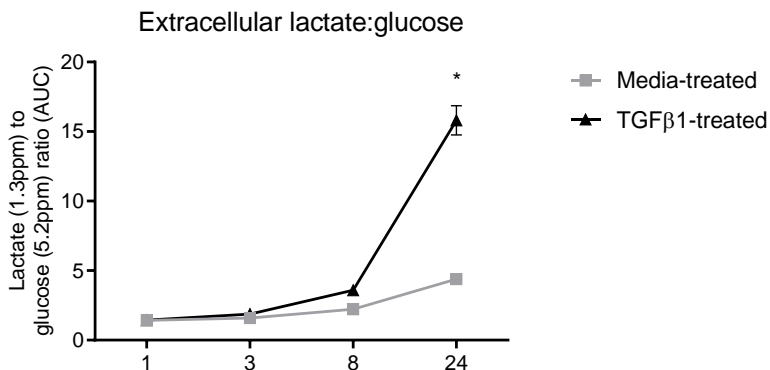
Figure 3-7. Effect of TGFβ1-stimulation on glycolytic flux.

Primary human lung fibroblasts were grown in serum-free conditions for 24 hours prior to stimulation with TGFβ1 (1ng/ml) or media control. Cell supernatants were then collected at the time points indicated and run on a 500MHz NMR spectrometer. Data shown represent the ratio between the AUC of the 1.3ppm (lactate) and 5.2 ppm (glucose) peaks after standardization to the 0ppm TSP peak (mean ± SEM, n=3 replicates). Difference between groups is evaluated with two-way ANOVA with Tukey correction for multiple comparisons. *p<0.05.

Overall, these results suggest that TGFβ1 stimulation increases the rate of glycolysis in pHLFs, with significant changes noted by 24 hours after TGFβ1 stimulation.

3.4. Effect of TGFβ1 stimulation on glucose uptake

In order to determine whether the increase in glucose uptake upon TGFβ1 stimulation is maintained once the cells have differentiated into myofibroblasts, the rate of glucose uptake was also compared between pHLFs exposed to 24 hours of media or of TGFβ1.

After 24 hours of media or TGFβ1 stimulation, uptake of radioactive 2-deoxy-D-glucose (5mM, containing 0.625μCi/ml [^{3}H]-2-deoxy- D-glucose) was measured over a period of 5 min. There was a 4-fold increase in [^{3}H]-2DG uptake in TGFβ1-stimulated cells relative to media-treated cells, suggesting that differentiated myofibroblasts maintain an increased rate of glucose uptake compared to undifferentiated fibroblasts (Figure 3-8).

Figure 3-8. Effect of TGFβ1-stimulation on glucose uptake.

Primary human lung fibroblasts were grown in serum-free conditions for 24 hours prior to stimulation with TGFβ1 (1ng/ml) or media control. Then, [^{3}H]-2DG was added and glucose uptake was assessed by determining the incorporated radioactivity over 5 minutes by liquid scintillation counting. Data shown represent the fold change in glucose uptake relative to media-treated cells (mean, n=3 replicates). Difference between groups is evaluated with unpaired t-test. *p<0.05.

3.5. Effect of TGFβ1 stimulation on glucose transporter gene expression and protein levels

Having shown an increase in glucose uptake and glycolytic flux during the process of TGFβ1-induced fibroblast differentiation, the next set of experiments was aimed at determining whether these metabolic changes were accompanied by increased expression of the glucose transporters type 1 and 3 (GLUT1 and GLUT3) known to be expressed in the lungs (see Introduction).

Figure 3-9 demonstrates that the mRNA levels of the *SLC2A1* gene which encodes the GLUT1 protein were increased significantly upon TGFβ1 stimulation when compared to media control at the 24-hour and 32-hour time points.
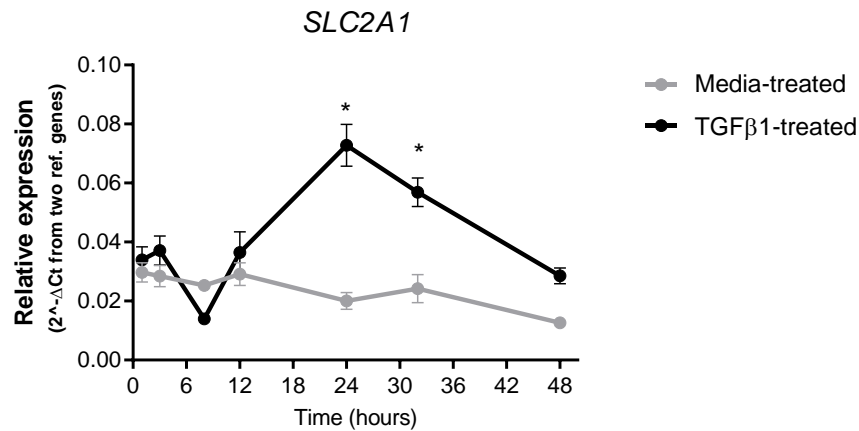
Figure 3-9. Effect of TGFβ1 on *SLC2A1* mRNA levels.
Primary human lung fibroblasts were grown in serum-free conditions for 24 hours prior to stimulation with TGFβ1 (1ng/ml) or media control. RNA was isolated at specified time points. Data shown represent the mRNA levels of *SLC2A1* relative to the geometric mean of *ATP5B* and *β2M* housekeeping genes (mean ± SEM, n=3 replicates). Difference between groups is evaluated with two-way ANOVA with Tukey correction for multiple comparisons. *p<0.05.

These effects were also noted at the protein levels, where TGFβ1 stimulation led to an increase in protein levels of GLUT1, most marked at the 24-hour and 32-hour time points (Figure 3-10). These findings were confirmed by immunoblotting of GLUT1 at the 24-hour time point using multiple replicates (Figure 3-11).
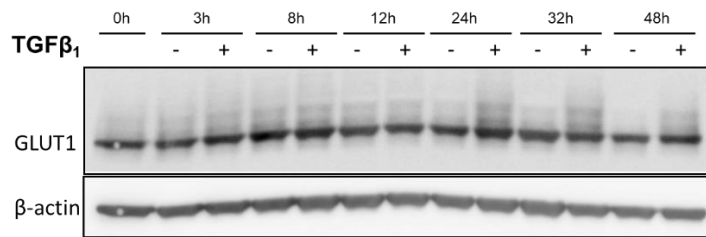
Figure 3-10. Effect of TGFβ1 on GLUT1 protein level over time.

Primary human lung fibroblasts were grown in serum-free conditions for 24 hours prior to stimulation with TGFβ1 (1ng/ml) or media control. Cells were lysed at the specified time points and immunoblotting was performed with anti-GLUT1 and β-actin antibodies.
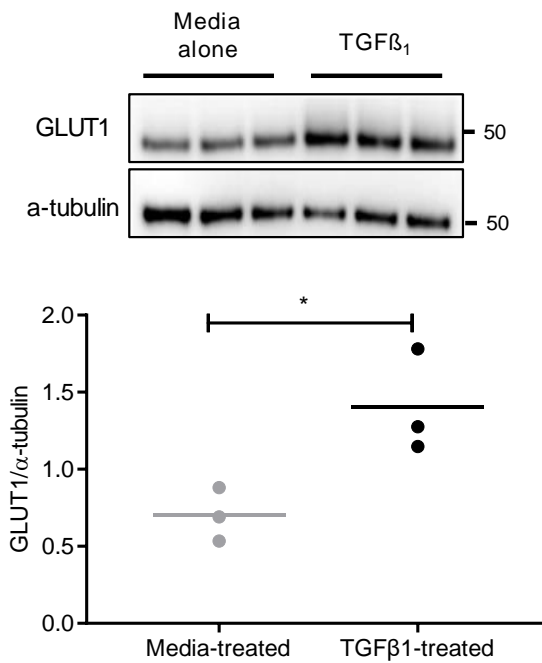
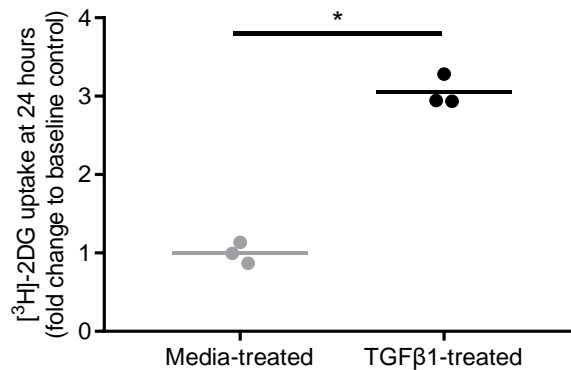**Figure 3-11. Effect of TGFβ1 on GLUT1 protein levels at 24 hours.**

Primary human lung fibroblasts were grown in serum-free conditions for 24 hours prior to stimulation with TGFβ1 (1ng/ml) or media control. Cells were lysed, followed by immunoblot with anti-GLUT1 and β-actin antibodies. Data shown represent the densitometry of GLUT1 relative to β-actin (mean, n=3 replicates). Difference between groups is evaluated with unpaired t-test *p<0.05.

In contrast, there were no significant differences in the mRNA levels of *GLUT3* at all time points

examined (Figure 3-12). Overall, these findings suggest that TGFβ1-stimulation is accompanied by increases in mRNA and protein levels of GLUT1 after 24 hours after stimulation.
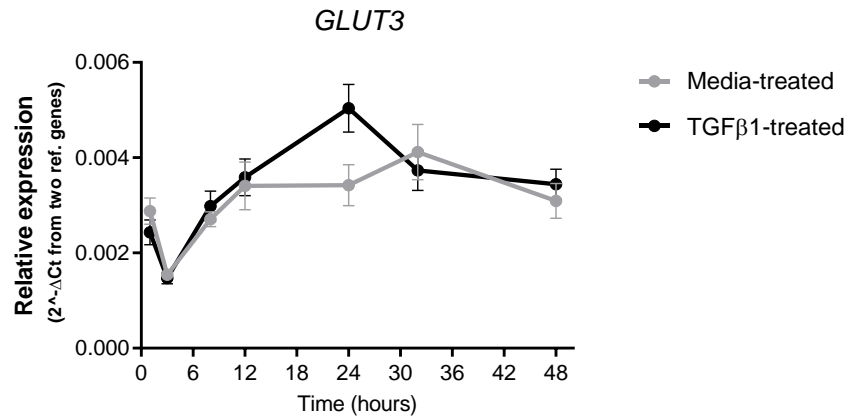
Figure 3-12. Effect of TGFβ1 on *GLUT3* mRNA levels.

Primary human lung fibroblasts were grown in serum-free conditions for 24 hours prior to stimulation with TGFβ1 (1ng/ml) or media control. RNA was isolated at specified time points. Data shown represent the mRNA levels of *GLUT3* relative to the geometric mean of *ATP5B* and *β2M* housekeeping genes (mean ± SEM, n=3 replicates). Difference between groups was evaluated with two-way ANOVA with Tukey correction for multiple comparisons. At each time point, there was no statistical difference between groups.

3.6. Effect of TGFβ1 stimulation on the expression of key glycolytic enzymes

Since the key regulatory glycolytic steps include (i) hexokinase, (ii) phosphofructokinase, and (iii) pyruvate kinase (see Introduction 1.5.1), the mRNA levels of the enzymes HK2, PFKFB3, PKM1 and PKM2 were also examined upon TGFβ1 stimulation. As extracellular lactate levels were found to be largely increased over time upon TGFβ1 stimulation, the mRNA levels of *LDHA* were also examined. HK2 catalyses the first rate-limiting step in glycolysis, while PFKFB3 catalyses the conversion of fructose-6-phosphate to fructose-2,6,-bisphosphate which is an allosteric activator of the glycolytic enzyme, phosphofructokinase-1 (PFK1) and a potent stimulator of glycolysis. Furthermore, *PKM1*, *PKM2* and *LDHA* encode the last 2 enzymes in the glycolytic pathway (pyruvate kinase and lactate dehydrogenase, respectively).

TGFβ1 stimulation led to a significant increase in the mRNA levels of *HKII* at 8 and 48 hours, of *PFKFB3* at 3 and 32 hours, and of *LDHA* at 8, 12 24 and 32 hours (Figure 3-13).
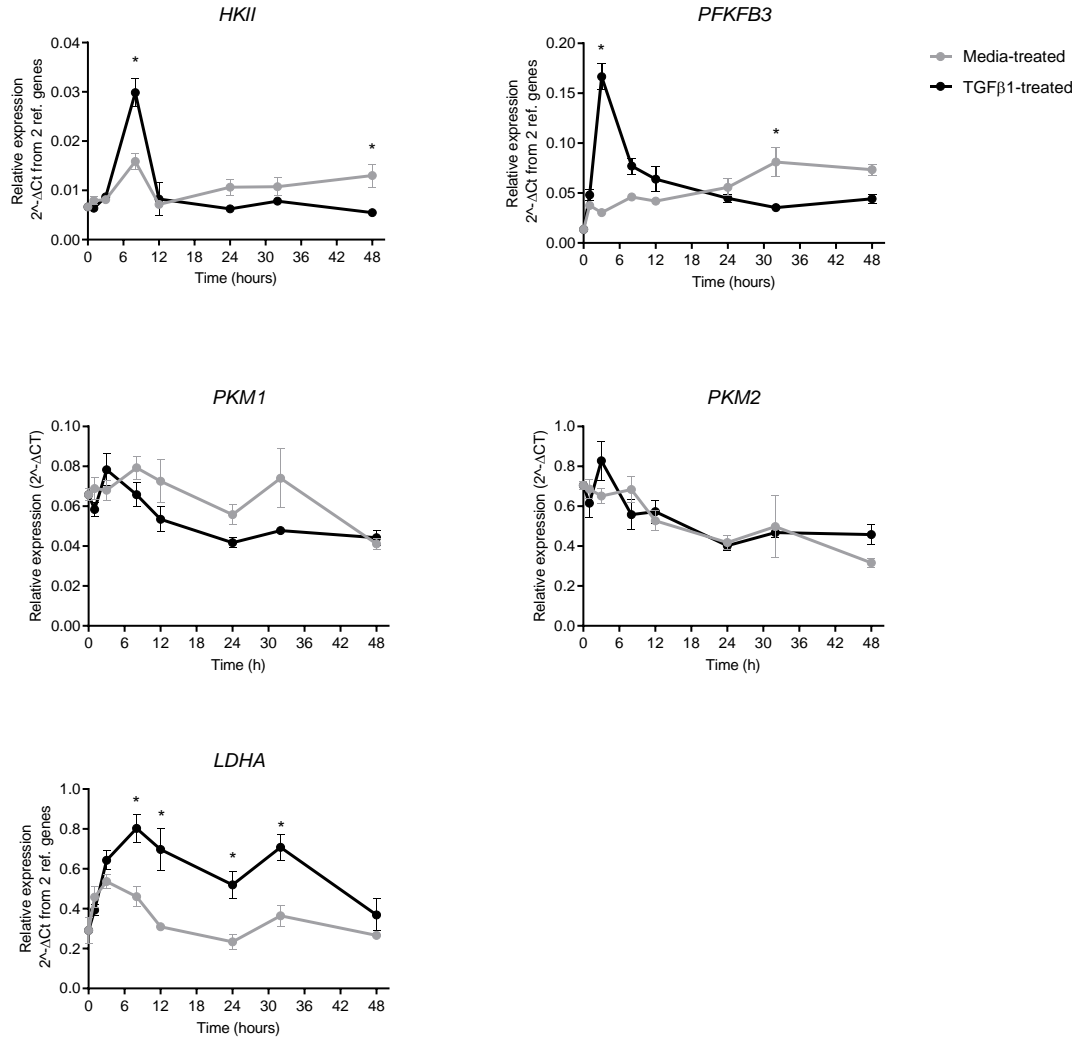
Figure 3-13. Effect of TGFβ1 on glycolytic genes expression.

Primary human lung fibroblasts were grown in serum-free conditions for 24 hours prior to stimulation with TGFβ1 (1ng/ml) or media control. RNA was isolated at specified time points. Data shown represent the mRNA levels of the genes mentioned relative to the geometric mean of *ATP5B* and *β2M* housekeeping genes (mean ± SEM, n=3 replicates). Difference between groups was evaluated with two-way ANOVA with Tukey correction for multiple comparisons. $*p < 0.05$.

These findings so far suggest that TGFβ1 stimulation leads to an increase in the expression of key rate-limiting glycolytic enzymes at various time points, with early increases in *PFKFB3* mRNA levels, followed by increases in *HK2* and *LDHA* levels. These findings occurred alongside an increase in glycolytic flux and glucose uptake during the process of fibroblast to myofibroblast differentiation.

63

In order to further delineate the metabolic changes that occur during this process, the following experiments sought to determine whether these metabolic changes induced by TGFβ1 stimulation represent aerobic glycolysis. To do so, the effects of TGFβ1 stimulation on mitochondrial respiration needed first to be examined.

3.7. Effect of TGFβ1 stimulation on oxygen consumption and extracellular acidification rates

The next set of experiments required the use of the Seahorse XFe96 Analyzer, a platform that measures the oxygen consumption rate (OCR) and extracellular acidification rate (ECAR) of live adherent cells in a 96-well plate format. The OCR and ECAR are considered key indicators of mitochondrial respiration and glycolysis, respectively.

Although very appealing, effective use of the Seahorse XFe96 Analyzer proved to be quite challenging and required many months to build an appropriate protocol for our primary cells. This prolonged work, summarized below, required optimizing many variables such as cell density, cell passage and culture conditions.

3.7.1. Protocol optimization

The Seahorse XF96e Analyzer measures OCR and ECAR on 96-well plates that have been coated with adherent cells. A schematic diagram representative of my initial protocol is shown below.
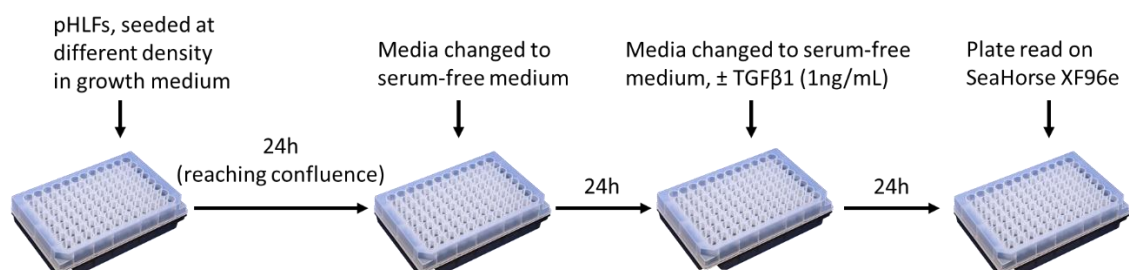
Figure 3-14. Schematic diagram of the early cell culture methods for the SeaHorse XF96e assay.
These methods were performed to obtain the data obtained in Figure 3-15, Figure 3-16 and Figure 3-17. Full experimental details can be found in the Methods 2.9 section of this thesis. pHLFs: Primary human lung fibroblasts.

Although initial results were encouraging, it quickly became evident that these experiments provided data that were very poorly reproducible. Close inspection of the wells, unfortunately,

revealed significant cell detachment upon TGFβ1-stimulation, as shown in Figure 3-15.

Media-treated

TGFβ1-treated
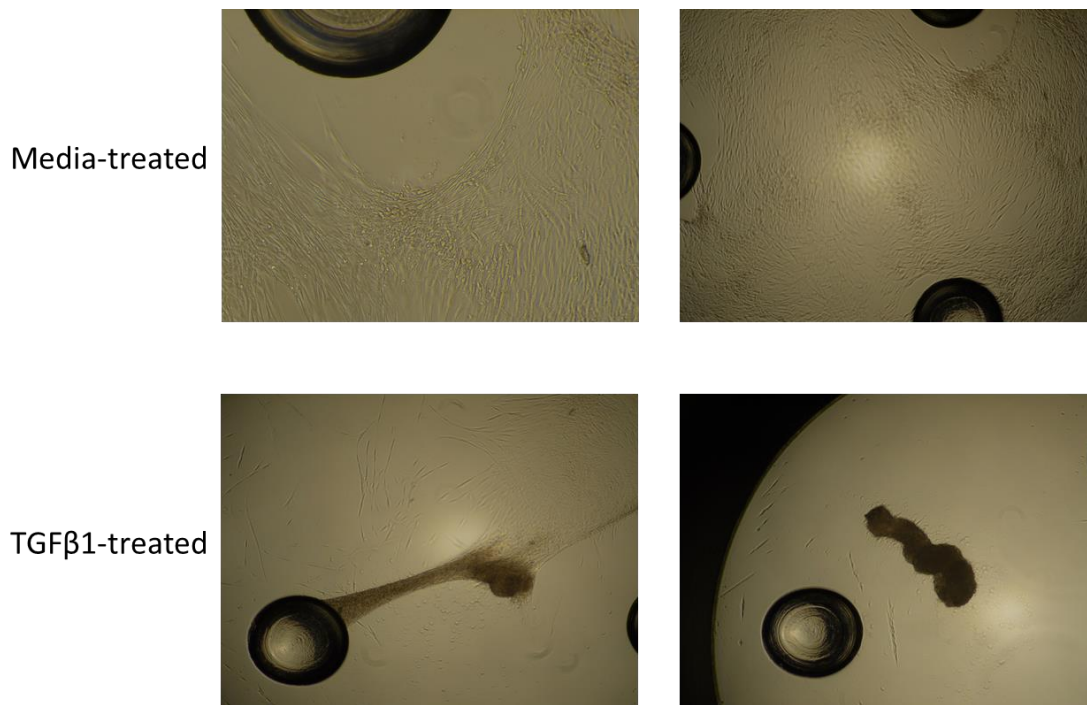
Figure 3-15. Representative images of early results with the SeaHorse XF96e Analyzer.
Representative images of primary human lung fibroblasts attached to the culture plate in the presence, or absence, of TGFβ1 stimulation. TGFβ1 caused impressive cell clumping and detachment from the wells, which led to the need for major protocol optimization.

To remedy this situation, I first attempted to coat the plates with adhering compounds, as described in previous publications. This included polyethyleneimine (PEI) polymer coating (Gerencser et al., 2009), Cell-Tak coating (Kang et al., 2014)and rat-tail collagen coating (Wang et al., 2015). Unfortunately, coating cells with PEI or Cell-Tak made no difference in cell detachment (Figure 3-16). Although rat-tail collagen coating did prevent cell detachment, it removed any TGFβ1 signal on OCR, which I hypothesized was due to the direct impact collagen may have on fibroblast differentiation (Asano et al., 2017) (Figure 3-17).

PEI-coated

CellTak-coated
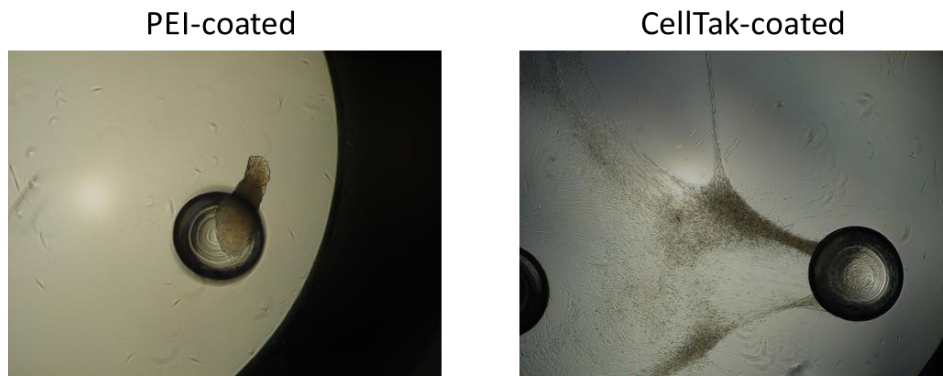
Figure 3-16. Representative images obtained with well-coating with the SeaHorse XF96e Analyzer.
Representative images of primary human lung fibroblasts attached to the culture plate in the presence of TGFβ1 stimulation under different cell-coating conditions. PEI: polyethyleneimine.

Collagen-coated
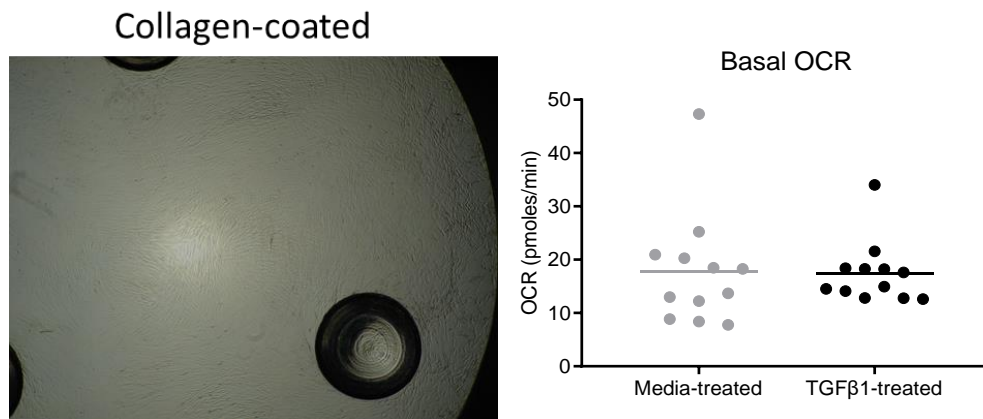
Basal OCR

Figure 3-17. Representative image and basal OCR obtained after rat-tail collagen well coating.
Representative image of primary human lung fibroblasts attached to the culture plate in the presence of TGFβ1 stimulation in rat-tail collagen plate coating. Basal oxygen consumption rate (OCR) was measured and found to be similar 24 hours after media or TGFβ1-treatment (mean, n=12 replicates). Difference between groups is evaluated with unpaired t-test.

For this reason and upon discussion with supervisors and collaborators, I chose to abandon cell coating and adjust the protocol such that low-density fibroblasts, at a low passage, would be seeded for a longer time prior to TGFβ1-stimulation, with the idea that it would provide enough time for the cells to lay down their own matrix. After multiple attempts at optimization, I finally decided to seed 10^4 cells/well for 72 hours at passage 4 (P4). This optimized protocol proved highly reproducible and led to a very effective method for measuring both OCR and ECAR in pHLFs (Figure 3-18).
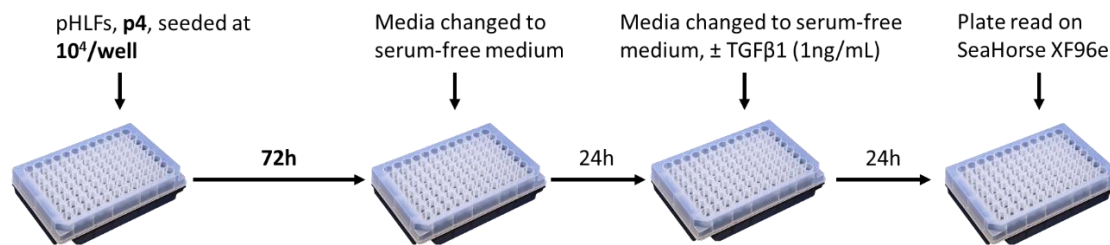
Figure 3-18. Schematic diagram of the optimized cell culture methods for the SeaHorse XF96e assay. Schematic diagram of the cell culture methods performed to obtain the data obtained for all the following assays performed with the SeaHorse XF96e. Full experimental details can be found in the Methods 2.9 section of this thesis. Note the change in cell density, cell passage and time of incubation relative to the previous experimental methods found in Figure 3-14.

3.7.2. Effect of TGFβ1 stimulation on oxygen consumption rate

First, the effect of TGFβ1 on OCR over time was evaluated. TGFβ1 caused an increase in OCR as early as 3 hours after stimulation and rising to its peak at 24 hours. Furthermore, this effect was not attributable to differences in cell count at these different time points (Figure 3-19).
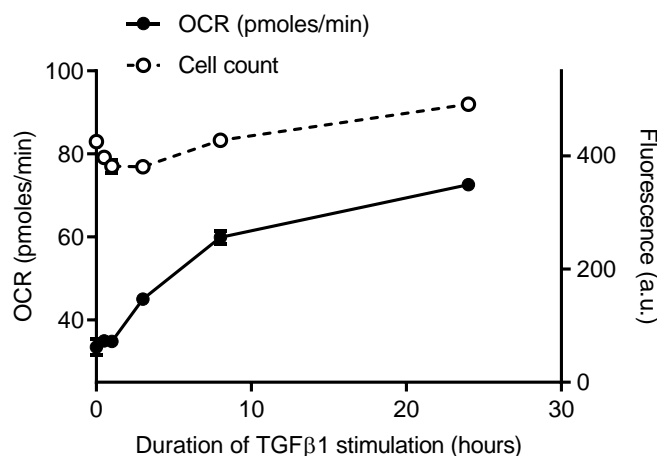
Figure 3-19. Effect of TGFβ1 on the oxygen consumption rate (OCR) of pHLFs over time.

OCR was measured in primary human lung fibroblasts exposed to TGFβ1 (1ng/ml) stimulation over a period of 24 hours. Following the experiment, cell count was measured using a fluorescence assay, as described in the Methods section (2.10). Data shown represent the OCR at each time point and corresponding cell count (mean ± SEM, n=6-12 replicates).

Next, a mitochondrial stress test was performed 24 hours after media-control or TGFβ1 stimulation, as described in detail in the Methods section of this thesis (2.9). Briefly, the mitochondrial stress test is a standard assay designed by Agilent© that assesses multiple parameters of mitochondrial function.

After measuring the oxygen consumption rate of cells at baseline ('*basal OCR*'), the first compound injected into the cell culture medium is oligomycin, an inhibitor of ATP synthase (complex V). When this enzyme is inhibited, mitochondrial ATP production is blocked, and the oxygen consumption measured corresponds to the small leak of protons that occurs along the mitochondrial membrane ('*proton leak*'). The difference in OCR prior to, and after oligomycin injection can be therefore viewed at the OCR contributing to the production of ATP ('*ATP production*'). The second injection is of FCCP (Carbonyl cyanide-p-trifluoromethoxyphenylhydrazone), a powerful uncoupler that disrupts the mitochondrial membrane potential. This leads to a rapid loss of the proton gradient across the mitochondrial membrane, such that oxygen consumption then massively increases to the '*maximal OCR*' in order to reinstitute that gradient. The third and last injection are of antimycin A (complex III inhibitor) and rotenone (complex I inhibitor). These compounds shut down mitochondrial respiration, such that the measured oxygen consumption rate is related to non-

mitochondrial respiration (eg. cellular oxygen consumption occurring outside mitochondria).

Primary human lung fibroblasts were subjected to the mitochondrial stress test 24 hours after media-control or TGFβ1-stimulation (Figure 3-20). Repeated independent experiments (n=6) confirmed that at that time point, TGFβ1 stimulation caused a significant increase in basal, ATP-related and maximal respiration (Figure 3-21).
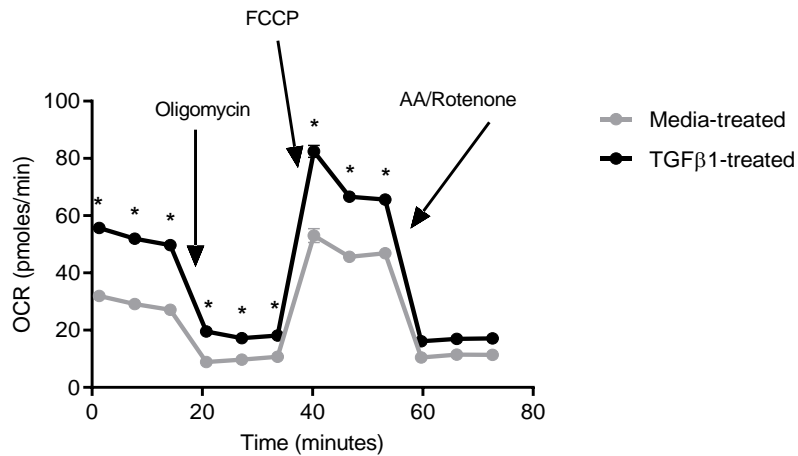
Figure 3-20. Mitochondrial stress test showing the OCR of pHLFs exposed to TGFβ1 for 24 hours.
Oxygen consumption rate (OCR) was measured in primary human lung fibroblasts after media-control or TGFβ1 (1ng/ml) stimulation for 24 hours. Data shown represent the measured OCR at each time point of the assay, (mean ± SEM, n=44-46 replicates). Difference between groups was evaluated by two-way ANOVA with Tukey correction for multiple comparisons. $*p<0.05$. (FCCP: Carbonyl cyanide-p-trifluoromethoxyphenylhydrazone; AA: Antimycin A)
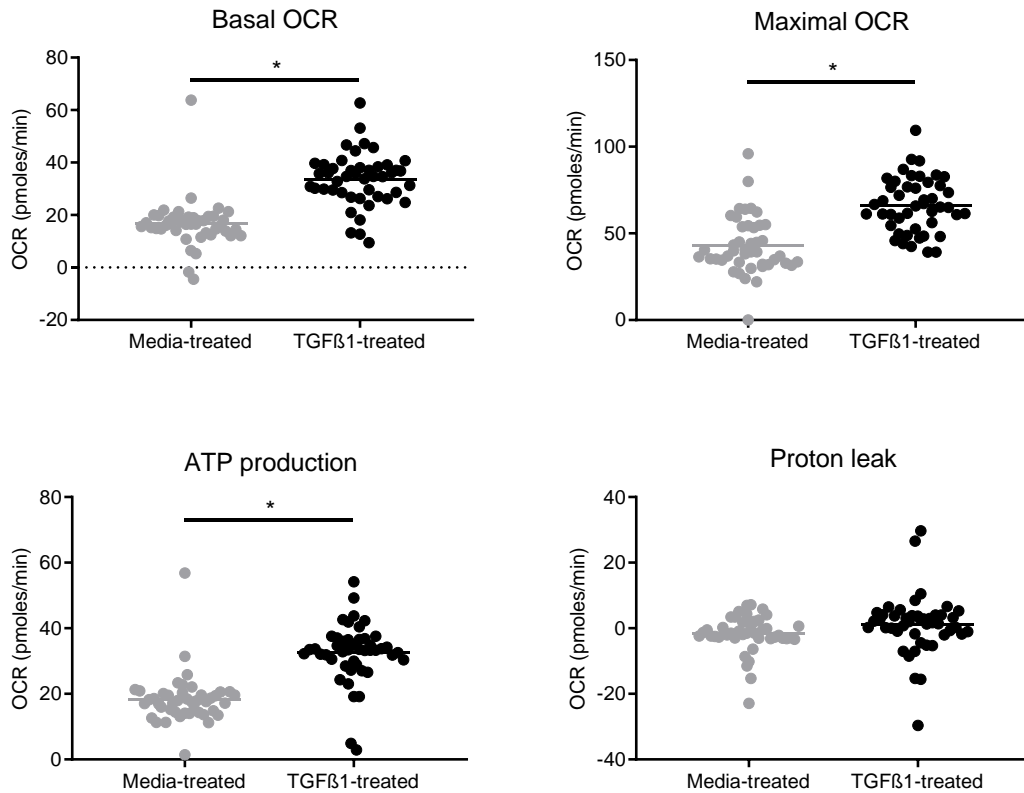
Figure 3-21. Effect of TGFβ1 on various measures of mitochondrial respiration after 24 hours of stimulation. The data obtained from Figure 3-20 allowed for the calculation of basal, maximal, ATP production-related and proton-leak-related OCR (mean, n=44-46 replicates). Difference between groups is evaluated with unpaired t-test. *p<0.05.

3.7.3. Effect of TGFβ1 stimulation on extracellular acidification rate

In addition to measuring the effect of TGFβ1 on mitochondrial respiration, the SeaHorse XF96e Analyzer also allows the measurement of the extracellular acidification rate (ECAR), a surrogate marker of glycolysis. Upon 24 hours of TGFβ1 stimulation, ECAR was found to be significantly elevated, as shown in Figure 3-22.
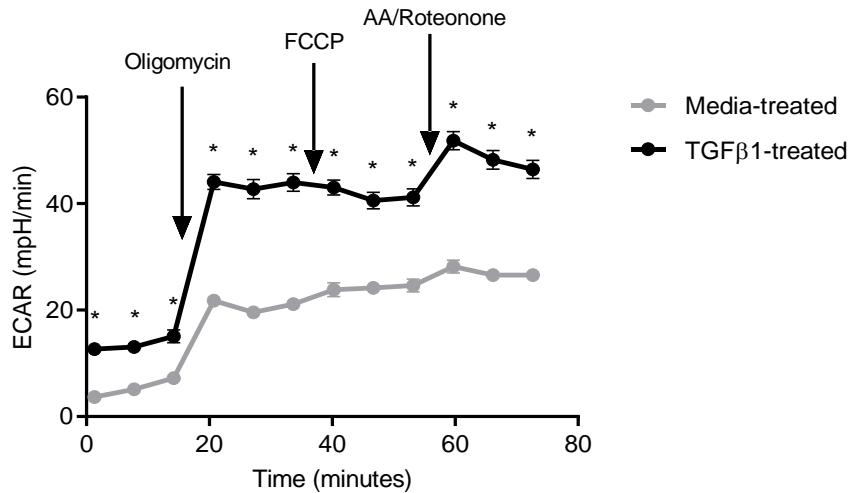
Figure 3-22. Mitochondrial stress test showing the ECAR of pHLFs exposed to TGFβ1 for 24 hours.

Extracellular acidification rate (ECAR) was measured in primary human lung fibroblasts after media-control or TGFβ1 (1ng/ml) stimulation for 24 hours, using the mitochondrial stress test protocol. Data shown represent the measured ECAR at each time point of the assay, (mean ± SEM, n=44-46 replicates). Difference between groups was evaluated by two-way ANOVA with Tukey correction for multiple comparisons. *$p<0.05$ (AA: Antimycin A)

3.7.4. Effect of TGFβ1 stimulation on aerobic glycolysis

Next, the effect of TGFβ1 on the OCR and ECAR of pHLFs was compared in order to determine the effect of TGFβ1 on the overall metabolic profile of fibroblasts. As depicted in the phenogram below (Figure 3-24), fibroblasts exposed to TGFβ1 for 24 hours increase both their OCR and their ECAR.
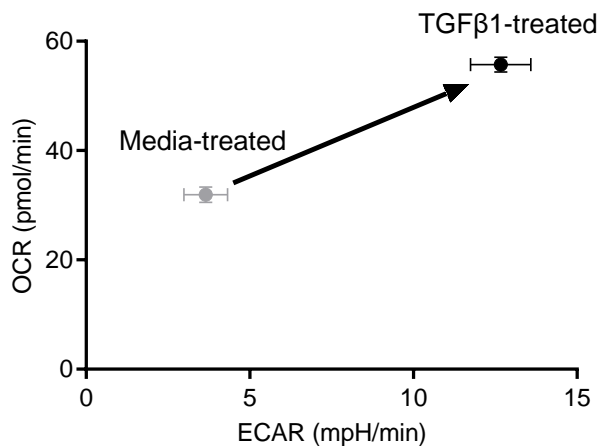
Figure 3-23. Effect of 24-hour stimulation of TGFβ1 on the changes in OCR and ECAR.

Oxygen consumption rate (OCR) and extracellular acidification rate (ECAR) were measured in primary human lung fibroblasts after media-control or TGFβ1 (1ng/ml) stimulation for 24 hours. Data shown represent the changes in OCR and ECAR between the groups (mean ± SEM, n=44-46 replicates).

When the effect of TGFβ1-stimulation was compared on each of those metabolic parameters, ECAR was found to increase by 3.47 ± 0.25 -fold and the OCR by 1.75 ± 0.04 -fold (Figure 3-24). Overall, these findings suggest that TGFβ1 stimulation causes significant changes in both mitochondrial respiration and glycolysis, with more marked changes in glycolysis, a feature that could be suggestive of aerobic glycolysis.
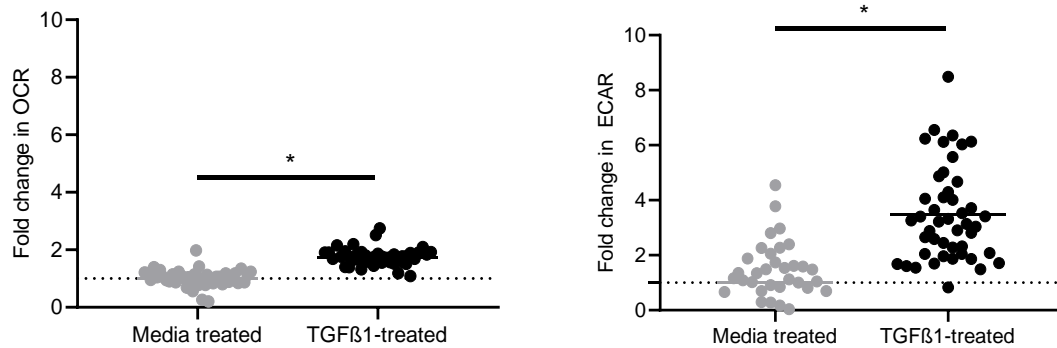
Figure 3-24. Effect of 24-hour stimulation of TGFβ1 on the changes in OCR and ECAR.

Oxygen consumption rate (OCR) and extracellular acidification rate (ECAR) were measured in primary human lung fibroblasts after media-control or TGFβ1 (1ng/ml) stimulation for 24 hours. Data shown represent the fold changes in OCR and ECAR for each group relative to media treatment (mean, n=44-46 replicates). Difference between groups is evaluated with unpaired t-test. *p<0.05.

Overall, these *in vitro* findings suggest that TGFβ1 stimulation causes a significant increase in glucose uptake and glycolytic flux, as well as an increase in oxygen consumption rate. The magnitude of the effect being stronger on glycolysis than on mitochondrial respiration suggests the presence of aerobic glycolysis. The next set of experiments was aimed at examining the molecular mechanisms that could underlie these metabolic changes.

3.8. PI3K-AKT-mTOR axis on glucose metabolism

The PI3K-AKT-mTOR signalling pathway is upregulated in many malignancies and is considered the key driver for the promotion of metabolic reprogramming in cancer (see Introduction). Furthermore, this axis has recently been implicated in the process of TGFβ1-induced fibroblast differentiation. The following experiments were therefore aimed at examining whether this axis mediates the TGFβ1-induced changes in glucose metabolism.

3.8.1. PI3K-AKT-mTOR axis on glycolytic flux

To examine the role of the PI3K-AKT-mTOR axis on TGFβ1-induced changes in glucose metabolism, pHLFs were incubated with the potent and selective ATP-competitive PI3 kinase inhibitor, GSK2864918A, the allosteric AKT inhibitor, MK2206, or with the specific ATP-competitive dual-complex inhibitor of mTOR, AZD8055. Details about the specificity and potency of each of these compounds can be found in the Methods 2.4 section of this thesis. The concentration used for each compound for the next set of experiments was at 1µM, based on previous work from our laboratory establishing significant inhibitory activity for its kinase without cell toxicity (Woodcock et al., 2019).

First, addition of AZD8055, a highly-potent ATP-competitive mTOR kinase inhibitor, significantly prevented the TGFβ1-induced reduction in extracellular glucose, increase in extracellular lactate and increase in glycolytic flux at 24 hours, as measured by the lactate: glucose peaks by 1H-NMR (Figure 3-25). However, pre-treatment of cells with either the pan PI3K-inhibitor, GSK2864918A, or with the AKT inhibitor, MK2206, had no effect on extracellular glucose or glycolytic flux. Surprisingly, there was a mild but significant increase in extracellular lactate upon TGFβ1-stimulation with GSK2864918A or with MK22016.
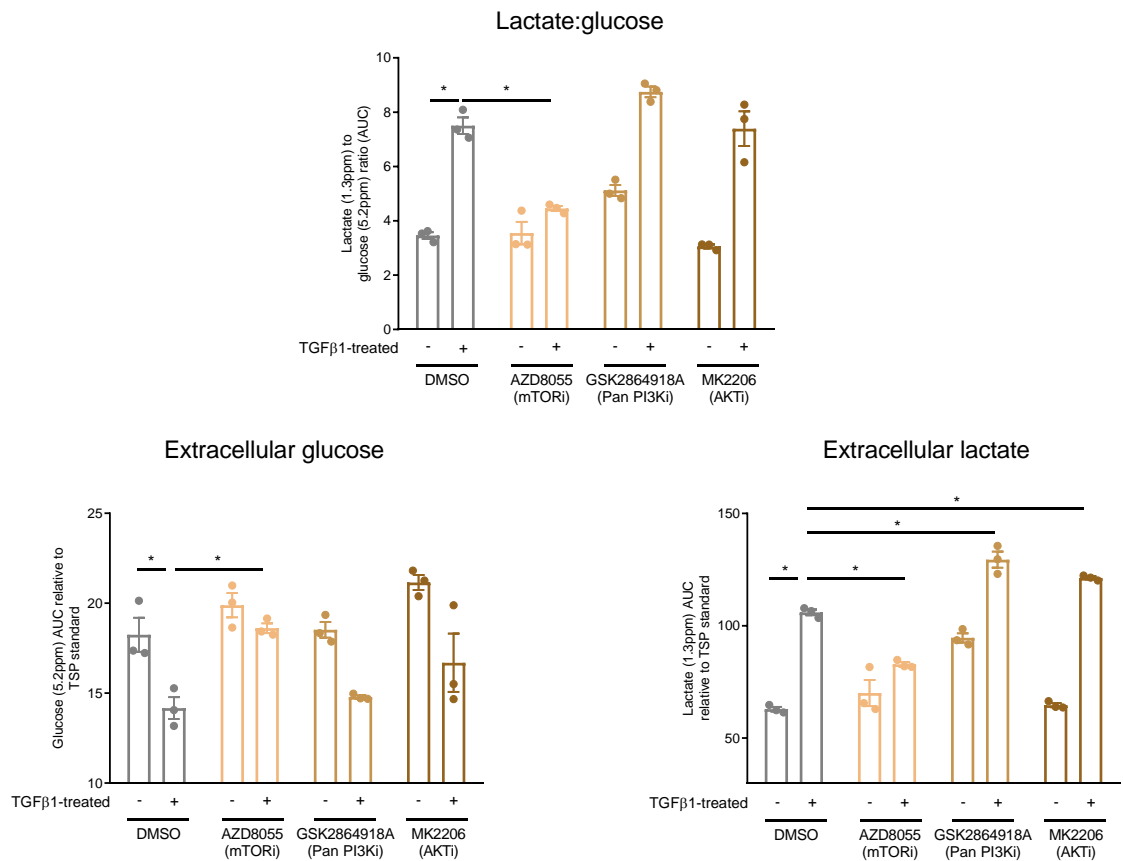
Figure 3-25. Effect of kinase inhibitors on TGFβ1-stimulation changes in extracellular levels of glucose and lactate.

Primary human lung fibroblasts were grown in serum-free conditions for 24 hours prior to pre-incubation with the compounds described. One hour later, samples were spiked with media control or TGFβ1 (1ng/ml) for 24 hours. Cell supernatants were then collected and run on a 500MHz NMR spectrometer. Data shown represent the AUC of the 1.3ppm and 5.2ppm peaks (representing respectively the lactate and glucose peaks) after standardization to the 0ppm TSP peak (mean, n=3 replicates). Difference between groups is evaluated with two-way ANOVA with Tukey correction for multiple comparisons. $*p<0.05$.

3.8.2. PI3K-AKT-mTOR axis on ECAR

The effects of the PI3K-AKT-mTOR axis on extracellular acidification rate were also assessed. ECAR was attenuated upon administration of the mTOR inhibitor AZD8055 but not of the PI3K inhibitor

GSK2864918A or with the AKT inhibitor MK2206 (Figure 3-26).
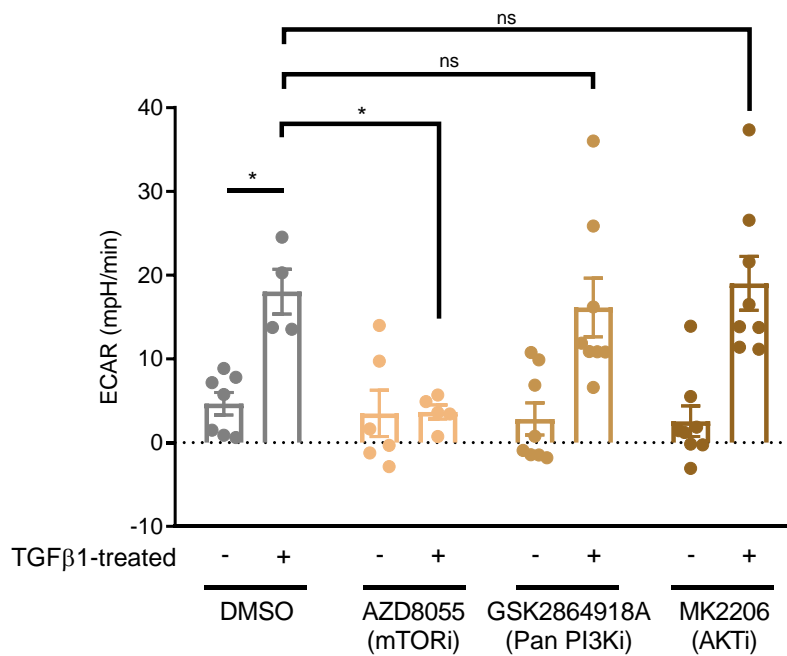
Figure 3-26. Effect of inhibitors of the PI3K-AKT-mTOR axis on ECAR.

Extracellular acidification rate (ECAR) was measured in primary human lung fibroblasts after media-control or TGFβ1 (1ng/ml) stimulation for 24 hours, using the mitochondrial stress test protocol, in the presence (or absence) of the mTOR inhibitor AZD8055 (1uM), pan-PI3K inhibitor GSK2864918A (1uM) or the AKT inhibitor MK2206 (1uM) and. Data shown represent the ECAR level (mean, n=4-8 replicates). Difference between groups is evaluated with two-way ANOVA with Tukey correction for multiple comparisons. *p<0.05

3.8.3. PI3K-AKT-mTOR axis on mitochondrial respiration

The role of the PI3K-AKT-mTOR axis was also examined on the TGFβ1-induced changes in oxygen consumption rate (OCR). Similar to our findings on glycolytic flux and ECAR, we found that only mTOR inhibition, but not PI3K or AKT inhibition, prevented the TGFβ1-induced changes in basal, maximal and ATP production-related OCR (Figure 3-27, Figure 3-28).
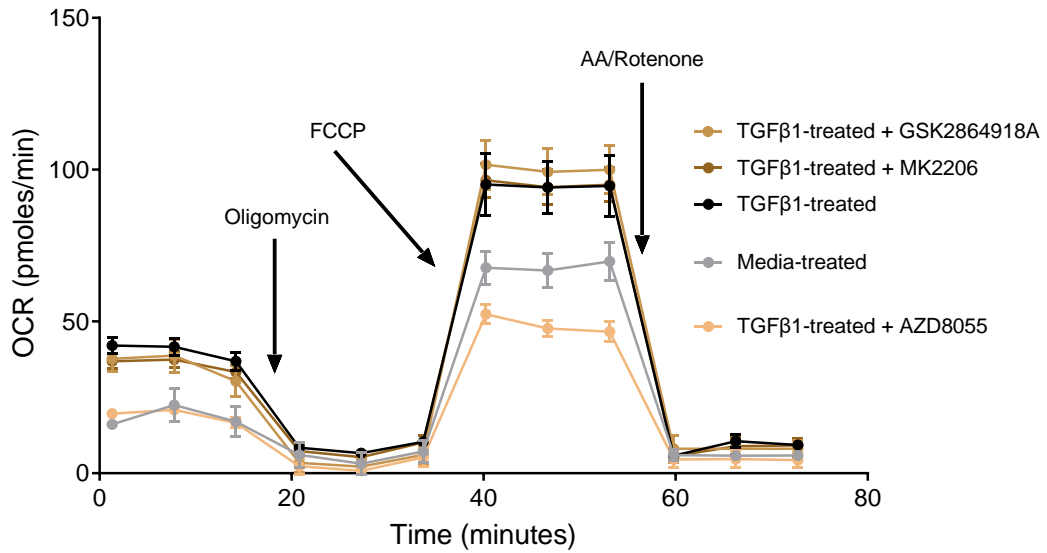
Figure 3-27. Effect of inhibitors of the PI3K-AKT-mTOR axis on the mitochondrial stress test.

Oxygen consumption rate (OCR) was measured in primary human lung fibroblasts after media-control or TGFβ1 (1ng/ml) stimulation for 24 hours, in the presence (or absence) of the pan-PI3K inhibitor GSK2864918A (1uM), the AKT inhibitor MK2206 (1uM) and the mTOR inhibitor AZD8055 (1uM). Data shown represent the measured OCR at each time point of the assay (mean ± SEM, n=4-8 replicates). (FCCP: Carbonyl cyanide-p-trifluoromethoxyphenylhydrazone; AA: Antimycin A).
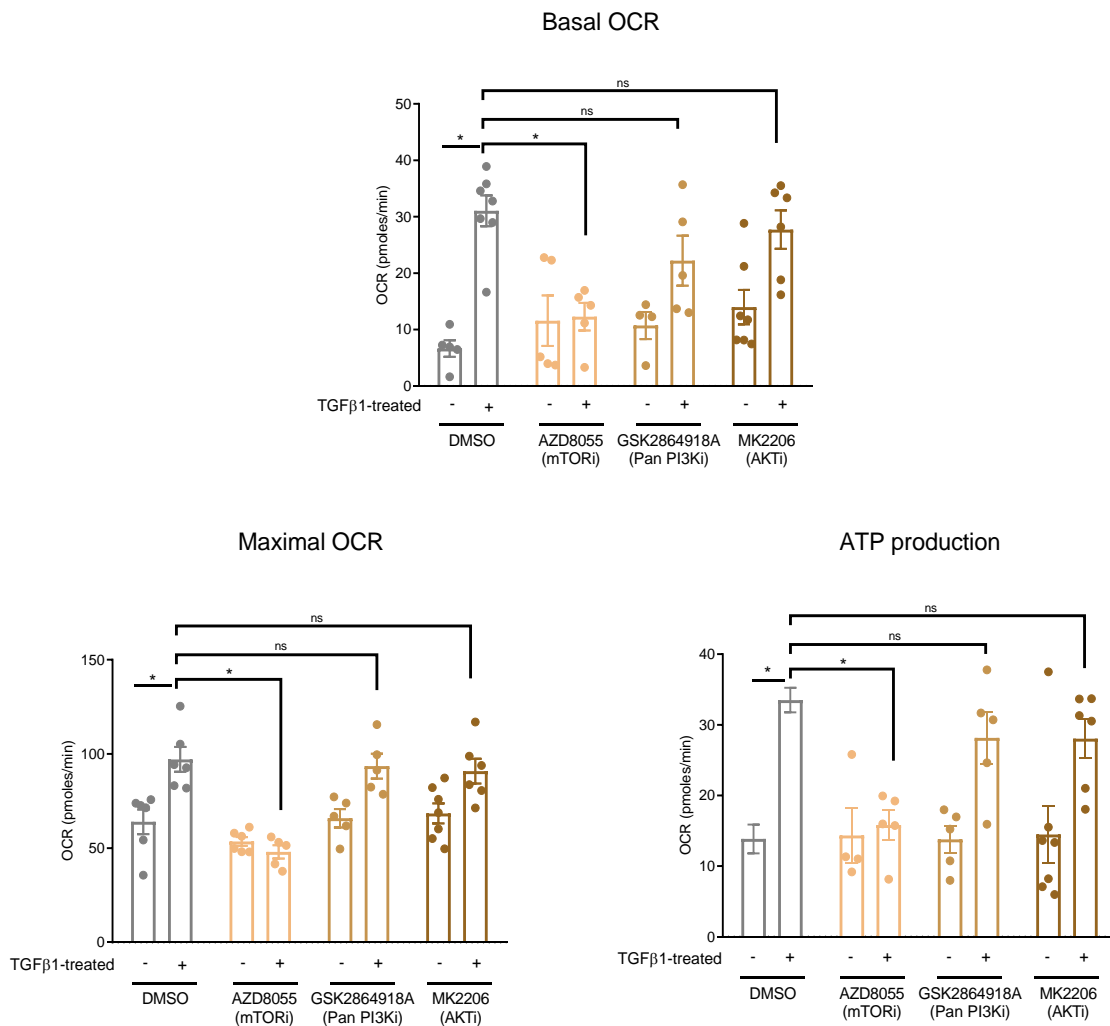
Figure 3-28. Effect of inhibitors of the PI3K-AKT-mTOR axis on various measures of mitochondrial respiration.

The data obtained from Figure 3-27 allowed for the calculation of basal, maximal, ATP production-related in each subgroup (mean, n=4-8 replicates). Difference between groups is evaluated with two-way ANOVA with Tukey correction for multiple comparisons. *p<0.05

In order to estimate the potency of each of the compounds on OCR, a concentration-response curve of basal OCR was performed following a mitochondrial stress test assay for each of the compound. There was a concentration-dependent reduction in TGFβ1-induced basal OCR with AZD8055 (mTORi), with an IC50 of 148nM (Figure 3-29). Furthermore, we saw no drop in cell count with concentrations up to 10^{-5}M.
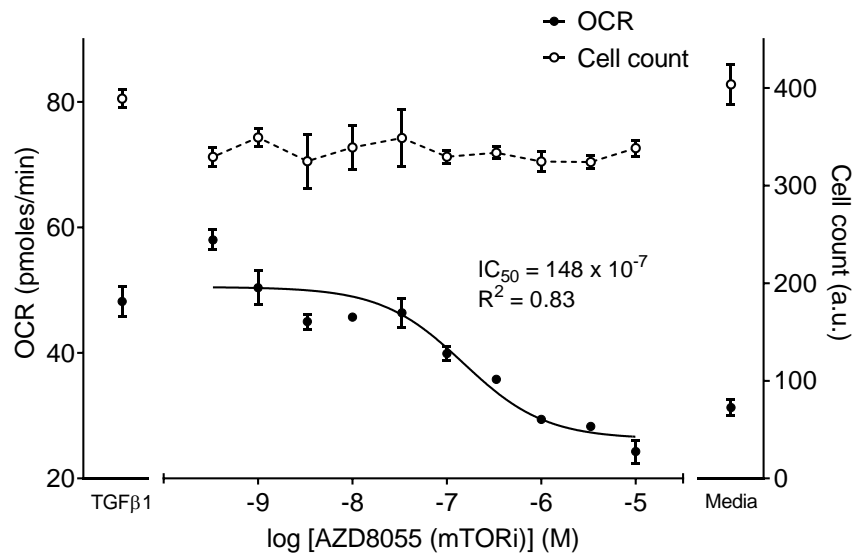
Figure 3-29. Concentration-dependent effect of AZD8055 on TGFβ1-stimulation changes in oxygen consumption rate (OCR).

Primary human lung fibroblasts were grown in serum-free conditions for 24 hours prior to pre-incubation with AZD8055 at the concentrations described. One hour later, samples were spiked with media control or TGFβ1 (1ng/ml) for 24 hours. A mitochondrial stress test was then performed, and the basal OCR was then measured using the Seahorse XF96e platform. Data shown represent basal OCR (mean ± SEM, n=4-8 replicates). Three-parameter concentration-inhibition curve linear fit was performed to obtain the IC_{50}.

In contrast, the pan-PI3K inhibitor GSK2864918A had no effect on TGFβ1-induced OCR, despite concentrations ranging up to 10^{-5}M, while the AKT inhibitor MK2206 led to an inhibition of TGFβ1-induced OCR only at the top concentration of 10^{-5}M (Figure 3-30), a concentration well above what is required to inhibit AKT signalling (Woodcock et al., 2019). Again, neither compound was associated with a significant drop in cell count during the assay (Figure 3-30).
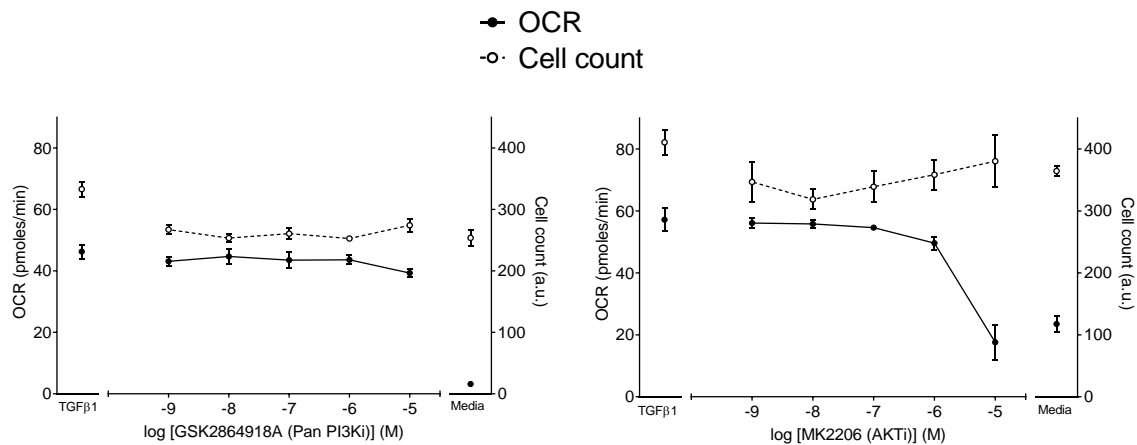
Figure 3-30. Concentration-dependent effect of the pan PI3K inhibitor GSK2864918A or with the AKT inhibitor MK2206 on TGFβ1-stimulation changes in oxygen consumption rate (OCR).

Primary human lung fibroblasts were grown in serum-free conditions for 24 hours prior to pre-incubation with GSK2864918A or MK2206 at the concentrations described. One hour later, samples were spiked with media control or TGFβ1 (1ng/ml) for 24 hours. A mitochondrial stress test was then performed, and the basal OCR was then measured using the Seahorse XF96e platform. Data shown represent basal OCR (mean ± SEM, n=4-8 replicates).

During the course of this work, I was given access to 2 other pharmacological inhibitors made available thanks to my work in a GSK facility. These included the mTOR inhibitor GSK3080501 and the AKT inhibitor GSK2119126. Again, there was a concentration-dependent reduction in basal OCR with the mTOR inhibitor GSK3080501 but not with the AKT inhibitor GSK2119126 (Figure 3-31).
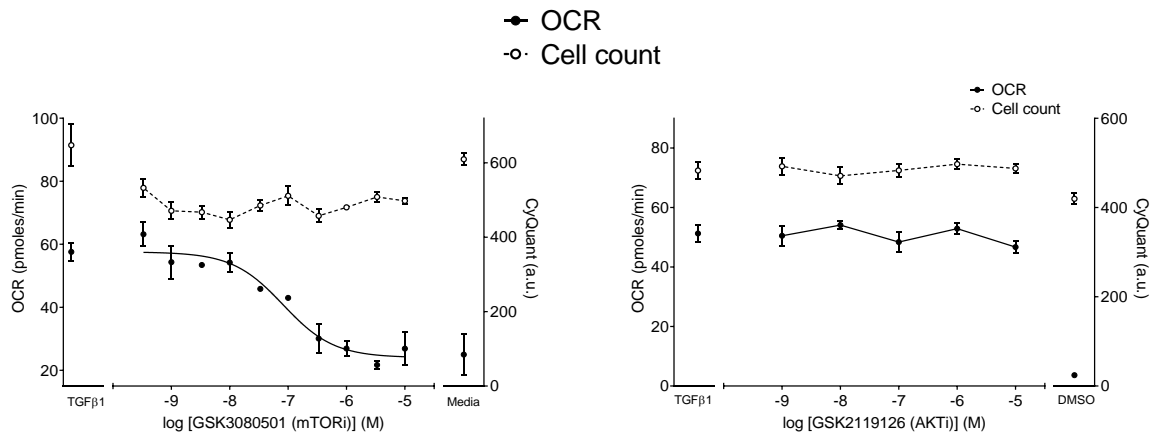
Figure 3-31. Concentration-dependent effect of the mTOR inhibitor GSK3080501 and with the AKT inhibitor

80

GSK2119126 on TGFβ1-stimulation changes in oxygen consumption rate (OCR).
Primary human lung fibroblasts were grown in serum-free conditions for 24 hours prior to pre-incubation with the mTOR inhibitor GSK3080501 or the AKT inhibitor GSK2119126 at the concentrations described. One hour later, samples were spiked with media control or TGFβ1 (1ng/ml) for 24 hours. A mitochondrial stress test was then performed, and the basal OCR was then measured using the Seahorse XF96e platform. Data shown represent basal OCR (mean ± SEM, n=4-8 replicates).

Overall, these findings suggest that TGFβ1-induced increase in mitochondrial respiration is regulated by mTOR, independently of PI3K and AKT.

3.8.4. PI3K-AKT-mTOR axis on aerobic glycolysis

Aerobic glycolysis was examined by comparing the changes in OCR and in ECAR that occur upon TGFβ1 stimulation in the presence, or absence, of the inhibitors of the PI3K-AKT-mTOR axis.

Consistent with earlier findings, the mTOR inhibitors AZD8055 and GSK3080501 attenuated the TGFβ1-induced increase in both OCR and ECAR (Figure 3-32), while the PI3K or AKT inhibitors had no impact on TGFβ1-induced OCR and ECAR (Figure 3-33).

Interestingly, one can appreciate that TGFβ1 still preferentially increases ECAR over OCR in the presence of PI3K or AKT inhibitors, suggesting they have no impact on TGFβ1-induced aerobic glycolysis.

.
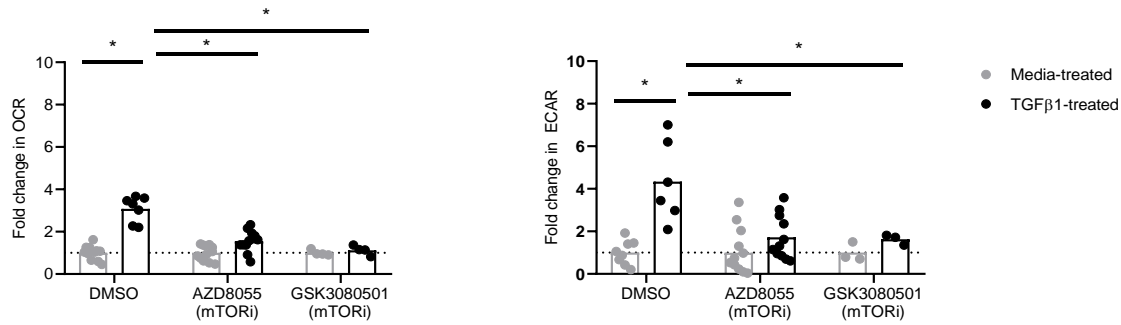
Figure 3-32. Effect of the mTOR inhibitors AZD8055 and GSK3080501 on the TGFβ1-induced changes in OCR and ECAR.

Oxygen consumption rate (OCR) and extracellular acidification rate (ECAR) were measured in primary human lung fibroblasts after media-control or TGFβ1 (1ng/ml) stimulation for 24 hours, in the presence (or absence) of the mTOR inhibitors AZD8055 and GSK3080501. Data shown represent the fold change in OCR and ECAR with TGFβ1 stimulation relative to media treatment with DMSO (mean, n=4-12 replicates). Difference between groups is evaluated with two-way ANOVA with Tukey correction for multiple comparisons. *p<0.05.
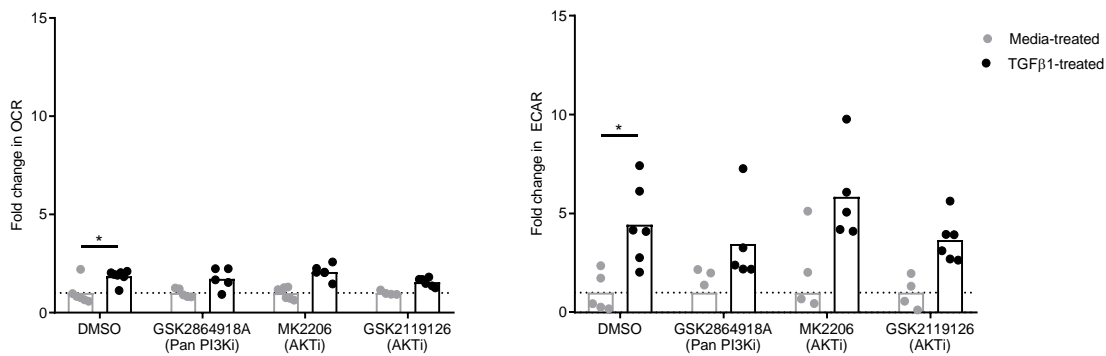

Figure 3-33. Effect of the PI3K inhibitor GSK2864918A and the AKT inhibitors MK2206 and GSK2110126 on the TGFβ1-induced changes in OCR and ECAR.

Oxygen consumption rate (OCR) and extracellular acidification rate (ECAR) were measured in primary human lung fibroblasts after media-control or TGFβ1 (1ng/ml) stimulation for 24 hours, in the presence (or absence) of the pan-PI3K inhibitor GSK2864918A (1uM) and the AKT inhibitor MK2206 (1uM) and GSK2119126 (1uM). Data shown represent the fold change in OCR and ECAR with TGFβ1 stimulation (mean, n=4-8 replicates). Difference between groups is evaluated with two-way ANOVA with Tukey correction for multiple comparisons. *p<0.05.

82

Overall, the metabolic phenotype of TGFβ1-stimulated fibroblasts can be represented using a phenogram, showing that mTOR regulates the metabolic changes upon TGFβ1 stimulation in a PI3K, AKT-independent manner (Figure 3-34).
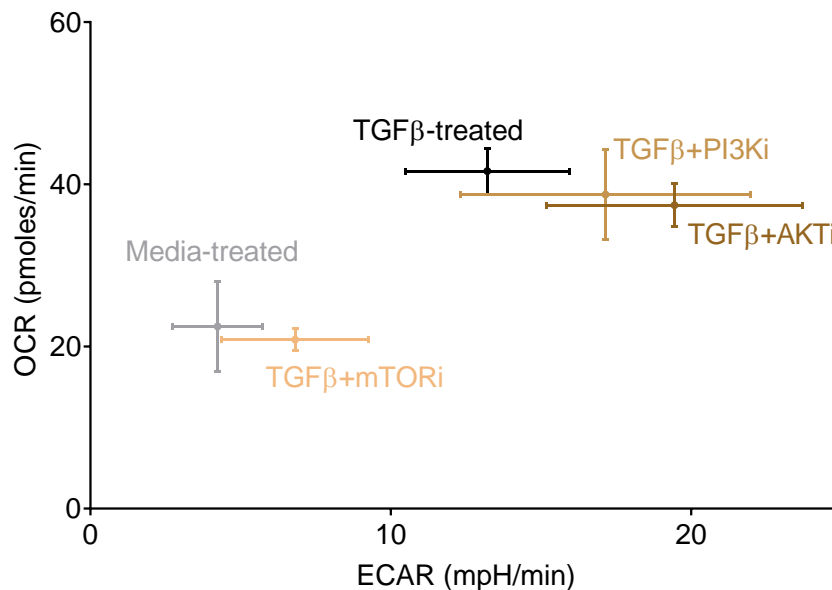
Figure 3-34. Phenogram representing the metabolic phenotype of TGFβ1-stimulated fibroblasts exposed to inhibitors of the PI3K-AKT-mTOR axis

Primary human lung fibroblasts were grown in serum-free conditions for 24 hours prior to pre-incubation with the compounds described. One hour later, samples were spiked with media control or TGFβ1 (1ng/ml) for 24 hours. OCR and ECAR were then measured using the Seahorse XF96e platform. Data shown represent the changes in OCR and ECAR between the groups (mean ± SEM, n=5-7 replicates).

3.8.5. Effect of AZD8055 on GLUT1 expression

Having established that mTOR regulates the TGFβ1-induced enhancement in glycolytic flux in a PI3K, AKT-independent manner, the final objective was to examine whether mTOR was also implicated in the TGFβ1-induced changes in GLUT1 mRNA and protein.

As depicted in Figure 3-35, SLC2A1 mRNA levels were significantly reduced when cells were pre-

treated with the mTOR inhibitor AZD8055 after 24 hours of TGFβ1 stimulation. Furthermore, treatment with AZD8055 also prevented the TGFβ1-induced increase in GLUT1 protein levels at 24 hours (Figure 3-36). These findings indicate that the effect of TGFβ1 on SLC2A1 and GLUT1 protein levels is mTOR dependent.
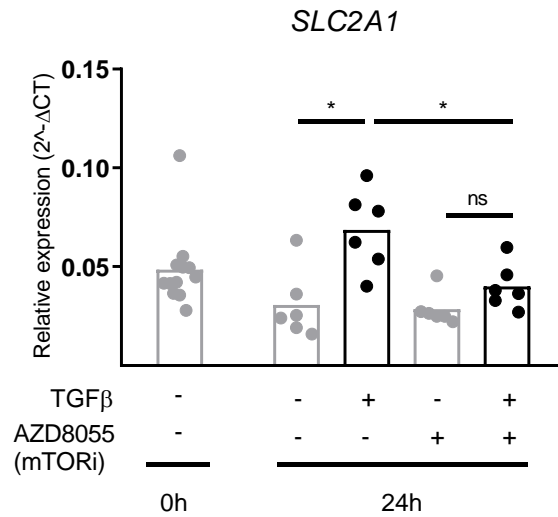
Figure 3-35. Effect of AZD8055 on TGFβ1-induced changes in *SLC2A1* mRNA levels.

Primary human lung fibroblasts were grown in serum-free conditions for 24 hours prior to pre-incubation with AZD8055 at 1uM. One hour later, samples were spiked with media control or TGFβ1 (1ng/ml) for 24 hours. RNA was then isolated at the specified time points. Data shown represent the mRNA levels of *SLC2A1* relative to the geometric mean of *ATP5B* and *β2M* housekeeping genes (mean, n=3 replicates). Difference between groups was evaluated with two-way ANOVA with Tukey correction for multiple comparisons. $*p < 0.05$.
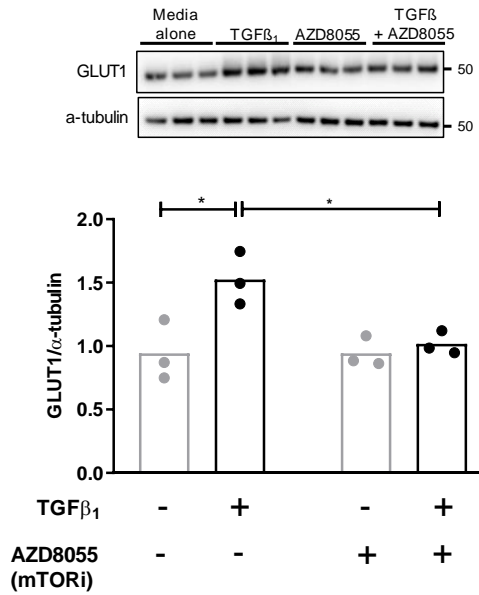
Figure 3-36. Effect of AZD8055 on TGFβ1-induced changes in GLUT1 protein levels.

Primary human lung fibroblasts were grown in serum-free conditions for 24 hours prior to pre-incubation with AZD8055 at 1uM. One hour later, samples were spiked with media control or TGFβ1 (1ng/ml) for 24 hours. Cells were lysed, followed by immunoblot with anti-GLUT1 and β-actin antibody. Data shown represent the densitometry of GLUT1/ β-actin (mean, n=3 replicates). Difference between groups is evaluated with 2-way ANOVA with Tukey correction for multiple comparisons. *p<0.05.

3.9. Glucose uptake in an experimental model of lung fibrosis

3.9.1. Pilot *in vivo* protocol

The first *in vivo* experiments assessed whether the process of lung fibrosis could be imaged in an experimental model of lung fibrosis. I chose to use the oropharyngeal bleomycin model, which is well established in the laboratory and commonly described in the literature. To that end, an initial pilot experiment was performed and involved the examination by ^{18}F-labeled fluoro-2-deoxyglucose-positron emission tomography-computed tomography ([18F]FDG-PET-CT) scanning of 4 mice aged 8-10 weeks, 21 days after oropharyngeal instillation of either bleomycin (1mg/kg, n=3) or normal saline (n=1) (Figure 3-37).
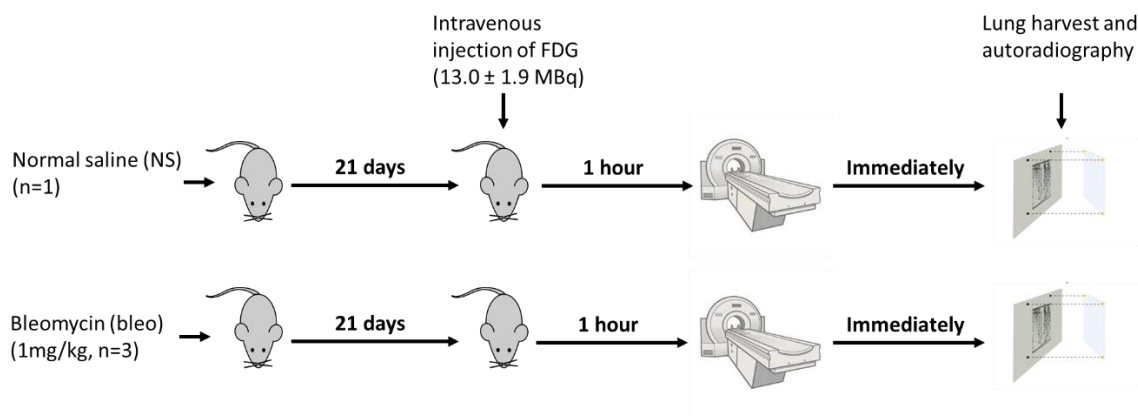
Figure 3-37. Schematic diagram of the pilot *in vivo* protocol of bleomycin-induced lung injury.
Schematic diagram of the initial *in vivo* experiment protocol performed to obtain the data obtained in Figure 3-39 and Figure 3-40. Full experimental details can be found in the 'Methods 2.11' section of this thesis.

As can be seen in Figure 3-38, the bulk of the PET signal emanated from the heart with minimal signal emanating from the lungs. On the CT images, one could appreciate little evidence for lung injury. PET-CT scanning was therefore deemed inadequate to qualitatively andéor quantitively correlate the levels of fibrosis and of [18F]FDG uptake in this mouse model.
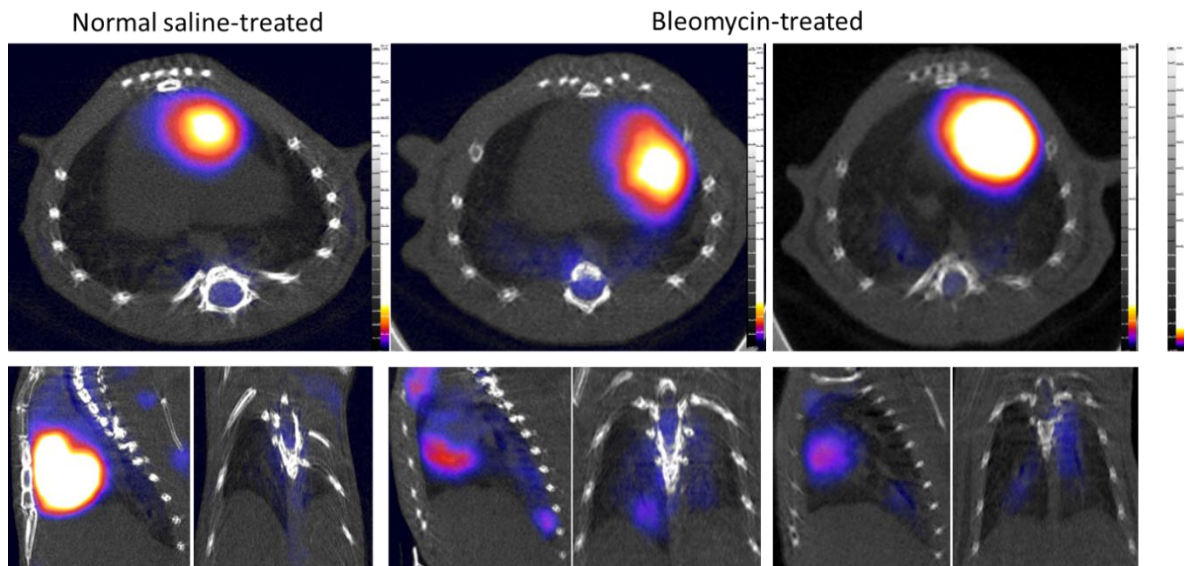
Figure 3-38 Representative [18F]FDG-PET-CT images of animals subjected to normal saline or bleomycin. Mice were oropharyngeally instilled with normal saline or bleomycin 21 days prior to [18F]FDG-PET-CT scanning, with the experimental protocol depicted in Figure 3-37. Representative axial, sagittal and coronal sections of the chest are shown.

While PET-CT scanning offered a poor image resolution of the organs, autoradiography provided a much better appreciation of the intensity of radioactivity representing [18F]FDG in the lungs. Sections of lungs were obtained immediately after the animals were subjected to the PET-CT protocol and submitted to autoradiography. In addition, adjacent lung sections were subjected to histology and stained with hematoxylin and eosin (H&E) (Figure 3-39). Unexpectedly, the extent of lung injury as assessed by histology in mice exposed to bleomycin was scant. However, radioactive signals were noticed in the autoradiography images but suspicion arose that the bulk of that signal emanated from blood vessels (Figure 3-39).
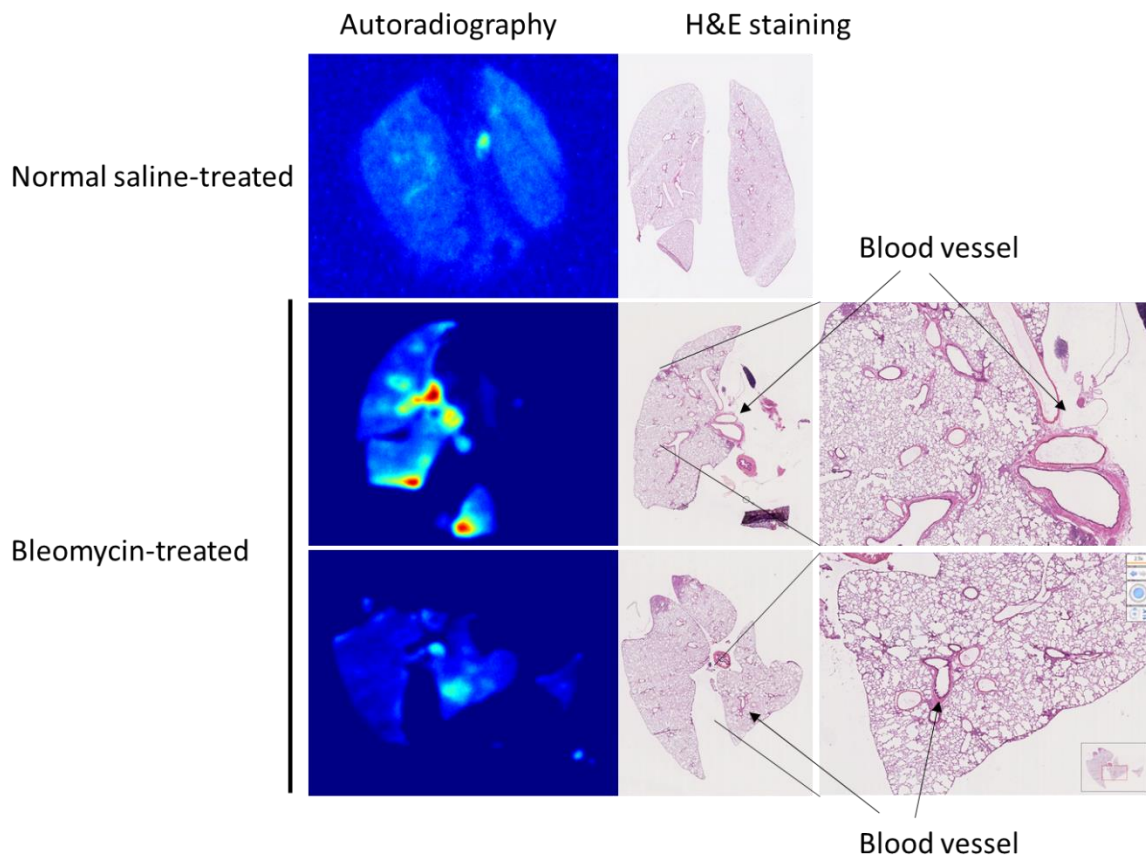
Figure 3-39. Representative images of lung sections from the pilot *in vivo* experiment.
Mice were oropharyngeally instilled with normal saline or bleomycin (1mg/kg) 21 days prior to sacrifice. Lungs were then sectioned and adjacent 5µm-thick lung slices were subjected to autoradiography and H&E staining. The autoradiography images have been pseudo-coloured to represent increased signal intensity from an original greyscale image for ease of visualization (red = high signal intensity, dark blue = low signal intensity).

3.9.2. Optimized *in vivo* protocol

Based on the results of this pilot experiment, I subsequently optimized the protocol by increasing the dose of bleomycin (from 1mg/kg to 2mg/kg) and increased the time between bleomycin instillation and animal sacrifice (from 21 days to 28 days). These changes were aimed at increasing the fibrotic response to bleomycin. In addition, another group of animals was added consisting of mice exposed to bleomycin in which the pulmonary circulation was flushed at the time of lung harvest by injecting normal saline (NS) through the right ventricle in order to eliminate the possible "vascular" contribution to the [^{18}F]FDG signal (bleo + flushed group) (Figure 3-40). Confirmation of

this successful flushing was obtained subjectively, by visualizing blanching of the lungs.
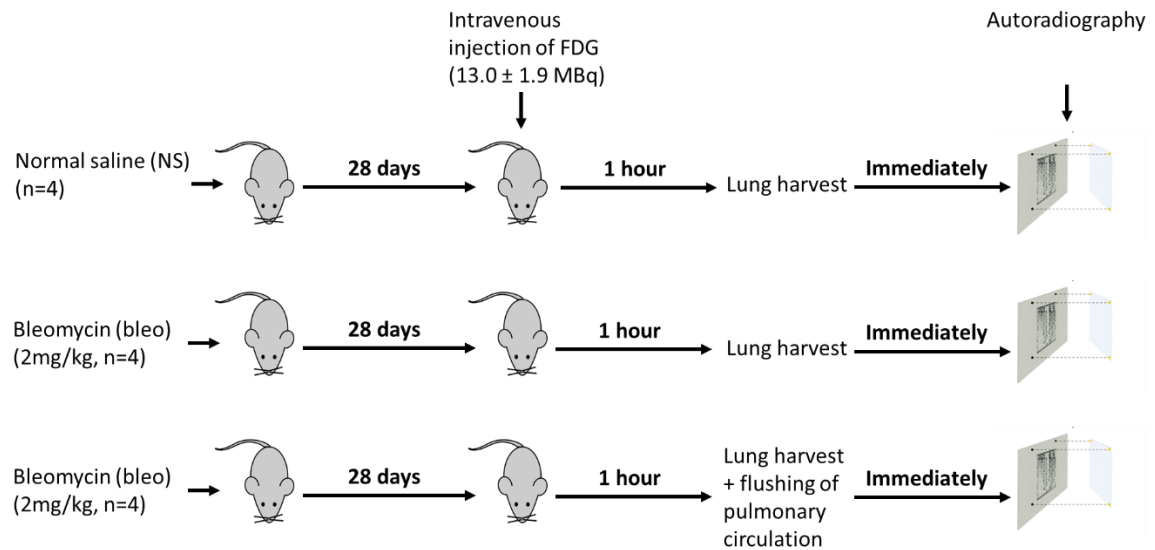
Figure 3-40. Schematic diagram of the optimized *in vivo* protocol of bleomycin-induced lung injury.
Schematic diagram of the optimized *in vivo* experiment protocol performed to obtain the data obtained in
Figure 3-41-Figure 3-45. Full experimental details can be found in the 'Methods' section of this thesis.

Using that optimized protocol, mice exposed to bleomycin (n=8) had their weight decrease to a nadir
at around 6 days after instillation, though every animal recovered their initial body weight by the
end of the experiment. No animal lost more than 20% of their initial body weight, a pre-specified
ethics requirement to allow animals to be monitored up to the point of sacrifice (Figure 3-41).
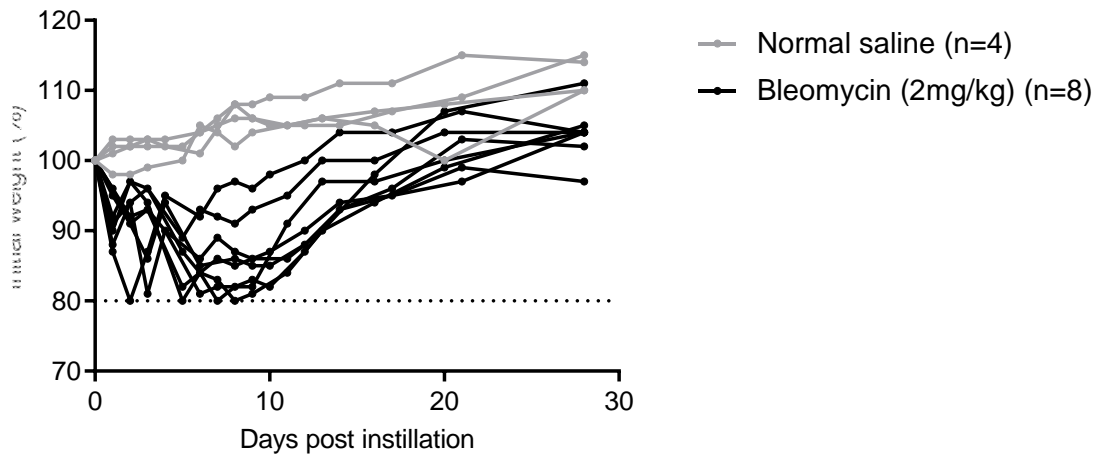
Figure 3-41. Animal weight following normal saline (NS) or bleomycin administration.

Mice were oropharyngeally instilled with normal saline or bleomycin (2mg/kg), as depicted in Figure 3-40. Data shown are the animal weights following NS or bleomycin instillation over time.

In normal-saline treated animals, lungs displayed normal healthy architecture as visualized by H&E staining of lung sections. In addition, low yet detectable ^{18}F activity in lungs from saline-treated mice was found by autoradiography (Figure 3-42).

Normal saline

| Autoradiography | H&E | H&E – higher magnification |
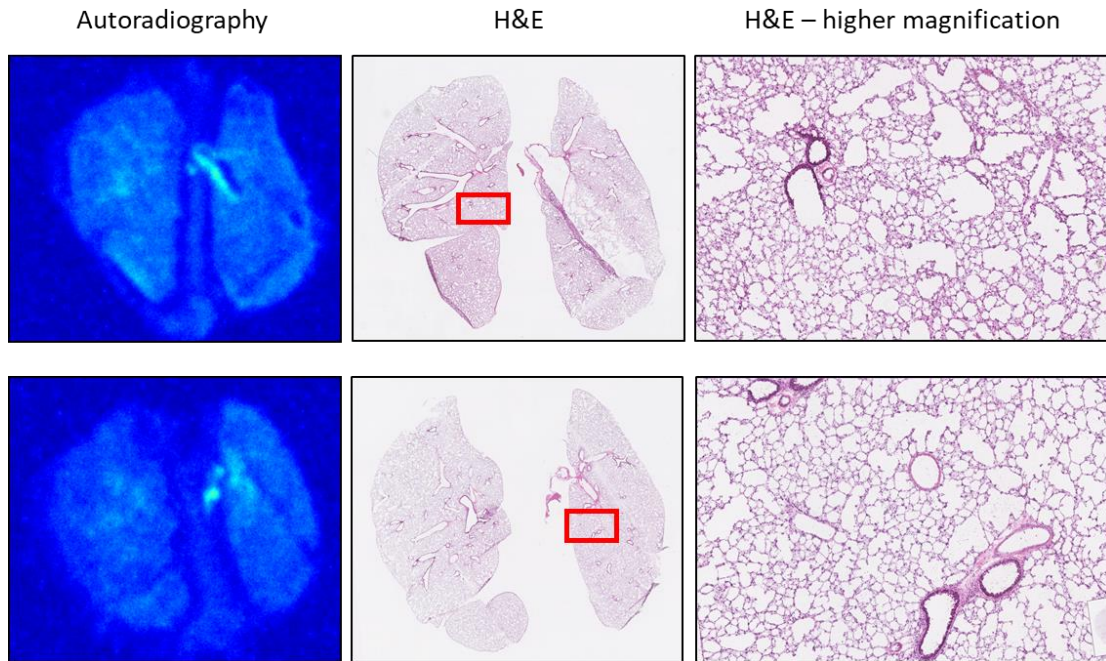
Figure 3-42. Representative images of lung sections of normal saline (NS)-treated animals.

Mice were oropharyngeally instilled with normal saline 28 days prior to sacrifice, as depicted in Figure 3-40. Lungs were then sectioned and adjacent 5μm-thick lung slices were subjected to autoradiography and H&E staining. The autoradiography images have been pseudo-coloured to represent increased signal intensity from an original greyscale image for ease of visualization (red = high signal intensity, dark blue = low signal intensity).

In comparison, bleomycin-challenged mouse lungs featured dense regions of subpleural and peri-bronchiolar fibrosis, with bronchiolization and extensive collagen deposition. By autoradiography, bleomycin-challenged lungs displayed increased ^{18}F activity in uninjured lung regions, with the most intense ^{18}F activity localised to regions of dense fibrosis, suggesting co-localisation of increased [^{18}F]FDG uptake with fibrotic lesions (Figure 3-43).
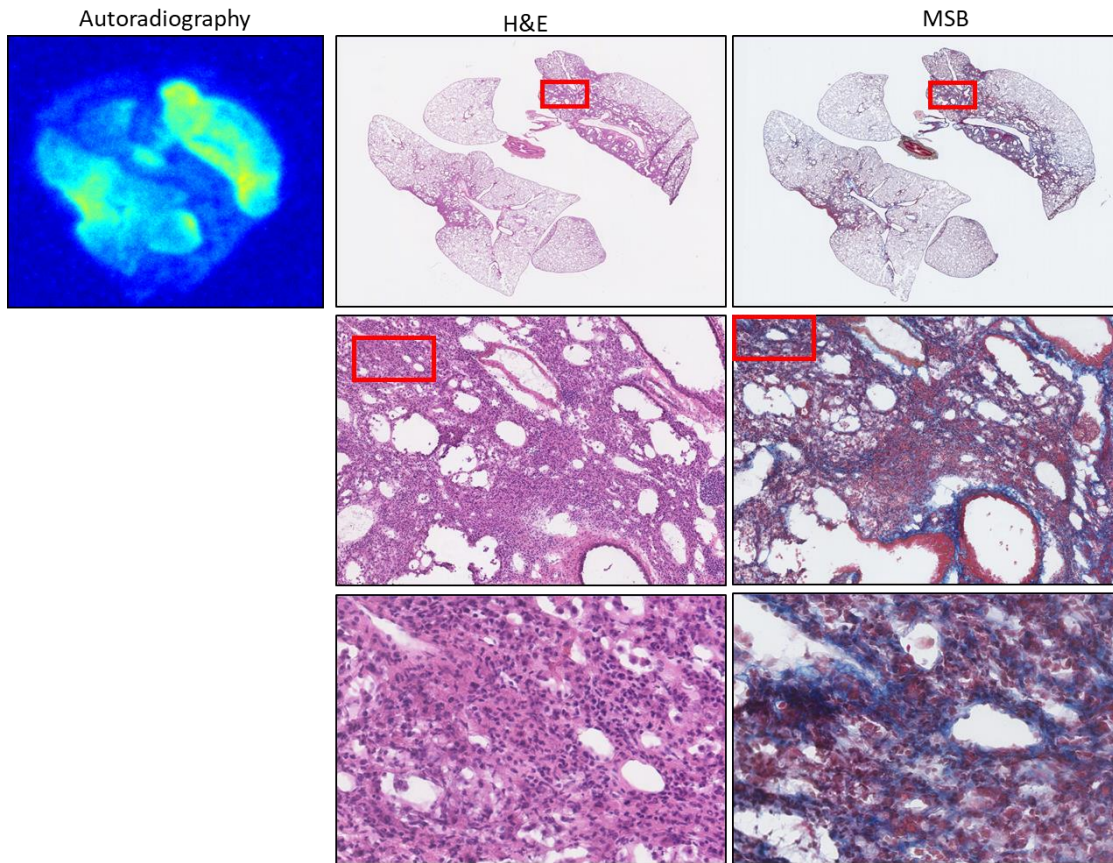
Figure 3-43. Representative images of lung sections of animals exposed to bleomycin.

Mice were oropharyngeally instilled with bleomycin (2mg/kg) 28 days prior to sacrifice, as depicted in Figure 3-40. Lungs were then sectioned and adjacent 5µm-thick lung slices were subjected to autoradiography, H&E and modified trichrome (MSB, collagen=blue) staining. The autoradiography images have been pseudo-coloured to represent increased signal intensity from an original greyscale image for ease of visualization (red = high signal intensity, dark blue = low signal intensity).

These findings were noted in all bleomycin-injured mice, including those whose pulmonary circulation was flushed (Figure 3-44).

Bleomycin + flushed

| Autoradiography | H&E | MSB |
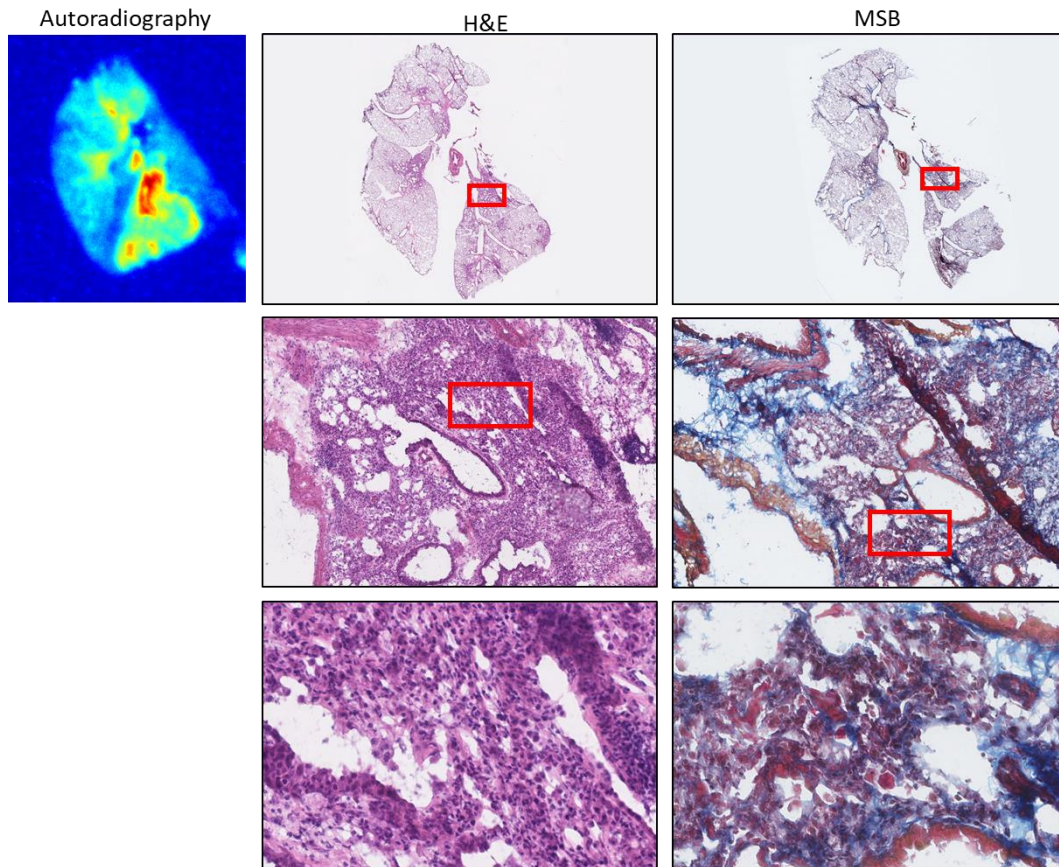
Figure 3-44. Representative images of lung sections of animals exposed to bleomycin with flushed pulmonary circulation.

Mice were oropharyngeally instilled with bleomycin (2mg/kg) 28 days prior to sacrifice, as depicted in Figure 3-40. Subsequently, normal saline was injected in the right ventricle to flush out the pulmonary circulation, at which point the lungs were seen blanching. Lungs were then sectioned and adjacent 5µm-thick lung slices were subjected to autoradiography, H&E and modified trichrome (MSB, collagen=blue) staining. The autoradiography images have been pseudo-coloured to represent increased signal intensity from an original greyscale image for ease of visualization (red = high signal intensity, dark blue = low signal intensity).

Furthermore, ^{18}F activity quantified from entire lung sections was significantly increased by autoradiography in both groups of bleomycin-challenged mice compared to saline-treated mice (Figure 3-45). Flushing the pulmonary circulation had no effect on ^{18}F activity, suggesting that the signal obtained did not emanate from the vascular compartment.
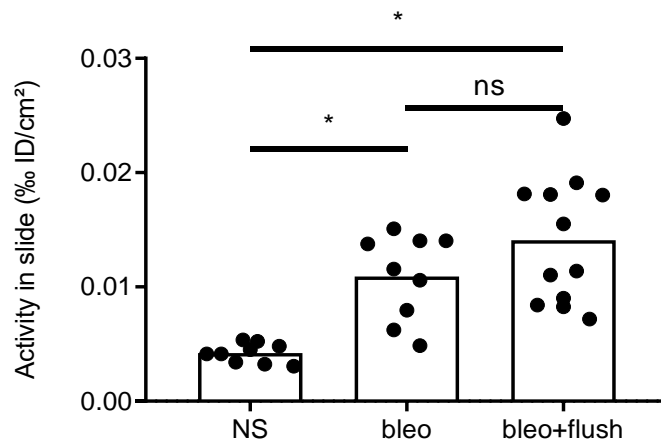
Figure 3-45. ^{18}F activity quantified on lung sections of animals subjected to normal saline or bleomycin with or without flushing of the pulmonary circulation.

Mice were oropharyngeally instilled with normal saline or bleomycin 28 days prior to sacrifice, as depicted in Figure 3-40. The Bleo+flush group had the pulmonary circulation flushed with NS prior to lung sectioning. Slices were then subjected to autoradiography (n= 3 sections per mouse, n = 3 mice), bleomycin-challenged (n = 3 sections per mouse, n = 4 mice) and bleo + flushed (n = 3 sections per mouse, n = 4 mice) lung sections. Data shown represent the differences in radioactivity per slice (mean). Difference between groups is evaluated with one-way ANOVA with Bonferroni correction for multiple comparisons. *$p<0.05$.

Overall, these findings suggest that in the bleomycin model of lung fibrosis, areas of parenchymal distortion are associated with increased glucose uptake and are not dependent on pulmonary vascular perfusion.

In view of the *in vitro* data showing that mTOR is key in promoting the changes in glucose metabolism of fibroblasts upon TGFβ1-stimulation, the next set of experiments planned involved examining the effect of mTOR inhibition on the bleomycin model of lung fibrosis. Unfortunately, such experiments could not be done due to time constraints during my MD(res) thesis.

4. Discussion

Idiopathic pulmonary fibrosis (IPF) is a devastating interstitial lung disease of unknown aetiology characterized by progressive scarring of the lung parenchyma. Transforming growth factor-β1 has been recognized as a key cytokine in the pathophysiology of IPF and acts largely by promoting the differentiation of fibroblasts into myofibroblasts, which in turn produce copious amounts of a collagen-rich extracellular matrix. This thesis examined whether the high biosynthetic demands associated with ECM production are accompanied by changes in glucose metabolism through the process of aerobic glycolysis, akin to that observed in rapidly proliferating cancer cells.

In this work, I first aimed to describe the changes in glucose metabolism that occur in primary human lung fibroblasts upon TGFβ1-induced fibroblast to myofibroblast differentiation and discovered that there are large cellular adaptations that occur during this process that are regulated by mTOR in a PI3K-AKT-independent manner.

Although changes in glucose metabolism have long been described in *proliferating* cells (eg. cancer cells), the concept of a role for metabolic changes during cell *differentiation* is only just emerging. This work shows that fibroblast to myofibroblast differentiation involves enhanced glucose metabolism, with an increase in glucose uptake through the upregulation of the GLUT1 transporter; as well as an increase in the expression of glycolytic enzymes and an increase in mitochondrial respiration. Furthermore, it also supports the notion that TGFβ1-induced fibroblast differentiation is associated with aerobic glycolysis and is regulated by mTOR independently of the linear PI3K and AKT axis. Finally, exploration of glucose metabolism in the bleomycin mouse model of pulmonary fibrosis revealed that fibrotic lesions are associated with large uptake of glucose and therefore support the link between the process of fibrogenesis and enhanced glycolysis *in vivo*.

Importantly, all the *in vitro* experiments described in this thesis were performed using fibroblasts obtained from a single healthy lung donor (single biological replicate) as mentioned in the Methods section of this thesis (Section 2.2). This is a significant limitation which must be acknowledged as it may affect the external validity, ie. generalizability of the results. For that reason, future experiments using fibroblasts derived from other lung donors, as well as using IPF-derived fibroblasts, could confirm and extend the findings reported in this thesis. Furthermore, it would be worthwhile examining whether the data obtained s are fibroblast-specific by testing other cell types (eg. epithelial cells and macrophages) which are known to play a rol in the pathogenesis of IPF.

4.1. Effect of TGFβ1 on fibroblast differentiation and collagen synthesis

Initial experiments aimed at validating the *in vitro* assay used for the process of TGFβ1-induced fibroblast differentiation. Although multiple published studies in this field have used varying concentrations of active TGFβ1 (ranging from 1-10ng/uL), I chose to use the minimum concentration required for maximal TGFβ1-induced collagen I deposition in order to minimize signalling via low-affinity receptors. I first determined that the lowest concentration of TGFβ1 to significantly increase collagen I expression was of 1 ng/uL, using an *in vitro* macromolecular crowding assay. This high-content imaging assay has been optimized in our laboratory by Dr Eley who has recently published a thesis detailing its protocol and benefits over standard 2D cultures (Eley, 2018). In brief, macromolecular crowding facilitates extracellular conversion of soluble procollagen monomers into insoluble collagen I fibrils and therefore monitors the complete biosynthetic cascade of collagen I formation (Chen et al., 2009; Mercer et al., 2016). Based on these results, all subsequent experiments were performed at a TGFβ1 concentration of 1ng/mL. At this concentration, activation of the canonical SMAD pathway was confirmed by monitoring the phosphorylation of SMAD3. In agreement with previous reports, peak phosphorylation of SMAD3 occurred 1 hour after TGFβ1 stimulation (Zi et al., 2012).

Following validation of these experimental methods, the time course for fibroblast to myofibroblast differentiation upon TGFβ1 stimulation was then examined. Peak expression of *ACTA2* and *COL1A1* genes occurred between 24-48 hours after TGFβ1 stimulation, much later than peak SMAD3 phosphorylation (peaking 1 hour after TGFβ1 stimulation). These findings suggest that although early activation of the SMAD pathway occurs upon TGFβ1 stimulation, other cellular processes are likely to be important for full myofibroblast differentiation to occur. Indeed, many non-SMAD pathways have been shown to be activated upon TGFβ1 activation, including the mTOR signalling hub, as has been reported in a recent publication emanating from our laboratory which found that mTOR activation was observed from 2-12 h after TGFβ1 stimulation (Woodcock et al., 2019).

4.2. Effect of TGFβ1 on glucose metabolism in fibroblasts

When this work was initiated, there were no previous reports in the literature regarding the effects of TGFβ1 stimulation on glucose metabolism in fibroblasts. Here, I show that TGFβ1, a pivotal cytokine known to play a critical role in the process of fibroblast differentiation and in the pathogenesis of IPF, promotes glucose uptake, glycolytic flux, lactate production and a shift towards aerobic glycolysis while still increasing oxidative phosphorylation in fibroblasts.

4.2.1. Effect of TGFβ1 on glucose uptake

To assess for changes in glucose uptake upon TGFβ1 stimulation, two complementary methods were used. First, the rate of decline of glucose levels in cell supernatants was measured using nuclear magnetic resonance spectroscopy (NMR). NMR, along with mass spectrometry (MS), are the most common analytical tools used in metabolomics research with exponential increases in metabolomic publications over the last decade based on these techniques (Emwas, 2015). NMR-based metabolomic analysis conveys significant advantages over mass spectrometry and is the method I chose for this work. With NMR, sample preparation protocols have been well established and have limited costs compared to MS. More importantly, the data obtained, in the form of NMR 'spectra' are highly reproducible and provide information on many metabolites over a very short period of time. In addition, NMR can be used for the assessment of extracellular metabolites without compromising cell integrity, so that they can be used in parallel with other experimental endpoints, such as assessment of protein or mRNA levels -which was performed in many of the experiments reported in this thesis and in other publications (Cuperlovic-Culf et al., 2016; Kostidis et al., 2017; Wagstaff et al., 2013). In general, the main limitations of NMR spectroscopy are its comparatively low sensitivity, especially compared to MS, as it can only identify metabolites in the high uM/mM range compared to the nM range with MS (not necessary for our current work) (Emwas et al., 2013). Of note, protocols used were based on previously established and published reports in highly regarded journals, such as Nature Protocols (Beckonert et al., 2007) with advice, guidance and support of members of the NMR Facility in the Department of Chemistry at the UCL School of Pharmacy.

The second assay that was used to assess glucose uptake was performed in collaboration with my colleague Dr B. Selvarajah. It involves directly comparing the rate of cellular glucose uptake prior to, and after 24 hours of TGFβ1 stimulation (undifferentiated fibroblast vs differentiated myofibroblast). This method, which has been published previously, required adding a minute amount of a non-metabolizable radioactive glucose analogue (^{3}H-2DG) and measuring radioactivity after cell lysis (Yamamoto et al., 2011), thereby informing us of the rate of glucose uptake at each time point.

Overall, the data obtained with these two assays were in general agreement and revealed that a significant increase in glucose consumption occurs upon TGFβ1 stimulation of fibroblasts. Indeed, over a 24 hour period, extracellular glucose levels were found to diminish twice as fast upon TGFβ1 stimulation relative to control media-treated cells (slopes -0.4292 ± 0.02 vs -0.21 ± 0.04, $p < 0.05$), with a significant difference in levels observed by 24 hours. At that time point, the rate of glucose uptake was found to be 3.05 ± 0.11 fold higher ($p < 0.05$) for TGFβ1-treated cells compared with control media-treated cells. Interestingly, the effect of TGFβ1 on glucose uptake was noticed as early as 8 hours after TGFβ1 stimulation, well before the rise in the mRNA levels of *COLA1A1* and of *ACTA2*, markers of fibroblast differentiation. These findings suggest that increased glucose uptake may, in fact, be necessary for myofibroblast differentiation to occur. Indeed, other experiments performed during the course of this work revealed that glycolysis is necessary for the process of TGFβ1-induced myofibroblast differentiation. For instance, depriving cells of glucose or pharmacologically inhibiting glycolysis significantly attenuated TGFβ1-induced collagen deposition. These experiments led to further work performed by my colleague Dr B. Selvarajah and resulted in a joint-first author publication in Science Signaling (Selvarajah, Azuelos et al., 2019).

Apart from being key for cellular energy production, intracellular glucose has many other roles, one of which is the post-translational modifications of proteins through the process of glycosylation. The glycolytic intermediate, fructose 6-phosphate, can be metabolized to glucosamine 6-phosphate via the hexosamine pathway. This leads to the formation of UPD-N-acetylglucosamine (UDP-GlcNAc), which can be used to generate glycoproteins and proteoglycans. Collagens also undergo a range of post-translational modifications, including glycosylation. Although the role of these modifications in collagens is still poorly understood, it has been suggested that collagen glycosylation may play a role in its turnover (Jürgensen et al., 2011). Also, direct glycosylation of the TGFβ1 receptor TβRII has been shown to influence the efficiency in TGFβ1 signalling by regulating the transport of the TβRII to the cell surface (Kim et al., 2012). The early increase in glycolytic flux may therefore contribute

to TGFβ1-induced fibroblast differentiation via multiple mechanisms. The relative contribution of these mechanisms was not explored further during the work performed in this thesis and will require extensive further experimentation.

4.2.2. Effect of TGFβ1 on extracellular lactate levels

To further validate the above findings, the levels of lactate were measured in the extracellular media as a marker of glycolytic activity using NMR spectroscopy. Although considered to be a 'waste product' of glycolysis, lactate plays an essential role in maintaining glycolytic flux by replenishing NAD^+ and thereby allowing glycolysis to continue. Lactate levels rose significantly over time upon TGFβ1 stimulation, with a 3.4-fold increase (slopes 1.67 ± 0.09 vs 5.68 ± 0.17, $p<0.05$) in observed lactate levels upon TGFβ1 stimulation over a 24 hour period. Significant changes in lactate levels were noted between groups at 8 and 24 hours after TGFβ1 stimulation. It is worth commenting that during the process of glycolysis, 1 molecule of glucose is converted to 2 molecules of pyruvate, which may be converted to acetyl-co-A in the mitochondria or to lactate in the cytoplasm. These data suggest that most of the increase in glucose consumption upon TGFβ1 stimulation is siphoned towards lactate production, as the rise in lactate levels approaches 2-fold the decline in glucose levels (TGFβ1 stimulation led to a 3.4-fold increase in lactate levels and a 2.0-fold decline in glucose levels), a feature described in aerobic glycolysis (Vander Heiden et al., 2009).

Extracellular lactate levels can be affected either by changes in lactate production or by changes in lactate transport across the plasma membrane via the monocarboxylate transporters (MCT). It has been reported that highly glycolytic cells, such as rapidly proliferating cancer cells, generally utilize MCT transporters to export lactate, although lactate can also be taken up from the extracellular space and used as a substrate to fuel metabolic pathways (Hui et al., 2017). Indeed, lactate can also be oxidized back into pyruvate and metabolized either for the generation of glycolytic intermediates or to the TCA cycle (Faubert et al., 2017). Therefore, although the increased level of lactate measured is a sign of enhanced glycolysis, other parameters affecting extracellular lactate levels may be at play during the process of TGFβ1-induced fibroblast differentiation. Further work examining specifically the intracellular levels of lactate and the levels and activity of MCT transporters would be needed to shed light on these potential possibilities.

The increase in lactate levels measured in our cell system follows a previous report showing that the concentrations of lactate are significantly increased in lung tissues of IPF patients compared with

healthy controls (Kottmann et al., 2012). In their report, the authors were also able to demonstrate that lactate directly promotes fibroblast differentiation by reducing extracellular pH and activating latent TGFβ1. Blocking lactate export using MCT inhibitors was subsequently shown to prevent TGFβ1 activation and myofibroblast differentiation, supporting MCT inhibitors as potential novel therapeutic agents in IPF (Colgan et al., 2015).

In summary, the findings reported here show that glycolytic flux is significantly enhanced during the process of fibroblast to myofibroblast differentiation and is accompanied by increases in glucose uptake and extracellular lactate levels. In order to determine the mechanism that accelerates glycolysis in pHLFs upon TGFβ1 stimulation, the key steps known to regulate glucose uptake and glycolysis were then evaluated.

4.2.3. Effect of TGFβ1 on glucose transporter levels

In the lung, GLUT1 and GLUT3 are the most commonly expressed glucose transporters (Devaskar and deMello, 1996) and in cancer cells, increased GLUT1 and GLUT3 expression is associated with augmented glucose uptake and cell proliferation (Birsoy et al., 2014; Macheda et al., 2005; Onodera et al., 2014; Szablewski, 2013). The work described in this thesis shows that GLUT1 mRNA and protein levels rose 24 hours after TGFβ1 stimulation while GLUT3 mRNA levels were not affected by TGFβ1 stimulation at any time point examined.

Only a few previous studies in mouse embryonic fibroblasts and in mesangial cells had revealed an induction in GLUT1 expression by TGFβ1 (Inoki et al., 1999; Kitagawa et al., 1991; Masumi et al., 1993). More recently, however, TGFβ1-induction in GLUT1 mRNA and protein levels were reported as early as 6 hours after TGFβ1 stimulation by others using mouse embryonic cells (Andrianifahanana et al., 2016). This earlier induction relative to my own data may be explained by the much higher concentration of TGFβ1 used in their experiments (10 ng/mL vs 1 ng/mL used here). In addition, their experiments were performed in mouse embryonic cells whilst mine were performed in primary human lung fibroblasts. Interestingly, however, these investigators also describe a large pool of GLUT1 protein in the plasma membrane upon TGFβ1 stimulation, suggesting that the GLUT1 protein may have translocated to its active site at the plasma membrane, thereby increasing its activity. Indeed, in addition to its cellular levels, the activity of GLUT1 can also be

affected by translocation to the plasma membrane and/or by post-translational modifications. In adipocytes, for instance, GLUT1 levels are markedly elevated in plasma membranes relative to intracellular membranes upon Ras overexpression (Kozma et al., 1993). Moreover, IL-7 was found to stimulate glucose uptake and cell-surface localization of GLUT1 (Wofford et al., 2008). Some of these effects could be mediated by the PI3K-AKT-mTOR axis as in lung adenocarcinoma cells, PI3K/mTOR inhibition effectively suppressed membrane localization of GLUT1, which, instead, accumulated in the cytoplasm(Makinoshima et al., 2015). It would therefore be interesting to examine whether GLUT1 translocation and GLUT1 activity are affected by TGFβ1 by performing cell fractionation followed by immunoblotting for GLUT1 in cytoplasmic and plasma membrane fractions; and/or the examination of GLUT1 cellular localization by immunofluorescence using confocal microscopy with appropriate intracellular localization markers. The effect of TGFβ1 and of inhibitors of the PI3K-AKT-mTOR axis could then be evaluated to examine their roles in GLUT1 translocation.

The association between GLUT1 expression and fibrogenesis has also recently been described, notably in the kidney fibrosis literature. For example, overexpression of GLUT1 in mice resulted in the development of changes consistent with diabetic glomerulosclerosis (Wang et al., 2010), suggesting that an increase in GLUT1-mediated glucose flux may be sufficient to drive pro-fibrotic pathways.

In order to further determine the mechanisms involved in glucose uptake, the expression levels of key enzymes involved in the glycolytic pathway were examined next.

4.2.4. Effect of TGFβ1 on glycolytic enzyme expression

After examining the effect of TGFβ1 on glucose transporter expression, I examined the changes in mRNA levels of key rate-limiting glycolytic genes. There was an increase in the mRNA levels of *PFKFB3* at 3 hours after TGFβ1 stimulation, and of *HK2* at 8 hours after stimulation. For *PKM1* and *PKM2*, the mRNA levels were unaffected by TGFβ1 stimulation, whilst TGFβ1 caused a consistent increase in *LDHA* mRNA levels over the first 32 hours after stimulation. Although PFK2 is not a rate-limiting glycolytic enzyme, it catalyses the conversion of fructose-6-phosphate to fructose-2, 6-bisphosphate, an allosteric activator of PFK1 and a potent stimulator of glycolysis. The decision to examine the mRNA levels of this enzyme was based on its key role in the process of aerobic glycolysis

in proliferating cells (De Bock et al., 2013).

Many of the key rate-limiting steps of glycolysis (HK, PFK and PK) have been reported to favour tumour initiation and growth (Bluemlein et al., 2011; Christofk et al., 2008; Dayton et al., 2016; De Bock et al., 2013; Patra et al., 2013; Ros and Schulze, 2013; Webb et al., 2015). Yet, the specific glycolytic enzymes that require upregulation for flux enhancement were not clearly elucidated until recently, when investigators systematically overexpressed enzymes that catalyze every glycolytic step and assessed its effect on glycolytic flux (Tanner et al., 2018). It was found that only four steps exert significant flux control when tested in 2 cell lines: hexokinase, phosphofructokinase, glucose import and lactate export. Interestingly, the enzymes past PFK, including PK, did not control glycolytic flux in both cell lines tested. This report supports the data obtained in the presents work, as TGFβ1 promoted an early induction of some of the key rate-limiting steps involved in glycolysis (eg. HK2 and PFKFB3). However, these steps are not the sole determinants of glycolytic flux. Further in-depth metabolomic analysis would provide valuable insight as many factors are felt to generally regulate the flux of a metabolic pathway. These include (1) the availability of the substrate (eg. glucose), (2) the concentration of the enzymes, (3) the activity of the enzymes which can be affected for instance by post-translational modifications and (4) the concentrations of metabolites that affect enzyme activity (eg. substrates and products of the reaction) (Chandel, 2015).

Although TGFβ1 stimulation led to an overall increase in glycolysis, it has been demonstrated that fibroblasts derived from IPF lungs may have a very different metabolic phenotype from TGFβ1-stimulated fibroblasts. For instance, IPF-derived fibroblasts were shown to have a tendency towards *reduced* glycolysis (as measured by the ECAR) and a *reduced* rise in ECAR upon TGFβ1 stimulation when compared to normal lung fibroblasts (Álvarez et al., 2017). In addition, using a combined metabolomic and microarray analysis, a recent report found a *decrease* in late-stage glycolytic metabolites including fructose 1,6-bisphosphate and phosphoenolpyruvate, along with a *decrease* in PFKFB3 in IPF whole lung tissue relative to normal human lung (Zhao et al., 2017). These findings suggest that IPF-derived fibroblasts may, in fact, have a diminished capacity to respond to TGFβ1 (Zank et al., 2018). Indeed, IPF-derived fibroblasts may have already been exposed and activated by the highly pro-fibrotic microenvironment in IPF when they are isolated and grown in culture, and therefore may already represent a fully activated phenotype with limited capacity to respond to further exogenous TGFβ1 stimulation.

Moreover, our findings indicate that TGFβ1 rapidly promotes glucose uptake, glycolytic expression and overall glycolytic flux well before the differentiation process of fibroblasts takes place. This

temporal difference raises the question as to whether these early metabolic changes observed are in fact required for the differentiation process to occur. Indeed, the process of cell differentiation involves the activation of many parts of the cell machinery, with extensive gene transcription requiring the synthesis of ribonucleotides, the turnover of transcripts and large amounts of amino acid synthesis and protein translation for the production of extracellular matrix proteins. All these cellular processes are known to require significant energy requirements in the form of ATP, which can be provided by glucose metabolism (Kafri et al., 2016; Lynch and Marinov, 2015).

In agreement with this hypothesis, our laboratory and others have shown that inhibiting glycolysis may attenuate TGFβ1-induced fibroblast differentiation and/or the extent of pulmonary fibrosis in experimental animal models. The compound 2-deoxyglucose (2-DG) is a glucose analogue that is phosphorylated by hexokinase to produce 2-deoxyglucose-6-phosphate, a molecule that cannot be further metabolized. As it accumulates in the cell, it competitively inhibits hexokinase and reduces glucose uptake. Although preclinical and early clinical studies have demonstrated anti-proliferative effects of 2-DG in cancer cells, its systemic toxicity made it an undesirable therapeutic option (LANDAU et al., 1958; Zhang et al., 2014). During the course of the work that led to this thesis, our laboratory has performed similar experiments using cultured primary human lung fibroblasts. We found that administration of 2-DG leads to a concentration-dependent reduction in collagen and α-sma expression upon TGFβ1-stimulation (Selvarajah, Azuelos et al., 2019). Similarly, a previous report showed that 2-DG, as well as another HK2 inhibitor, 3-bromopyruvate, and the PFKFB3 inhibitor 3-(3-Pyridinyl)-1-(4-pyridinyl)-2-propen-1-one (3PO) also inhibit TGFβ1–induced fibroblast differentiation (Xie et al., 2015). Finally, GLUT1 inhibition, either via shRNA knockdown or using the inhibitor, phloretin, was also shown to inhibit TGF-β1-induced increases in α-SMA expression, the defining marker for fibroblast differentiation (Cho et al., 2017). Similarly, the drug dichloroacetate (DCA) inhibits aerobic glycolysis by targeting and inhibiting the action of the enzyme pyruvate dehydrogenase kinase (PDK). PDK, which is overexpressed in several tumours, phosphorylates and inhibits pyruvate dehydrogenase (PDH). By inactivating PDH, pyruvate cannot enter the TCA cycle and is thus metabolized into lactate (Kim et al., 2006a). DCA, therefore, stimulates the conversion of pyruvate into acetyl-CoA and mitochondrial respiration. By doing so, DCA was shown to inhibit tumour growth *in vivo* (Michelakis et al., 2010) and was recently also found to inhibit TFGβ1-induced fibroblast differentiation and attenuate bleomycin-induced pulmonary fibrosis (Goodwin et al., 2018). Finally, the glycolytic enzyme, LDHA, is also a metabolic target in cancer. The LDHA inhibitor, gossypol, has been used in clinical trials but again, tolerability has limited its use in the

clinic (Ready et al., 2011). Pre-clinical studies with gossypol in the context of IPF have also shown interesting results with evidence for prevention of bleomycin and radiation-induced pulmonary fibrosis in murine models (Judge et al., 2017, 2018; Kottmann et al., 2015).

4.2.5. Effect of TGFβ1 on mitochondrial respiration and aerobic glycolysis

Much of this work so far has established a critical link between glycolytic flux and TGFβ1-induced fibroblast differentiation. In addition to glycolysis, however, intracellular glucose metabolism into pyruvate can also lead to its oxidation in the mitochondria to generate large amounts of energy in the form of ATP. In fact, mitochondrial oxidative phosphorylation can generate 15 times more ATP molecules per mole of glucose, when compared to glycolysis. To determine the impact of TGFβ1 on mitochondrial respiration, the oxygen consumption rate (OCR) was examined using the SeaHorse XF96e Analyzer, which provides a direct measurement of OCR in live adherent cells. These experiments revealed that the OCR largely increases upon TGFβ1 stimulation, relative to control media-treated cells with a significant increase noted as early as 3 hours after TGFβ1 stimulation.

This rapid increase in OCR after TGFβ1 stimulation suggests that TGFβ1 signalling likely has an impact on specific factors that regulate mitochondrial respiration. These may include a direct impact on the expression, levels, activity and/or efficiency of the mitochondrial electron transport chain enzymes (Benard et al., 2010). Such examples could include a leaky mitochondrial inner membrane forcing an increase in OCR without accompanied ATP generation, a concept called uncoupling. Also, changes in mitochondrial network shape and location within the cells (a concept labelled mitochondrial dynamics) may be affected directly or indirectly by TGFβ1 stimulation, as such changes in the mitochondrial network have been associated with changes in mitochondrial respiration (Mishra and Chan, 2016). Similarly, mitochondrial energy substrates, such as NADH and ADP, or total mitochondrial content, which is regulated by processes such as mitochondrial biogenesis and mitochondrial autophagy, may also be affected by TGFβ1 stimulation and would have an impact on mitochondrial respiration. Of all these regulatory factors, only the impact of TGFβ1 on mitochondrial biogenesis has been reported in the fibroblast literature. Indeed, recent reports of a TGFβ1-driven induction of mitochondrial biogenesis was reported in human fetal lung fibroblasts, as evidenced by an increase in overall OCR, an increase in active peroxisome proliferator-activated receptor gamma coactivator 1-alpha (PGC1α), a transcription factor that plays

a critical role in mitochondrial biogenesis and an increase in mitochondrial DNA. Remarkably, pharmacological inhibition of glycolysis or of mitochondrial respiration prevented TGFβ1-induced fibroblast to myofibroblast differentiation. Although TGFβ1 has also been linked to other effects on mitochondria, including modulating intracellular calcium balance (Casalena et al., 2012; Yoon et al., 2005; Zhang et al., 2015), its effects on mitochondrial function in primary human lung fibroblasts have not been clearly defined.

In addition to being the main sources of energy in the cell, mitochondria are critical in maintaining cellular homeostasis, with evidence of mitochondrial dysfunction seen in diabetes, neurodegenerative diseases and ageing (Srivastava, 2017). They are the major source of endogenous ROS, which if not properly regulated, can oxidize and damage the mitochondrial lipids, proteins, and DNA. Damaged mitochondria can in turn release even more ROS, thereby creating a vicious cycle of oxidative stress that may culminate in cell death. As described in the Introduction section of this thesis (1.3.1), ROS have been shown to activate latent TGFβ1. The observation of an increase in TGFβ1-induced OCR, therefore, could contribute to an increase in ROS production, with a feed-forward loop promoting further TGFβ1 activation and ongoing fibrogenesis (Bargagli et al., 2009). In addition, mitochondrial ROS are produced in larger quantities by dysfunctional mitochondria and TGFβ1 has also been shown, albeit in epithelial cells, to cause mitochondrial dysfunction by downregulating mitochondrial complex IV, thereby leading to further increase in mitochondrial ROS production (Yoon et al., 2005). Finally, the ROS-producing enzyme NADPH oxidase-4 (Nox4) was shown to be upregulated in IPF lung fibroblasts and was found to repress mitochondrial biogenesis (Amara et al., 2010; Bernard et al., 2017).

Much of the work examining mitochondrial dysfunction in the context of IPF has been performed in epithelial cells with little published in the fibroblast literature. Specifically, multiple studies have examined whether lung epithelial cell injury, thought to be the key driver in the development of pulmonary fibrosis, is a consequence of mitochondrial dysfunction or mitochondria-derived ROS release. For instance, deficient mitochondrial clearance ("mitophagy") has been associated with the development of pulmonary fibrosis in response to injury (Bueno et al., 2015; Patel et al., 2015; Sosulski et al., 2015). This leads to the accumulation of dysfunctional mitochondria that have reduced mitochondrial electron transport chain activity and that release more ROS, thereby causing cellular damage. Interestingly, enhancing mitophagya using thyroid hormone was shown to ameliorate lung fibrosis in experimental models (Yu et al., 2017).

In addition to examining OCR, the SeaHorse XF96e Analyzer assay also allows the measurement of

the extracellular acidification rate (ECAR), considered to be a surrogate measurement for lactic acid production. The magnitude of the increase in ECAR was much more pronounced than that of OCR, raising the notion that under TGFβ1 stimulation, glucose metabolism is more readily geared towards the glycolytic pathway than towards mitochondrial respiration, a feature consistent with our earlier findings of aerobic glycolysis.

Taken together, the work so far revealed that the process of fibroblast differentiation, when stimulated by TGFβ1, is accompanied by large changes in glucose metabolism with increases in both glycolytic flux and mitochondrial respiration.

4.3. Regulation of TGFβ1-induced glucose metabolism by the PI3K-AKT-mTOR axis

The next question aimed to determine whether the PI3K-AKT-mTOR signalling pathway regulates the TGFβ1-induced changes in glucose metabolism in fibroblasts. This work revealed that mTOR, in a PI3K-AKT independent manner, regulate various aspects of glucose metabolism that occur upon TGFβ1 stimulation.

It has now been established that the PI3K-AKT-mTOR axis plays a critical role in regulating glucose metabolism in cancer cells, largely by accelerating flux through glycolysis, by increasing the activity of key enzymes of the glycolytic pathway and by upregulating glucose uptake via glucose transporter GLUT1 (see Introduction 1.6). These changes in glucose metabolism represent a striking metabolic difference between cancer and most normal tissues, and for that reason, a vast amount of research has been focussed on targeting aerobic glycolysis in cancer (Doherty and Cleveland, 2013; Hamanaka and Chandel, 2012; Luengo et al., 2017; Zhao et al., 2013). Strategies have included approaches that *directly* inhibit glycolysis, and/or *indirectly* by inhibiting the PI3K-AKT-mTOR axis which regulates these changes in metabolism (Vernieri et al., 2016). Our findings in primary human lung fibroblasts confirm that targeting fibroblast metabolism using similar approaches may hold promise to limit the fibrogenesis in IPF.

In the current work, a significant inhibition in TGFβ1-induced glucose uptake, lactate production and oxygen consumption rate was noted when fibroblasts were pre-treated with the highly selective ATP-competitive mTOR inhibitor, AZD8055. However, these effects were not apparent when cells

were pre-treated with the PI3K inhibitor, GSK2864918A, or the AKT inhibitor, MK2206. In fact, the extracellular levels of lactate rose when cells were exposed to GSK2864918A and to MK2206, which may be attributable to cell death or changes in lactate export via MCTs. Further work examining the effect of these compounds on lactate transport across the cell membrane would be needed to shed further light on the likely mechanism involved. For these experiments, the concentration (1 µM) used for each of the compounds was previously shown to significantly inhibit specific downstream signalling of each respective kinase (Woodcock et al., 2019), without any associated cell toxicity in human lung fibroblasts.

Interestingly, a recent report found that although the PI3K-AKT axis is one of the best-characterized pathways leading to mTORC1 activation, specific PI3K or specific AKT inhibition had no impact on TGFβ1-induced mTORC1 downstream signalling and on TGFβ1-induced collagen synthesis (Woodcock et al., 2019). These findings suggest that another pathway may promote mTOR activation independent of PI3K-AKT. Whether TGFβ1-mediated mTOR activation occurs via the activation of specific kinases or via changes in the intracellular environment (e.g. amino acid uptake, redox status, changes in the AMP/ATP levels) is currently being intensely investigated in our laboratory. In any case, it is therefore very exciting to note that the effects we observed on TGFβ1-induced glucose metabolism were also sensitive to mTOR inhibition and independent of the linear PI3K-AKT pathway. The exact mechanism by which mTOR regulates glucose metabolism upon TGFβ1 stimulation has yet to be defined, although an attenuation in GLUT1 induction with AZD8055 was noted. In cancer, it is believed that the transcription factors, HIF-1 and c-myc, are largely regulated by mTOR signalling and thereby influence glucose metabolism. It would certainly be interesting to examine the expression and role of these transcription factors, especially as HIF-1 is induced upon TGFβ1 stimulation and has been shown to play an important role in mediating TGFβ1-induced fibroblast differentiation by other investigators (Goodwin et al., 2018; Kottmann et al., 2012).

AZD8055 is an ATP-competitive mTOR inhibitor which targets the FRAP1 kinase common to both mTORC1 and mTORC2. In this work, the contribution of each mTOR complex to the TGFβ1-induced changes in metabolism was not examined, although much work has already implicated mTORC1 as the critical node involved in regulating glucose metabolism in various cell types (see Introduction 1.4). Furthermore, the role of each mTOR complex in TGFβ1-induced fibroblast collagen deposition was thoroughly and recently examined, with the mTORC1-4EBP1 signalling axis found to be critical for TGFβ1-induced collagen deposition in fibroblasts (Woodcock et al., 2019). It would be worth examining whether this axis is also predominantly responsible for regulating the TGFβ1-induced

changes in glucose metabolism.

Overall, this work is in agreement with various studies examining the potential use of mTOR inhibitors for the treatment of cancer and pulmonary fibrosis. In the context of cancer, mTOR inhibitors have already been shown to exert antitumour effects and are currently approved for the treatment of a variety of cancers, including advanced renal cell carcinoma, neuroendocrine cancers and certain breast cancers (Chiarini et al., 2015). Recently our laboratory has shown that omipalisib, a potent and novel pan- PI3K and mTOR inhibitor, inhibits fibroblast proliferation and TGFβ1-induced collagen deposition *in vitro* and [^{18}F]FDG-uptake in a small proof of mechanism trial in IPF (Lukey et al., 2019; Mercer et al., 2016).

Interestingly, one of the current medications shown to slow down the progression of the disease is the tyrosine kinase inhibitor nintedanib. Nintedanib is an inhibitor of the FGF, VEGF and PDGF-receptors, which are known to signal through PI3K. In fact, nintedanib was initially approved as an anti-neoplastic drug and was found to reduce cancer progression, while reducing glucose uptake, glycolysis and lactate production in cancer (Navarro et al., 2016). Similarly, metformin, which is a commonly prescribed anti-diabetic agent, activates the AMP-activated protein kinase (AMPK) pathway, resulting in the phosphorylation of TSC2 thereby promoting its inhibition of Rheb and mTORC1. Metformin was shown to reduce TGFβ1-induced fibroblast differentiation and attenuate lung fibrosis in the bleomycin mouse model (Sato et al., 2016). A recent report further revealed that metformin promotes fibrosis resolution by inducing myofibroblast-to-lipofibroblast transdifferentiation (Kheirollahi et al., 2019). There are additional glycolytic modulators currently in clinical trials (phase I and II) which have already shown potential in the cancer setting (Sborov et al., 2015) and may provide further therapeutic opportunities for fibrotic disorders.

4.4. Glucose uptake in the bleomycin model of lung fibrosis

Following the work describing the changes in glucose metabolism occurring in TGFβ1-stimulated fibroblasts, the final section of this thesis examined whether changes in glucose uptake were linked to fibrogenesis in an experimental model of lung fibrosis.

For these experiments, the bleomycin model of lung fibrosis was used. This is the most widely used and best-characterized animal model of pulmonary fibrosis. Following the ATS workshop

recommendations, the study was performed in male mice, the recommended gender species for initial preclinical testing, and further employed a "single oropharyngeal administration of bleomycin" (Jenkins et al., 2017), as previously described by our laboratory (Scotton and Chambers, 2010; Scotton et al., 2013). In order to confirm the development of fibrosis, the animals were sacrificed during the fibrotic stage of lung injury; that is, 28 days after administration of bleomycin. At that time point, histologic examination of the lungs revealed multiple areas of lung injury with peri-bronchiolar fibrosis with bronchiolization and extensive collagen deposition.

To assess and correlate glucose uptake in the lungs following bleomycin-induced lung injury with fibrotic lesions, I examined [^{18}F]FDG uptake by autoradiography of lung slices. Multiple studies have now demonstrated that the [^{18}F]FDG signal is increased in IPF lungs, is reproducible, and can be objectively measured (Groves et al., 2009; Win et al., 2012). In humans, [^{18}F]FDG activity correlates with physiologic outcomes and even with mortality (Justet et al., 2017; Win et al., 2018) although key methodological assessments, such as considering fibrotic lung density appears to be critical and is the subject of methodological research in this field (Castiaux et al.; Chen et al., 2017; Holman et al., 2015; Lambrou et al., 2011).

In the present work, [^{18}F]FDG uptake was higher in the healthy lung sections of mice exposed to bleomycin compared to lung sections of saline-control challenged mice. These findings are in agreement with a study showing increased [^{18}F]FDG uptake in areas of normal lungs of IPF patients when compared to healthy subjects (Win et al., 2014). This further suggests that changes in glucose metabolism occur throughout the IPF lung prior to any evidence of overt pathological or radiological changes. These findings further support the notion that changes in glucose metabolism in the IPF lung may precede the deposition of the extracellular matrix, at which point potentially irreversible fibrosis has developed.

Second, there was a clear correlation between the extent of lung injury and the extent of [^{18}F]FDG uptake in the bleomycin-challenged lungs. Overall quantification of the [^{18}F]FDG activity across the entire lung sections demonstrated significantly greater [^{18}F]FDG uptake in the bleomycin-challenged lungs compared to the saline-challenged control lungs. These findings are in agreement with a previous report revealing that increased [^{18}F]FDG uptake in bleomycin-challenged mice correlated with bleomycin concentration and histologic score of fibrosis (Bondue et al., 2015).

Evidence from our *in vitro* work in fibroblasts raises the possibility that the increase in glucose uptake occurring during TGFβ1-induced fibroblast differentiation may explain the increase in

[18F]FDG signal noted in IPF lungs. However, a previous report (El-Chemaly et al., 2013) based on immunohistochemical analysis of normal and fibrotic lungs found that GLUT1 is predominantly expressed on the surface of erythrocytes and inflammatory cells, such as neutrophils and macrophages. Their findings suggest that enhanced [18F]FDG-PET uptake in pulmonary fibrosis may, in fact, stem from an increase in inflammatory cell infiltration, as as well as an increase in lung parenchymal vasculature due to angiogenesis in fibrotic areas, rather than upregulation of the metabolic rate of fibroblasts. These investigators also noted that in a UIP biopsy sample, GLUT1 was found to be present in erythrocytes and inflammatory cells and not in mesenchymal cells in fibroblastic foci. In view of this published report, the contribution of erythrocytes to [18F]FDG activity in fibrotic regions was investigated by adding a group of mice exposed to bleomycin which, following terminal anaesthesia, had their pulmonary vasculature flushed with normal saline to remove circulating erythrocytes. The lungs of these mice were histologically similar to bleomycin-challenged (not perfused) lungs and had similar [18F]FDG uptake. These findings suggest that the [18F]FDG signal may not be simply be emanating from the vasculature in this animal model.

One limitation of this work is that is was based on a single model and was not investigated in other established models of lung fibrosis (radiation-induced or TGFβ1-overexpression models). Indeed, the bleomycin model of lung injury is far from perfect in terms of representing a faithful animal model of IPF. Indeed, the peribronchiolar location of lung injury is not typically observed in UIP (histological pattern seen in IPF, see introduction 1.8) which is classically and predominantly subpleural and peripheral. In addition, the inflammatory cell infiltrate that was noted is much more extensive than what is usually seen in the UIP pattern although such findings have been described previously by other groups (Degryse et al., 2010; Liu et al., 2017).

Overall, the data presented in this thesis reveal that the process of fibrogenesis in the bleomycin model of lung injury is associated with increased glucose uptake in the lung, suggesting that [18F]FDG uptake could potentially be used as a clinical biomarker and/or a marker of therapeutic response. In fact, the antifibrotic compound pirfenidone was found to significantly reduce [18F]FDG uptake in mice exposed to bleomycin, although [18F]FDG uptake in the lungs of IPF patients did not change over 3 months of treatment (Bondue et al., 2019). More interestingly, the PI3K-mTOR inhibitor omipalisib was found to induce an exposure-dependent reduction in [18F]FDG uptake in fibrotic areas of IPF lungs (Lukey et al., 2019).

5. Conclusion and future work

Idiopathic pulmonary fibrosis (IPF) is a chronic and progressive lung disease that carries a poor prognosis, with an estimated survival of only 3-5 years from diagnosis. There is currently an urgent clinical need for the development of novel therapeutic options that halt rather than simply slow-down disease progression. The pathology of IPF is underpinned by the accumulation and aberrant activation of highly synthetic myofibroblasts, which produce an excessive collagen-rich extracellular matrix leading to irreversible loss of lung function.

The work presented examined the changes that occur upon TGFβ1-stimulation during the process of fibroblast to myofibroblast differentiation. This process is associated with large increases in glucose uptake, glycolytic flux and lactate production, as well as increases in mitochondrial respiration. These changes suggest the development of aerobic glycolysis, a process previously and classically described in proliferating cancer cells. Mechanistic studies using highly potent and selective pharmacological kinase inhibitors revealed that TGFβ1-induced changes in glucose metabolism in fibroblasts are regulated by mTOR in a PI3K-AKT independent manner, opening up further avenues for testing mTOR inhibitors for clinical use in IPF. Furthermore, an increase in glucose uptake was also noted *in vivo*, in fibrotic areas of the lungs of mice exposed to bleomycin. These findings suggest there is potential for using glucose uptake as a marker of therapeutic response and/or prognosis in IPF patients, although further work in this regard is clearly needed.

These data have led to multiple reports that have been published (Azuelos et al., 2018; Forty et al., 2017; Selvarajah et al., 2016, 2017, 2019), and others in preparation. In addition, this work offers the potential for many more experiments that could help improve our understanding of the pathogenesis of IPF and offer therapeutic options for patients affected by this disease.

First, deciphering how the TGFβ1-mTOR axis exerts its effect on promoting glycolysis could be examined. Based on my data, examining the activity and cellular localization of the GLUT1 transporter upon TGFβ1 stimulation would be warranted. In addition, the activity rather than enzyme levels of the rate-limiting glycolytic enzymes should be assessed, as this may offer a potential target to mitigate the TGFβ1 effect on glycolysis. Furthermore, this work revealed significant increases in extracellular lactate levels upon TGFβ1 stimulation. As described above, extracellular lactate levels can be modulated by lactate production and lactate transport across the plasma membrane, via MCT transporters. Examining the levels and activity of these transporters

would further help in understanding the effect of TGFβ1 on overall glucose metabolism in fibroblasts and may similarly offer new therapeutic opportunities.

The work presented also revealed the critical importance of the mTOR kinase in promoting changes in glucose metabolism. However, the downstream mechanism by which mTOR promotes glycolysis was not examined further. Interestingly, the mTORC1-4EBP1 axis was recently shown to be key in mediating fibroblast to myofibroblast differentiation. It would be interesting to examine whether this axis also mediates the TGFβ1-induced changes in glucose metabolism.

Finally, this work involved the use of the bleomycin model of lung fibrosis. The next experiment that could not be completed due to limited time was to assess whether administering an mTOR inhibitor *in vivo* to bleomycin-challenged mice could prevent both [^{18}F]FDG uptake in the lungs and overall lung fibrosis.

6. References

Abraham, A.G., and O'Neill, E. (2014). PI3K/Akt-mediated regulation of p53 in cancer. Biochem. Soc. Trans. *42*, 798–803.

Adekola, K., Rosen, S.T., and Shanmugam, M. (2012). Glucose transporters in cancer metabolism. Curr. Opin. Oncol. *24*, 650–654.

Ahluwalia, N., Shea, B.S., and Tager, A.M. (2014). New therapeutic targets in idiopathic pulmonary fibrosis. Aiming to rein in runaway wound-healing responses. Am. J. Respir. Crit. Care Med. *190*, 867–878.

Alessi, D.R., James, S.R., Downes, C.P., Holmes, A.B., Gaffney, P.R., Reese, C.B., and Cohen, P. (1997). Characterization of a 3-phosphoinositide-dependent protein kinase which phosphorylates and activates protein kinase Balpha. Curr. Biol. *7*, 261–269.

Álvarez, D., Cárdenes, N., Sellarés, J., Bueno, M., Corey, C., Hanumanthu, V.S., Peng, Y., D'Cunha, H., Sembrat, J., Nouraie, M., et al. (2017). IPF lung fibroblasts have a senescent phenotype. Am. J. Physiol. Cell. Mol. Physiol. *313*, L1164–L1173.

Amara, N., Goven, D., Prost, F., Muloway, R., Crestani, B., and Boczkowski, J. (2010). NOX4/NADPH oxidase expression is increased in pulmonary fibroblasts from patients with idiopathic pulmonary fibrosis and mediates TGF 1-induced fibroblast differentiation into myofibroblasts. Thorax *65*, 733–738.

American Thoracic Society, and European Respiratory Society (2002). American Thoracic Society/European Respiratory Society International Multidisciplinary Consensus Classification of the Idiopathic Interstitial Pneumonias. This joint statement of the American Thoracic Society (ATS), and the European Respiratory Society (E. Am. J. Respir. Crit. Care Med. *165*, 277–304.

Andrianifahanana, M., Hernandez, D.M., Yin, X., Kang, J.-H.J.-H., Jung, M.-Y., Wang, Y., Yi, E.S., Roden, A.C., Limper, A.H., and Leof, E.B. (2016). Profibrotic up-regulation of glucose transporter 1 by TGF- involves activation of MEK and mammalian target of rapamycin complex 2 pathways. FASEB J. *30*, 3733–3744.

Asano, S., Ito, S., Takahashi, K., Furuya, K., Kondo, M., Sokabe, M., and Hasegawa, Y. (2017). Matrix stiffness regulates migration of human lung fibroblasts. Physiol. Rep. *5*.

Ask, K., Bonniaud, P., Maass, K., Eickelberg, O., Margetts, P.J., Warburton, D., Groffen, J., Gauldie, J., and Kolb, M. (2008). Progressive pulmonary fibrosis is mediated by TGF-β isoform 1 but not TGF-β3. Int. J. Biochem. Cell Biol. *40*, 484–495.

Azuelos, I., Selvarajah, B., Plate, M., Woodcock, H., Taylor, A., Brunori, G., Blanchard, A., Mercer, P., and

Chambers, R. (2018). MTOR regulates TGFß-induced collagen synthesis via increased glycine biosynthesis. In Mechanisms of Lung Injury and Repair, (European Respiratory Society), p. LSC-1186.

Bárdos, J.I., and Ashcroft, M. (2004). Hypoxia-inducible factor-1 and oncogenic signalling. BioEssays *26*, 262–269.

Bargagli, E., Olivieri, C., Bennett, D., Prasse, A., Muller-Quernheim, J., and Rottoli, P. (2009). Oxidative stress in the pathogenesis of diffuse lung diseases: A review. Respir. Med. *103*, 1245–1256.

Bauer, Y., Tedrow, J., de Bernard, S., Birker-Robaczewska, M., Gibson, K.F., Guardela, B.J., Hess, P., Klenk, A., Lindell, K.O., Poirey, S., et al. (2015). A Novel Genomic Signature with Translational Significance for Human Idiopathic Pulmonary Fibrosis. Am. J. Respir. Cell Mol. Biol. *52*, 217–231.

Beckonert, O., Keun, H.C., Ebbels, T.M.D., Bundy, J., Holmes, E., Lindon, J.C., and Nicholson, J.K. (2007). Metabolic profiling, metabolomic and metabonomic procedures for NMR spectroscopy of urine, plasma, serum and tissue extracts. Nat. Protoc. *2*, 2692–2703.

Benard, G., Bellance, N., Jose, C., Melser, S., Nouette-Gaulain, K., and Rossignol, R. (2010). Multi-site control and regulation of mitochondrial energy production. (Elsevier).

Bentley, J., Itchayanan, D., Barnes, K., McIntosh, E., Tang, X., Downes, C.P., Holman, G.D., Whetton, A.D., Owen-Lynch, P.J., and Baldwin, S.A. (2003). Interleukin-3-mediated Cell Survival Signals Include Phosphatidylinositol 3-Kinase-dependent Translocation of the Glucose Transporter GLUT1 to the Cell Surface. J. Biol. Chem. *278*, 39337–39348.

Bernard, K., Logsdon, N.J., Miguel, V., Benavides, G.A., Zhang, J., Carter, A.B., Darley-Usmar, V.M., and Thannickal, V.J. (2017). NADPH Oxidase 4 (Nox4) Suppresses Mitochondrial Biogenesis and Bioenergetics in Lung Fibroblasts via a Nuclear Factor Erythroid-derived 2-like 2 (Nrf2)-dependent Pathway. J. Biol. Chem. *292*, 3029–3038.

Bhaskar, P.T., Nogueira, V., Patra, K.C., Jeon, S.-M., Park, Y., Robey, R.B., and Hay, N. (2009). mTORC1 hyperactivity inhibits serum deprivation-induced apoptosis via increased hexokinase II and GLUT1 expression, sustained Mcl-1 expression, and glycogen synthase kinase 3beta inhibition. Mol. Cell. Biol. *29*, 5136–5147.

Birsoy, K., Possemato, R., Lorbeer, F.K., Bayraktar, E.C., Thiru, P., Yucel, B., Wang, T., Chen, W.W., Clish, C.B., and Sabatini, D.M. (2014). Metabolic determinants of cancer cell sensitivity to glucose limitation and biguanides. Nature *508*, 108–112.

Blancher, C., Moore, J.W., Robertson, N., and Harris, A.L. (2001). Effects of ras and von Hippel-Lindau (VHL) gene mutations on hypoxia-inducible factor (HIF)-1alpha, HIF-2alpha, and vascular endothelial growth factor expression and their regulation by the phosphatidylinositol 3'-kinase/Akt signaling pathway. Cancer Res. *61*,

7349–7355.

Bluemlein, K., Grüning, N.-M., Feichtinger, R.G., Lehrach, H., Kofler, B., Ralser, M., Bluemlein, K., Grüning, N.-M., Feichtinger, R.G., Lehrach, H., et al. (2011). No evidence for a shift in pyruvate kinase PKM1 to PKM2 expression during tumorigenesis. Oncotarget *2*, 393–400.

Bondue, B., Sherer, F., Van Simaeys, G., Doumont, G., Egrise, D., Yakoub, Y., Huaux, F., Parmentier, M., Rorive, S., Sauvage, S., et al. (2015). PET/CT with 18F-FDG- and 18F-FBEM-Labeled Leukocytes for Metabolic Activity and Leukocyte Recruitment Monitoring in a Mouse Model of Pulmonary Fibrosis. J. Nucl. Med. *56*, 127–132.

Bondue, B., Castiaux, A., Van Simaeys, G., Mathey, C., Sherer, F., Egrise, D., Lacroix, S., Huaux, F., Doumont, G., and Goldman, S. (2019). Absence of early metabolic response assessed by 18F-FDG PET/CT after initiation of antifibrotic drugs in IPF patients. Respir. Res. *20*, 10.

Bonniaud, P., Margetts, P.J., Kolb, M., Schroeder, J.A., Kapoun, A.M., Damm, D., Murphy, A., Chakravarty, S., Dugar, S., Higgins, L., et al. (2005). Progressive transforming growth factor beta1-induced lung fibrosis is blocked by an orally active ALK5 kinase inhibitor. Am. J. Respir. Crit. Care Med. *171*, 889–898.

BORZONE, G., MORENO, R., URREA, R., MENESES, M., OYARZÚN, M., and LISBOA, C. (2001). Bleomycin-Induced Chronic Lung Damage Does Not Resemble Human Idiopathic Pulmonary Fibrosis. Am. J. Respir. Crit. Care Med. *163*, 1648–1653.

Brahimi-Horn, M.C., Chiche, J., and Pouysségur, J. (2007). Hypoxia signalling controls metabolic demand. Curr. Opin. Cell Biol. *19*, 223–229.

Buck, M.D., O'Sullivan, D., Pearce, E.L., Sullivan, D.O., and Pearce, E.L. (2015). T cell metabolism drives immunity. J. Exp. Med. *212*, 1345–1360.

Buck, M.D., Sowell, R.T., Kaech, S.M., and Pearce, E.L. (2017). Metabolic Instruction of Immunity. Cell *169*, 570–586.

Bueno, M., Lai, Y., Romero, Y., Brands, J., Croix, C.M.S., Kamga, C., Corey, C., Herazo-maya, J.D., Sembrat, J., Lee, J.S., et al. (2015). PINK1 deficiency impairs mitochondrial homeostasis and promotes lung fibrosis. *125*, 521–538.

Buller, C., Loberg, R., and Fan, M. (2008). A GSK-3 / TSC2 / mTOR pathway regulates glucose uptake and GLUT1 glucose transporter expression. Am. J. … *0680*, 836–843.

Burgess, J.K., Mauad, T., Tjin, G., Karlsson, J.C., and Westergren-Thorsson, G. (2016). The Extracellular Matrix - the under-recognised element in lung disease? J. Pathol. 397–409.

Cai, Y., Zhu, L., Zhang, F., Niu, G., Lee, S., Kimura, S., and Chen, X. (2013). Noninvasive monitoring of

pulmonary fibrosis by targeting matrix metalloproteinases (MMPs). Mol. Pharm. *10*, 2237–2247.

Casalena, G., Daehn, I., and Bottinger, E. (2012). Transforming Growth Factor-??, Bioenergetics, and Mitochondria in Renal Disease. Semin. Nephrol. *32*, 295–303.

Castiaux, A., Van Simaeys, G., Goldman, S., and Bondue, B. Assessment of 18F-FDG uptake in idiopathic pulmonary fibrosis: influence of lung density changes.

Chambers, R.C., and Mercer, P.F. (2015). Mechanisms of alveolar epithelial injury, repair, and fibrosis. Ann. Am. Thorac. Soc. *12*, S16–S20.

Chambers, R.C., Leoni, P., Kaminski, N., Laurent, G.J., and Heller, R. a. (2003). Global Expression Profiling of Fibroblast Responses to Transforming Growth Factor-β1 Reveals the Induction of Inhibitor of Differentiation-1 and Provides Evidence of Smooth Muscle Cell Phenotypic Switching. Am. J. Pathol. *162*, 533–546.

Chandel, N.S. (2015). Navigating Metabolism (John Inglis).

Chang, W., Wei, K., Ho, L., Berry, G.J., Jacobs, S.S., Chang, C.H., and Rosen, G.D. (2014). A critical role for the mTORC2 pathway in lung fibrosis. PLoS One *9*.

Chaponnier, C., and Gabbiani, G. (2004). Pathological situations characterized by altered actin isoform expression. J. Pathol. *204*, 386–395.

Chen, C.Z.C., Peng, Y.X., Wang, Z.B., Fish, P. V, Kaar, J.L., Koepsel, R.R., Russell, a J., Lareu, R.R., and Raghunath, M. (2009). The Scar-in-a-Jar: studying potential antifibrotic compounds from the epigenetic to extracellular level in a single well. Br. J. Pharmacol. *158*, 1196–1209.

Chen, D.L., Cheriyan, J., Chilvers, E.R., Choudhury, G., Coello, C., Connell, M., Fisk, M., Groves, A.M., Gunn, R.N., Holman, B.F., et al. (2017). Quantification of Lung PET Images: Challenges and Opportunities. J. Nucl. Med. *58*, 201–207.

Cheng, K., and Hao, M. (2016). Metformin Inhibits TGF-β1-Induced Epithelial-to-Mesenchymal Transition via PKM2 Relative-mTOR/p70s6k Signaling Pathway in Cervical Carcinoma Cells. Int. J. Mol. Sci. *17*.

Chiarini, F., Evangelisti, C., McCubrey, J.A., and Martelli, A.M. (2015). Current treatment strategies for inhibiting mTOR in cancer. Trends Pharmacol. Sci. *36*, 124–135.

Cho, S.J., Moon, J.-S., Lee, C.-M., Choi, A.M.K., and Stout-Delgado, H.W. (2017). Glucose Transporter 1–Dependent Glycolysis Is Increased during Aging-Related Lung Fibrosis, and Phloretin Inhibits Lung Fibrosis. Am. J. Respir. Cell Mol. Biol. *56*, 521–531.

Christofk, H.R., Vander Heiden, M.G., Harris, M.H., Ramanathan, A., Gerszten, R.E., Wei, R., Fleming, M.D., Schreiber, S.L., and Cantley, L.C. (2008). The M2 splice isoform of pyruvate kinase is important for cancer

metabolism and tumour growth. Nature *452*, 230–233.

Colgan, D.A., Judge, J.L., Wahl, L.A., Sime, P.J., and Kottmann, R.M. (2015). The Lactate Transporter Inhibitor, Alpha-Cyano-4-Hydroxycinnamic Acid, Inhibits Tgf-Beta Induced Myofibroblast Differentiation. Am. J. Respir. Crit. Care Med. *191*, A4923.

Cong, L.-N., Chen, H., Li, Y., Zhou, L., McGibbon, M.A., Taylor, S.I., and Quon, M.J. (1997). Physiological Role of Akt in Insulin-Stimulated Translocation of GLUT4 in Transfected Rat Adipose Cells. Mol. Endocrinol. *11*, 1881–1890.

Conte, E., Fruciano, M., Fagone, E., Gili, E., Caraci, F., Iemmolo, M., Crimi, N., and Vancheri, C. (2011). Inhibition of PI3K Prevents the Proliferation and Differentiation of Human Lung Fibroblasts into Myofibroblasts: The Role of Class I P110 Isoforms. PLoS One *6*, e24663.

Conte, E., Gili, E., Fruciano, M., Korfei, M., Fagone, E., Iemmolo, M., Lo Furno, D., Giuffrida, R., Crimi, N., Guenther, A., et al. (2013). PI3K p110γ overexpression in idiopathic pulmonary fibrosis lung tissue and fibroblast cells: In vitro effects of its inhibition. Lab. Investig. *93*, 566–576.

Cramer, T., and Editors, C.A.S. (2016). Metabolism in Cancer.

Cuperlovic-Culf, M., Cormier, K., Touaibia, M., Reyjal, J., Robichaud, S., Belbraouet, M., and Turcotte, S. (2016). (1) H NMR metabolomics analysis of renal cell carcinoma cells: Effect of VHL inactivation on metabolism. Int. J. Cancer *138*, 2439–2449.

Cutroneo, K.R., White, S.L., Phan, S.H., and Ehrlich, H.P. (2007). Therapies for bleomycin induced lung fibrosis through regulation of TGF-β1 induced collagen gene expression. J. Cell. Physiol. *211*, 585–589.

Dancer, R.C.A., Wood, A.M., and Thickett, D.R. (2011). Metalloproteinases in idiopathic pulmonary fibrosis. Eur. Respir. J. *38*, 1461–1467.

Dayton, T.L., Jacks, T., and Vander Heiden, M.G. (2016). PKM2, cancer metabolism, and the road ahead. EMBO Rep. *17*, 1721–1730.

De Bock, K., Georgiadou, M., Schoors, S., Kuchnio, A., Wong, B.W., Cantelmo, A.R., Quaegebeur, A., Ghesquière, B., Cauwenberghs, S., Eelen, G., et al. (2013). Role of PFKFB3-Driven Glycolysis in Vessel Sprouting. Cell *154*, 651–663.

Degryse, A.L., Tanjore, H., Xu, X.C., Polosukhin, V. V, Jones, B.R., McMahon, F.B., Gleaves, L.A., Blackwell, T.S., and Lawson, W.E. (2010). Repetitive intratracheal bleomycin models several features of idiopathic pulmonary fibrosis. Am. J. Physiol. Lung Cell. Mol. Physiol. *299*, L442-52.

Deprez, J., Vertommen, D., Alessi, D.R., Hue, L., and Rider, M.H. (1997). Phosphorylation and activation of heart 6-phosphofructo-2-kinase by protein kinase B and other protein kinases of the insulin signaling

cascades. J. Biol. Chem. *272*, 17269–17275.

Derynck, R., and Zhang, Y.E. (2003). Smad-dependent and Smad-independent pathways in TGF-β family signalling. Nature *425*, 577–584.

Desmoulière, A., Geinoz, A., Gabbiani, F., and Gabbiani, G. (1993). Transforming growth factor-beta 1 induces alpha-smooth muscle actin expression in granulation tissue myofibroblasts and in quiescent and growing cultured fibroblasts. J. Cell Biol. *122*, 103–111.

Desmoulière, A., Redard, M., Darby, I., and Gabbiani, G. (1995). Apoptosis mediates the decrease in cellularity during the transition between granulation tissue and scar. Am. J. Pathol. *146*, 56–66.

Devaskar, S.U., and deMello, D.E. (1996). Cell-specific localization of glucose transporter proteins in mammalian lung. J. Clin. Endocrinol. Metab. *81*, 4373–4378.

Devic, S. (2016). Warburg Effect - a Consequence or the Cause of Carcinogenesis? J. Cancer *7*, 817–822.

Dickson, M.C., Martin, J.S., Cousins, F.M., Kulkarni, A.B., Karlsson, S., and Akhurst, R.J. (1995). Defective haematopoiesis and vasculogenesis in transforming growth factor-beta 1 knock out mice. Development *121*, 1845–1854.

Dodd, K.M., Yang, J., Shen, M.H., Sampson, J.R., and Tee, A.R. (2015). mTORC1 drives HIF-1α and VEGF-A signalling via multiple mechanisms involving 4E-BP1, S6K1 and STAT3. Oncogene *34*, 2239–2250.

Doherty, J.R., and Cleveland, J.L. (2013). Targeting lactate metabolism for cancer therapeutics. J. Clin. Invest. *123*, 3685–3692.

Duchemann, B., Annesi-Maesano, I., Jacobe de Naurois, C., Sanyal, S., Brillet, P.-Y., Brauner, M., Kambouchner, M., Huynh, S., Naccache, J.M., Borie, R., et al. (2017). Prevalence and incidence of interstitial lung diseases in a multi-ethnic county of Greater Paris. Eur. Respir. J. *50*, 1602419.

Düvel, K., Yecies, J.L., Menon, S., Raman, P., Lipovsky, A.I., Souza, A.L., Triantafellow, E., Ma, Q., Gorski, R., Cleaver, S., et al. (2010). Activation of a metabolic gene regulatory network downstream of mTOR complex 1. Mol. Cell *39*, 171–183.

Eickelberg, O., and Laurent, G.J. (2010). The Quest for the Initial Lesion in Idiopathic Pulmonary Fibrosis. Am. J. Respir. Cell Mol. Biol. *42*, 1–2.

Eickelberg, O., Köhler, E., Reichenberger, F., Bertschin, S., Woodtli, T., Erne, P., Perruchoud, A.P., and Roth, M. (1999). Extracellular matrix deposition by primary human lung fibroblasts in response to TGF-beta1 and TGF-beta3. Am. J. Physiol. *276*, L814-24.

Eilers, M., and Eisenman, R.N. (2008). Myc's broad reach. Genes Dev. *22*, 2755–2766.

El-Chemaly, S., Malide, D., Yao, J., Nathan, S.D., Rosas, I.O., Gahl, W.A., Moss, J., and Gochuico, B.R. (2013). Glucose transporter-1 distribution in fibrotic lung disease: Association with [18F]-2-fluoro-2-deoxyglucose-PET scan uptake, inflammation, and neovascularization. Chest *143*, 1685–1691.

Eley, J.D. (2018). Investigating the role of mTOR signalling in mediating the pro-fibrotic effects of TGF-β1. University College London.

Emwas, A.-H.M. (2015). The strengths and weaknesses of NMR spectroscopy and mass spectrometry with particular focus on metabolomics research. Methods Mol. Biol. *1277*, 161–193.

Emwas, A.-H.M., Salek, R.M., Griffin, J.L., and Merzaban, J. (2013). NMR-based metabolomics in human disease diagnosis: applications, limitations, and recommendations. Metabolomics *9*, 1048–1072.

Engelman, J.A., Chen, L., Tan, X., Crosby, K., Guimaraes, A.R., Upadhyay, R., Maira, M., McNamara, K., Perera, S.A., Song, Y., et al. (2008). Effective use of PI3K and MEK inhibitors to treat mutant Kras G12D and PIK3CA H1047R murine lung cancers. Nat. Med. *14*, 1351–1356.

Esposito, D.B., Lanes, S., Donneyong, M., Holick, C.N., Lasky, J.A., Lederer, D., Nathan, S.D., O'Quinn, S., Parker, J., and Tran, T.N. (2015). Idiopathic Pulmonary Fibrosis in United States Automated Claims. Incidence, Prevalence, and Algorithm Validation. Am. J. Respir. Crit. Care Med. *192*, 1200–1207.

Everts, B., Amiel, E., Huang, S.C.-C., Smith, A.M., Chang, C.-H., Lam, W.Y., Redmann, V., Freitas, T.C., Blagih, J., van der Windt, G.J.W., et al. (2014). TLR-driven early glycolytic reprogramming via the kinases TBK1-IKKε supports the anabolic demands of dendritic cell activation. Nat. Immunol. *15*, 323–332.

Faubert, B., Li, K.Y., Cai, L., Hensley, C.T., Kim, J., Zacharias, L.G., Yang, C., Do, Q.N., Doucette, S., Burguete, D., et al. (2017). Lactate Metabolism in Human Lung Tumors. Cell *171*, 358–371.e9.

Fernandez, I.E., and Eickelberg, O. (2012). The Impact of TGF-β on Lung Fibrosis. Proc. Am. Thorac. Soc. *9*, 111–116.

Forty, E., Azuelos, I., Kalber, T., Gendron, T., Zaw-Thin, M., Vitulli, G., Barrett, J., Anastasiou, D., Mercer, P., Blanchard, A., et al. (2017). LSC - 2017 - Targeting glucose metabolism in experimental lung injury and fibrosis. In Mechanisms of Lung Injury and Repair, (European Respiratory Society), p. PA3470.

Fruman, D.A., and Rommel, C. (2014). PI3K and cancer: lessons, challenges and opportunities. Nat. Rev. Drug Discov. *13*, 140–156.

Galligan, C.L., and Fish, E.N. (2013). The role of circulating fibrocytes in inflammation and autoimmunity. J. Leukoc. Biol. *93*, 45–50.

García-Martínez, J.M., and Alessi, D.R. (2008). mTOR complex 2 (mTORC2) controls hydrophobic motif phosphorylation and activation of serum- and glucocorticoid-induced protein kinase 1 (SGK1). Biochem. J.

416, 375–385.

Gerencser, A.A., Neilson, A., Choi, S.W., Edman, U., Yadava, N., Oh, R.J., Ferrick, D.A., Nicholls, D.G., and Brand, M.D. (2009). Quantitative microplate-based respirometry with correction for oxygen diffusion. Anal. Chem. *81*, 6868–6878.

Gerriets, V.A., and Rathmell, J.C. (2012). Metabolic pathways in T cell fate and function. Trends Immunol. *33*, 168–173.

Goldsmith, K.T., Gammon, R.B., and Garver, R.I. (1991). Modulation of bFGF in lung fibroblasts by TGF-beta and PDGF. Am. J. Physiol. *261*, L378-85.

Goodwin, J., Choi, H., Hsieh, M., Neugent, M.L., Ahn, J.-M., Hayenga, H.N., Singh, P.K., Shackelford, D.B., Lee, I.-K., Shulaev, V., et al. (2018). Targeting Hypoxia-Inducible Factor-1a/Pyruvate Dehydrogenase Kinase 1 Axis by Dichloroacetate Suppresses Bleomycin-induced Pulmonary Fibrosis. Am. J. Respir. Cell Mol. Biol. *58*, 216–231.

Gregory, M.A., Qi, Y., and Hann, S.R. (2003). Phosphorylation by Glycogen Synthase Kinase-3 Controls c-Myc Proteolysis and Subnuclear Localization. J. Biol. Chem. *278*, 51606–51612.

Grimminger, F., Günther, A., and Vancheri, C. (2015). The role of tyrosine kinases in the pathogenesis of idiopathic pulmonary fibrosis. Eur. Respir. J. *45*, 1426–1433.

Grotendorst, G.R., Okochi, H., and Hayashi, N. (1996). A novel transforming growth factor beta response element controls the expression of the connective tissue growth factor gene. Cell Growth Differ. *7*, 469–480.

Groves, A.M., Win, T., Screaton, N.J., Berovic, M., Endozo, R., Booth, H., Kayani, I., Menezes, L.J., Dickson, J.C., and Ell, P.J. (2009). Idiopathic Pulmonary Fibrosis and Diffuse Parenchymal Lung Disease: Implications from Initial Experience with 18F-FDG PET/CT. J. Nucl. Med. *50*, 538–545.

Gui, Y.-S.S., Wang, L., Tian, X., Li, X., Ma, A., Zhou, W., Zeng, N., Zhang, J., Cai, B., Zhang, H., et al. (2015). mTOR Overactivation and Compromised Autophagy in the Pathogenesis of Pulmonary Fibrosis. PLoS One *10*, e0138625.

Guillermet-Guibert, J., Bjorklof, K., Salpekar, A., Gonella, C., Ramadani, F., Bilancio, A., Meek, S., Smith, A.J.H., Okkenhaug, K., and Vanhaesebroeck, B. (2008). The p110 isoform of phosphoinositide 3-kinase signals downstream of G protein-coupled receptors and is functionally redundant with p110. Proc. Natl. Acad. Sci. *105*, 8292–8297.

Gwinn, D.M., Shackelford, D.B., Egan, D.F., Mihaylova, M.M., Mery, A., Vasquez, D.S., Turk, B.E., and Shaw, R.J. (2008). AMPK Phosphorylation of Raptor Mediates a Metabolic Checkpoint. Mol. Cell *30*, 214–226.

Haar, E. Vander, Lee, S., Bandhakavi, S., Griffin, T.J., and Kim, D.-H. (2007). Insulin signalling to mTOR

mediated by the Akt/PKB substrate PRAS40. Nat. Cell Biol. *9*, 316–323.

Haissaguerre, M., Saucisse, N., and Cota, D. (2014). Influence of mTOR in energy and metabolic homeostasis. Mol. Cell. Endocrinol. *397*, 67–77.

Hamanaka, R.B., and Chandel, N.S. (2012). Targeting glucose metabolism for cancer therapy. J. Exp. Med. *209*, 211–215.

Hamid, Q., Martin, J., and Shannon, J.R. (2005). Physiologic Basis of Respiratory Disease (Hamilton, Ontario: BC Decker).

Vander Heiden, M.G., Plas, D.R., Rathmell, J.C., Fox, C.J., Harris, M.H., and Thompson, C.B. (2001). Growth factors can influence cell growth and survival through effects on glucose metabolism. Mol. Cell. Biol. *21*, 5899–5912.

Vander Heiden, M.G., Cantley, L.C., and Thompson, C.B. (2009). Understanding the Warburg effect: the metabolic requirements of cell proliferation. Science *324*, 1029–1033.

Heldin, C.-H., and Moustakas, A. (2016). Signaling Receptors for TGF-β Family Members. Cold Spring Harb. Perspect. Biol. *8*, a022053.

Higashiyama, H., Yoshimoto, D., Kaise, T., Matsubara, S., Fujiwara, M., Kikkawa, H., Asano, S., and Kinoshita, M. (2007). Inhibition of activin receptor-like kinase 5 attenuates bleomycin-induced pulmonary fibrosis. Exp. Mol. Pathol. *83*, 39–46.

Hinz, B. (2009). Tissue stiffness, latent TGF-beta1 activation, and mechanical signal transduction: implications for the pathogenesis and treatment of fibrosis. Curr. Rheumatol. Rep. *11*, 120–126.

Hinz, B., Phan, S.H., Thannickal, V.J., Prunotto, M., Desmoulière, A., Varga, J., De Wever, O., Mareel, M., and Gabbiani, G. (2012). Recent Developments in Myofibroblast Biology. Am. J. Pathol. *180*, 1340–1355.

Hirschey, M.D., DeBerardinis, R.J., Diehl, A.M.E., Drew, J.E., Frezza, C., Green, M.F., Jones, L.W., Ko, Y.H., Le, A., Lea, M.A., et al. (2015). Dysregulated metabolism contributes to oncogenesis. Semin. Cancer Biol. *35*, S129–S150.

HMDB (2010). Human Metabolome Database. Http://Www.Hmdb.Ca/ 12–14.

Ho, W.-T., Chang, J.-S., Su, C.-C., Chang, S.-W., Hu, F.-R., Jou, T.-S., and Wang, I.-J. (2015). Inhibition of Matrix Metalloproteinase Activity Reverses Corneal Endothelial-Mesenchymal Transition. Am. J. Pathol. *185*, 2158–2167.

Holman, B.F., Cuplov, V., Millner, L., Hutton, B.F., Maher, T.M., Groves, A.M., and Thielemans, K. (2015). Improved correction for the tissue fraction effect in lung PET/CT imaging. Phys. Med. Biol. *60*, 7387–7402.

Huang, S., and Czech, M.P. (2007). The GLUT4 Glucose Transporter. Cell Metab. *5*, 237–252.

Hui, S., Ghergurovich, J.M., Morscher, R.J., Jang, C., Teng, X., Lu, W., Esparza, L.A., Reya, T., Le Zhan, Yanxiang Guo, J., et al. (2017). Glucose feeds the TCA cycle via circulating lactate. Nature *551*, 115–118.

Huse, M., Muir, T.W., Xu, L., Chen, Y.G., Kuriyan, J., and Massagué, J. (2001). The TGF beta receptor activation process: an inhibitor- to substrate-binding switch. Mol. Cell *8*, 671–682.

Hutchinson, J., Fogarty, A., Hubbard, R., and McKeever, T. (2015). Global incidence and mortality of idiopathic pulmonary fibrosis: a systematic review. Eur. Respir. J. *46*, 795–806.

Hynes, R.O. (2002). Integrins: bidirectional, allosteric signaling machines. Cell *110*, 673–687.

Inoki, K., Haneda, M., Maeda, S., Koya, D., Kikkawa, R., and Science, M. (1999). TGF-beta 1 stimulates glucose uptake by enhancing GLUT1 expression in mesangial cells. Kidney Int. *55*, 1704–1712.

Inoki, K., Zhu, T., and Guan, K.-L. (2003). TSC2 Mediates Cellular Energy Response to Control Cell Growth and Survival. Cell *115*, 577–590.

Ito, K., and Suda, T. (2014). Metabolic requirements for the maintenance of self-renewing stem cells. Nat. Rev. Mol. Cell Biol. *15*, 243–256.

Jacobs, S.R., Herman, C.E., Maciver, N.J., Wofford, J.A., Wieman, H.L., Hammen, J.J., and Rathmell, J.C. (2008). Glucose uptake is limiting in T cell activation and requires CD28-mediated Akt-dependent and independent pathways. J. Immunol. *180*, 4476–4486.

Jenkins, R.G., Moore, B.B., Chambers, R.C., Eickelberg, O., Königshoff, M., Kolb, M., Laurent, G.J., Nanthakumar, C.B., Olman, M.A., Pardo, A., et al. (2017). An Official American Thoracic Society Workshop Report: Use of Animal Models for the Preclinical Assessment of Potential Therapies for Pulmonary Fibrosis. Am. J. Respir. Cell Mol. Biol. *56*, 667–679.

Jha, A.K., Huang, S.C.-C., Sergushichev, A., Lampropoulou, V., Ivanova, Y., Loginicheva, E., Chmielewski, K., Stewart, K.M., Ashall, J., Everts, B., et al. (2015). Network Integration of Parallel Metabolic and Transcriptional Data Reveals Metabolic Modules that Regulate Macrophage Polarization. Immunity *42*, 419–430.

Judge, J.L., Lacy, S.H., Ku, W.-Y., Owens, K.M., Hernady, E., Thatcher, T.H., Williams, J.P., Phipps, R.P., Sime, P.J., and Kottmann, R.M. (2017). The Lactate Dehydrogenase Inhibitor Gossypol Inhibits Radiation-Induced Pulmonary Fibrosis. Radiat. Res. *188*, 35–43.

Judge, J.L., Nagel, D.J., Owens, K.M., Rackow, A., Phipps, R.P., Sime, P.J., and Kottmann, R.M. (2018). Prevention and treatment of bleomycin-induced pulmonary fibrosis with the lactate dehydrogenase inhibitor gossypol. PLoS One *13*, e0197936.

Jürgensen, H.J., Madsen, D.H., Ingvarsen, S., Melander, M.C., Gårdsvoll, H., Patthy, L., Engelholm, L.H., and Behrendt, N. (2011). A novel functional role of collagen glycosylation: interaction with the endocytic collagen receptor uparap/ENDO180. J. Biol. Chem. *286*, 32736–32748.

Justet, A., Laurent-Bellue, A., Thabut, G., Dieudonné, A., Debray, M.-P., Borie, R., Aubier, M., Lebtahi, R., and Crestani, B. (2017). [18F]FDG PET/CT predicts progression-free survival in patients with idiopathic pulmonary fibrosis. Respir. Res. *18*, 74.

Juvekar, A., Burga, L.N., Hu, H., Lunsford, E.P., Ibrahim, Y.H., Balmañà, J., Rajendran, A., Papa, A., Spencer, K., Lyssiotis, C.A., et al. (2012). Combining a PI3K inhibitor with a PARP inhibitor provides an effective therapy for BRCA1-related breast cancer. Cancer Discov. *2*, 1048–1063.

Kafri, M., Metzl-Raz, E., Jona, G., and Barkai, N. (2016). The Cost of Protein Production. Cell Rep. *14*, 22–31.

Kaira, K., Serizawa, M., Koh, Y., Takahashi, T., Yamaguchi, A., Hanaoka, H., Oriuchi, N., Endo, M., Ohde, Y., Nakajima, T., et al. (2014). Biological significance of 18F-FDG uptake on PET in patients with non-small-cell lung cancer. Lung Cancer *83*, 197–204.

Kang, J.-G., Wang, P., and Hwang, P.M. (2014). Cell-based measurements of mitochondrial function in human subjects. Methods Enzymol. *542*, 209–221.

Kaunisto, J., Salomaa, E.-R., Hodgson, U., Kaarteenaho, R., and Myllärniemi, M. (2013). Idiopathic pulmonary fibrosis--a systematic review on methodology for the collection of epidemiological data. BMC Pulm. Med. *13*, 53.

Keerthisingam, C.B., Jenkins, R.G., Harrison, N.K., Hernandez-Rodriguez, N.A., Booth, H., Laurent, G.J., Hart, S.L., Foster, M.L., and McAnulty, R.J. (2001). Cyclooxygenase-2 Deficiency Results in a Loss of the Anti-Proliferative Response to Transforming Growth Factor-β in Human Fibrotic Lung Fibroblasts and Promotes Bleomycin-Induced Pulmonary Fibrosis in Mice. Am. J. Pathol. *158*, 1411–1422.

Khalil, N., O'Connor, R.N., Unruh, H.W., Warren, P.W., Flanders, K.C., Kemp, A., Bereznay, O.H., and Greenberg, A.H. (1991). Increased production and immunohistochemical localization of transforming growth factor-beta in idiopathic pulmonary fibrosis. Am. J. Respir. Cell Mol. Biol. *5*, 155–162.

Kheirollahi, V., Wasnick, R.M., Biasin, V., Vazquez-Armendariz, A.I., Chu, X., Moiseenko, A., Weiss, A., Wilhelm, J., Zhang, J.-S., Kwapiszewska, G., et al. (2019). Metformin induces lipogenic differentiation in myofibroblasts to reverse lung fibrosis. Nat. Commun. *10*, 2987.

Kim, D.-H., Sarbassov, D.D., Ali, S.M., King, J.E., Latek, R.R., Erdjument-Bromage, H., Tempst, P., and Sabatini, D.M. (2002). mTOR interacts with raptor to form a nutrient-sensitive complex that signals to the cell growth machinery. Cell *110*, 163–175.

Kim, J., Tchernyshyov, I., Semenza, G.L., and Dang, C. V. (2006a). HIF-1-mediated expression of pyruvate dehydrogenase kinase: A metabolic switch required for cellular adaptation to hypoxia. Cell Metab. *3*, 177–185.

Kim, J. -w., Zeller, K.I., Wang, Y., Jegga, A.G., Aronow, B.J., O'Donnell, K.A., and Dang, C. V. (2004). Evaluation of Myc E-Box Phylogenetic Footprints in Glycolytic Genes by Chromatin Immunoprecipitation Assays. Mol. Cell. Biol. *24*, 5923–5936.

Kim, K.K., Kugler, M.C., Wolters, P.J., Robillard, L., Galvez, M.G., Brumwell, A.N., Sheppard, D., and Chapman, H.A. (2006b). Alveolar epithelial cell mesenchymal transition develops in vivo during pulmonary fibrosis and is regulated by the extracellular matrix. Proc. Natl. Acad. Sci. *103*, 13180–13185.

Kim, Y.-W., Park, J., Lee, H.-J., Lee, S.-Y., and Kim, S.-J. (2012). TGF-β sensitivity is determined by N-linked glycosylation of the type II TGF-β receptor. Biochem. J. *445*, 403–411.

King, C.S., and Nathan, S.D. (2015). Practical considerations in the pharmacologic treatment of idiopathic pulmonary fibrosis. Curr. Opin. Pulm. Med. *21*, 479–489.

King, T.E., Schwarz, M.I., Brown, K., Tooze, J.A., Colby, T. V, Waldron, J.A., Flint, A., Thurlbeck, W., and Cherniack, R.M. (2001). Idiopathic pulmonary fibrosis: relationship between histopathologic features and mortality. Am. J. Respir. Crit. Care Med. *164*, 1025–1032.

King, T.E., Bradford, W.Z., Castro-Bernardini, S., Fagan, E. a, Glaspole, I., Glassberg, M.K., Gorina, E., Hopkins, P.M., Kardatzke, D., Lancaster, L., et al. (2014). A Phase 3 Trial of Pirfenidone in Patients with Idiopathic Pulmonary Fibrosis. N. Engl. J. Med. 1–10.

King, T.E., Pardo, A., and Selman, M. (2016). Idiopathic Pulmonary Fibrosis (European Respiratory Society).

Kitagawa, T., Masumi, A., and Akamatsu, Y. (1991). Transforming growth factor-beta 1 stimulates glucose uptake and the expression of glucose transporter mRNA in quiescent Swiss mouse 3T3 cells. J. Biol. Chem. *266*, 18066–18071.

Kobayashi, H., Enomoto, A., Woods, S.L., Burt, A.D., Takahashi, M., and Worthley, D.L. (2019). Cancer-associated fibroblasts in gastrointestinal cancer. Nat. Rev. Gastroenterol. Hepatol.

Kohn, A.D., Summers, S.A., Birnbaum, M.J., and Roth, R.A. (1996). Expression of a constitutively active Akt Ser/Thr kinase in 3T3-L1 adipocytes stimulates glucose uptake and glucose transporter 4 translocation. J. Biol. Chem. *271*, 31372–31378.

Kostidis, S., Addie, R.D., Morreau, H., Mayboroda, O.A., and Giera, M. (2017). Quantitative NMR analysis of intra- and extracellular metabolism of mammalian cells: A tutorial. Anal. Chim. Acta *980*, 1–24.

Kottmann, R.M., Kulkarni, A. a, Smolnycki, K. a, Lyda, E., Dahanayake, T., Salibi, R., Honnons, S., Jones, C.,

Isern, N.G., Hu, J.Z., et al. (2012). Lactic acid is elevated in idiopathic pulmonary fibrosis and induces myofibroblast differentiation via pH-dependent activation of transforming growth factor-β. Am. J. Respir. Crit. Care Med. *186*, 740–751.

Kottmann, R.M., Trawick, E., Judge, J.L., Wahl, L.A., Epa, A.P., Owens, K.M., Thatcher, T.H., Phipps, R.P., and Sime, P.J. (2015). Pharmacologic inhibition of lactate production prevents myofibroblast differentiation. Am. J. Physiol. Cell. Mol. Physiol. *309*, L1305–L1312.

Kozma, L., Baltensperger, K., Klarlund, J., Porras, A., Santos, E., and Czech, M.P. (1993). The ras signaling pathway mimics insulin action on glucose transporter translocation. Proc. Natl. Acad. Sci. *90*, 4460–4464.

Kubiczkova, L., Sedlarikova, L., Hajek, R., and Sevcikova, S. (2012). TGF-β - an excellent servant but a bad master. J. Transl. Med. *10*.

Kuhn, C., Boldt, J., King, T.E., Crouch, E., Vartio, T., and McDonald, J.A. (1989). An Immunohistochemical Study of Architectural Remodeling and Connective Tissue Synthesis in Pulmonary Fibrosis. Am. Rev. Respir. Dis. *140*, 1693–1703.

Kulkarni, A.B., Huh, C.G., Becker, D., Geiser, A., Lyght, M., Flanders, K.C., Roberts, A.B., Sporn, M.B., Ward, J.M., and Karlsson, S. (1993). Transforming growth factor beta 1 null mutation in mice causes excessive inflammatory response and early death. Proc. Natl. Acad. Sci. U. S. A. *90*, 770–774.

Kunz-Schughart, L.A., and Knuechel, R. (2002). Tumor-associated fibroblasts (part I): Active stromal participants in tumor development and progression? Histol. Histopathol. *17*, 599–621.

Lambrou, T., Groves, A.M., Erlandsson, K., Screaton, N., Endozo, R., Win, T., Porter, J.C., and Hutton, B.F. (2011). The importance of correction for tissue fraction effects in lung PET: preliminary findings. Eur. J. Nucl. Med. Mol. Imaging *38*, 2238–2246.

Lamouille, S., and Derynck, R. (2011). Emergence of the phosphoinositide 3-kinase-Akt-mammalian target of rapamycin axis in transforming growth factor-β-induced epithelial-mesenchymal transition. Cells. Tissues. Organs *193*, 8–22.

Lamouille, S., Connolly, E., Smyth, J.W., Akhurst, R.J., and Derynck, R. (2012). TGF-β-induced activation of mTOR complex 2 drives epithelial-mesenchymal transition and cell invasion. J. Cell Sci. *125*, 1259–1273.

LANDAU, B.R., LASZLO, J., STENGLE, J., and BURK, D. (1958). Certain metabolic and pharmacologic effects in cancer patients given infusions of 2-deoxy-D-glucose. J. Natl. Cancer Inst. *21*, 485–494.

Laplante, M., and Sabatini, D.M. (2013). Regulation of mTORC1 and its impact on gene expression at a glance. J. Cell Sci. *126*, 1713–1719.

Della Latta, V., Cecchettini, A., Del Ry, S., and Morales, M.A.A. (2015). Bleomycin in the setting of lung

fibrosis induction: From biological mechanisms to counteractions. Pharmacol. Res. *97*, 122–130.

Laughner, E., Taghavi, P., Chiles, K., Mahon, P.C., and Semenza, G.L. (2001). HER2 (neu) Signaling Increases the Rate of Hypoxia-Inducible Factor 1 (HIF-1) Synthesis: Novel Mechanism for HIF-1-Mediated Vascular Endothelial Growth Factor Expression. Mol. Cell. Biol. *21*, 3995–4004.

Lawson, W.E., Polosukhin, V. V., Stathopoulos, G.T., Zoia, O., Han, W., Lane, K.B., Li, B., Donnelly, E.F., Holburn, G.E., Lewis, K.G., et al. (2005). Increased and Prolonged Pulmonary Fibrosis in Surfactant Protein C-Deficient Mice Following Intratracheal Bleomycin. Am. J. Pathol. *167*, 1267–1277.

Leask, A., Holmes, A., Black, C.M., and Abraham, D.J. (2003). Connective tissue growth factor gene regulation. Requirements for its induction by transforming growth factor-beta 2 in fibroblasts. J. Biol. Chem. *278*, 13008–13015.

LEASK, A., and ABRAHAM, D.J. (2004). TGF-β signaling and the fibrotic response. FASEB J. *18*, 816–827.

Leese, H.J., and Barton, A.M. (1984). Pyruvate and glucose uptake by mouse ova and preimplantation embryos. J. Reprod. Fertil. *72*, 9–13.

Ley, B., Collard, H.R., and King, T.E. (2011). Clinical course and prediction of survival in idiopathic pulmonary fibrosis. Am. J. Respir. Crit. Care Med. *183*, 431–440.

Li, W., Wei, Z., Liu, Y., Li, H., Ren, R., and Tang, Y. (2010). Increased 18F-FDG uptake and expression of Glut1 in the EMT transformed breast cancer cells induced by TGF-β. Neoplasma *57*, 234–240.

Liebow, A.A. (1975). Definition and Classification of Interstitial Pneumonias in Human Pathology1. *8*, 1–33.

Lin, G., Gai, R., Chen, Z., Wang, Y., Liao, S., Dong, R., Zhu, H., Gu, Y., He, Q., and Yang, B. (2014). The dual PI3K/mTOR inhibitor NVP-BEZ235 prevents epithelial-mesenchymal transition induced by hypoxia and TGF-β1. Eur. J. Pharmacol. *729*, 45–53.

Liu, T., De Los Santos, F.G., and Phan, S.H. (2017). The Bleomycin Model of Pulmonary Fibrosis. In Fibrosis: Methods and Protocols, L. Rittié, ed. (New York, NY: Springer New York), pp. 27–42.

Luengo, A., Gui, D.Y., and Vander Heiden, M.G. (2017). Review Targeting Metabolism for Cancer Therapy. Cell Chem. Biol. *24*, 1161–1180.

Lukey, P.T., Harrison, S.A., Yang, S., Man, Y., Holman, B.F., Rashidnasab, A., Azzopardi, G., Grayer, M., Simpson, J.K., Bareille, P., et al. (2019). A Randomised, Placebo-Controlled Study of Omipalisib (PI3K/mTOR) in Idiopathic Pulmonary Fibrosis. Eur. Respir. J. 1801992.

Lunt, S.Y., and Vander Heiden, M.G. (2011). Aerobic glycolysis: meeting the metabolic requirements of cell proliferation. Annu. Rev. Cell Dev. Biol. *27*, 441–464.

Lynch, M., and Marinov, G.K. (2015). The bioenergetic costs of a gene. Proc. Natl. Acad. Sci. 201514974.

Macheda, M.L., Rogers, S., and Best, J.D. (2005). Molecular and cellular regulation of glucose transporter (GLUT) proteins in cancer. J. Cell. Physiol. *202*, 654–662.

Macintyre, A.N., Gerriets, V.A., Nichols, A.G., Michalek, R.D., Rudolph, M.C., Deoliveira, D., Anderson, S.M., Abel, E.D., Chen, B.J., Hale, L.P., et al. (2014). The Glucose Transporter Glut1 Is Selectively Essential for CD4 T Cell Activation and Effector Function. Cell Metab. *20*, 61–72.

Majewski, N., Nogueira, V., Robey, R.B., and Hay, N. (2004). Akt inhibits apoptosis downstream of BID cleavage via a glucose-dependent mechanism involving mitochondrial hexokinases. Mol. Cell. Biol. *24*, 730–740.

Makinoshima, H., Takita, M., Saruwatari, K., Umemura, S., Obata, Y., Ishii, G., Matsumoto, S., Sugiyama, E., Ochiai, A., Abe, R., et al. (2015). Signaling through the Phosphatidylinositol 3-Kinase (PI3K)/Mammalian Target of Rapamycin (mTOR) Axis Is Responsible for Aerobic Glycolysis mediated by Glucose Transporter in Epidermal Growth Factor Receptor (EGFR)-mutated Lung Adenocarcinoma. J. Biol. Chem. *290*, 17495–17504.

Margadant, C., and Sonnenberg, A. (2010). Integrin–TGF-β crosstalk in fibrosis, cancer and wound healing. EMBO Rep. *11*, 97–105.

Massagué, J. (2008). TGFβ in Cancer. Cell *134*, 215–230.

Massagué, J. (2012). TGFβ signalling in context. Nat. Rev. Mol. Cell Biol. *13*, 616–630.

Masumi, A., Akamatsu, Y., and Kitagawa, T. (1993). Modulation of the synthesis and glycosylation of the glucose transporter protein by transforming growth factor-[beta]1 in Swiss 3T3 fibroblasts. Biochim. Biophys. Acta - Biomembr. *1145*, 227–234.

Mathupala, S.P., Ko, Y.H., and Pedersen, P.L. (2006). Hexokinase II: cancer's double-edged sword acting as both facilitator and gatekeeper of malignancy when bound to mitochondria. Oncogene *25*, 4777–4786.

McAnulty, R.J., Campa, J.S., Cambrey, A.D., and Laurent, G.J. (1991). The effect of transforming growth factor beta on rates of procollagen synthesis and degradation in vitro. Biochim. Biophys. Acta *1091*, 231–235.

Meissner, H.-H., Soo Hoo, G.W., Khonsary, S.A., Mandelkern, M., Brown, C. V, and Santiago, S.M. (2006). Idiopathic pulmonary fibrosis: evaluation with positron emission tomography. Respiration. *73*, 197–202.

Mercer, P.F., Woodcock, H. V, Eley, J.D., Platé, M., Sulikowski, M.G., Durrenberger, P.F., Franklin, L., Nanthakumar, C.B., Man, Y., Genovese, F., et al. (2016). Exploration of a potent PI3 kinase/mTOR inhibitor as a novel anti-fibrotic agent in IPF. Thorax *71*, 701–711.

Michelakis, E.D., Sutendra, G., Dromparis, P., Webster, L., Haromy, A., Niven, E., Maguire, C., Gammer, T.L., Mackey, J.R., Fulton, D., et al. (2010). Metabolic Modulation of Glioblastoma with Dichloroacetate. Sci. Transl. Med. *2*, 31ra34-31ra34.

Millis, S.Z., Ikeda, S., Reddy, S., Gatalica, Z., and Kurzrock, R. (2016). Landscape of Phosphatidylinositol-3-Kinase Pathway Alterations Across 19 784 Diverse Solid Tumors. JAMA Oncol. *0658*, 1–9.

Mishra, P., and Chan, D.C. (2016). Metabolic regulation of mitochondrial dynamics. J. Cell Biol. *212*, 379–387.

Moore, B.B., Lawson, W.E., Oury, T.D., Sisson, T.H., Raghavendran, K., Hogaboam, C.M., B Moore, B., Lawson, W.E., Oury, T.D., Sisson, T.H., et al. (2013). Animal models of fibrotic lung disease. Am. J. Respir. Cell Mol. Biol. *49*, 167–179.

Moreno-Sánchez, R., Rodríguez-Enríquez, S., Marín-Hernández, A., and Saavedra, E. (2007). Energy metabolism in tumor cells. FEBS J. *274*, 1393–1418.

Morita, M., Gravel, S.-P.P., Hulea, L., Larsson, O., Pollak, M., St-Pierre, J., and Topisirovic, I. (2015). MTOR coordinates protein synthesis, mitochondrial activity. Cell Cycle *14*, 473–480.

Munger, J.S., Huang, X., Kawakatsu, H., Griffiths, M.J., Dalton, S.L., Wu, J., Pittet, J.F., Kaminski, N., Garat, C., Matthay, M.A., et al. (1999). The integrin alpha v beta 6 binds and activates latent TGF beta 1: a mechanism for regulating pulmonary inflammation and fibrosis. Cell *96*, 319–328.

Naik, P.K., and Moore, B.B. (2010). Viral infection and aging as cofactors for the development of pulmonary fibrosis. Expert Rev. Respir. Med. *4*, 759–771.

Navale, A.M., and Paranjape, A.N. (2016). Glucose transporters: physiological and pathological roles. Biophys. Rev. *8*, 5–9.

Navaratnam, V., Fleming, K.M., West, J., Smith, C.J.P., Jenkins, R.G., Fogarty, A., and Hubbard, R.B. (2011). The rising incidence of idiopathic pulmonary fibrosis in the U.K. Thorax *66*, 462–467.

Navarro, P., Bueno, M.J., Zagorac, I., Mondejar, T., Sanchez, J., Mourón, S., Muñoz, J., Gómez-López, G., Jimenez-Renard, V., Mulero, F., et al. (2016). Targeting Tumor Mitochondrial Metabolism Overcomes Resistance to Antiangiogenics. Cell Rep. *15*, 2705–2718.

Neill, L.A.J.O., and Pearce, E.J. (2016). Immunometabolism governs dendritic cell and macrophage function. 15–23.

Nocera, M., and Chu, T.M. (1995). Characterization of latent transforming growth factor-beta from human seminal plasma. Am. J. Reprod. Immunol. *33*, 282–291.

Nusair, S., Rubinstein, R., Freedman, N.M., Amir, G., Bogot, N.R., Izhar, U., and Breuer, R. (2007). Positron

emission tomography in interstitial lung disease. Respirology *12*, 843–847.

O'Neill, L.A.J., and Hardie, D.G. (2013). Metabolism of inflammation limited by AMPK and pseudo-starvation. Nature *493*, 346–355.

O'Neill, L.A.J., Kishton, R.J., and Rathmell, J.C. (2016). A guide to immunometabolism for immunologists. Nat. Rev. Immunol.

Okada, T., Kawano, Y., Sakakibara, T., Hazeki, O., and Ui, M. (1994). Essential role of phosphatidylinositol 3-kinase in insulin-induced glucose transport and antilipolysis in rat adipocytes. Studies with a selective inhibitor wortmannin. J. Biol. Chem. *269*, 3568–3573.

Olsen, J.M., Sato, M., Dallner, O.S., Sandstr??m, A.L., Pisani, D.F., Chambard, J.C., Amri, E.Z., Hutchinson, D.S., Bengtsson, T., Sandström, A.L., et al. (2014). Glucose uptake in brown fat cells is dependent on mTOR complex 2-promoted GLUT1 translocation. J. Cell Biol. *207*, 365–374.

Onodera, Y., Nam, J.-M., and Bissell, M.J. (2014). Increased sugar uptake promotes oncogenesis via EPAC/RAP1 and O-GlcNAc pathways. J. Clin. Invest. *124*, 367–384.

Osthus, R.C., Shim, H., Kim, S., Li, Q., Reddy, R., Mukherjee, M., Xu, Y., Wonsey, D., Lee, L.A., and Dang, C. V. (2000). Deregulation of Glucose Transporter 1 and Glycolytic Gene Expression by c-Myc. J. Biol. Chem. *275*, 21797–21800.

Otto Warburg, B., Wind, F., and Negelein, N. (1923). THE METABOLISM OF TUMORS IN THE BODY. The Journal of General Physiology. Biochem. Z. Biochem. Z. Biochem. Z.. Biol. Chem *309*, 397–519.

Overall, C.M., Wrana, J.L., and Sodek, J. (1989). Transforming growth factor-beta regulation of collagenase, 72 kDa-progelatinase, TIMP and PAI-1 expression in rat bone cell populations and human fibroblasts. Connect. Tissue Res. *20*, 289–294.

Palmer, C.S., Ostrowski, M., Balderson, B., Christian, N., and Crowe, S.M. (2015). Glucose Metabolism Regulates T Cell Activation, Differentiation, and Functions. Front. Immunol. *6*, 1.

Pantaleon, M., and Kaye, P.L. (1998). Glucose transporters in preimplantation development. Rev. Reprod. *3*, 77–81.

Park, J.S., Park, H.J., Park, Y.S., Lee, S.-M., Yim, J.-J., Yoo, C.-G., Han, S.K., and Kim, Y.W. (2014). Clinical significance of mTOR, ZEB1, ROCK1 expression in lung tissues of pulmonary fibrosis patients. BMC Pulm. Med. *14*, 168.

Parker, M.W., Rossi, D., Peterson, M., Smith, K., Sikström, K., White, E.S., Connett, J.E., Henke, C.A., Larsson, O., and Bitterman, P.B. (2014). Fibrotic extracellular matrix activates a profibrotic positive feedback loop. J. Clin. Invest. *124*, 1622–1635.

Patching, S. (2015). Roles of facilitative glucose transporter GLUT1 in [18F]FDG positron emission tomography (PET) imaging of human diseases. J. Diagnostic Imaging Ther. *2*, 30–102.

Patel, A.S., Song, J.W., Chu, S.G., Mizumura, K., Osorio, J.C., Shi, Y., El-Chemaly, S., Lee, C.G., Rosas, I.O., Elias, J. a., et al. (2015). Epithelial Cell Mitochondrial Dysfunction and PINK1 Are Induced by Transforming Growth Factor- Beta1 in Pulmonary Fibrosis. PLoS One *10*, e0121246.

Patra, K.C.C., Wang, Q., Bhaskar, P.T.T., Miller, L., Wang, Z., Wheaton, W., Chandel, N., Laakso, M., Muller, W.J.J., Allen, E.L.L., et al. (2013). Hexokinase 2 is required for tumor initiation and maintenance and its systemic deletion is therapeutic in mouse models of cancer. Cancer Cell *24*, 213–228.

Powell, D.W., Mifflin, R.C., Valentich, J.D., Crowe, S.E., Saada, J.I., and West, A.B. (1999). Myofibroblasts. I. Paracrine cells important in health and disease. Am. J. Physiol. Physiol. *277*, C1–C19.

Raghow, R., Postlethwaite, A.E., Keski-Oja, J., Moses, H.L., and Kang, A.H. (1987). Transforming growth factor-beta increases steady state levels of type I procollagen and fibronectin messenger RNAs posttranscriptionally in cultured human dermal fibroblasts. J. Clin. Invest. *79*, 1285–1288.

Raghu, G., Collard, H.R., Egan, J.J., Martinez, F.J., Behr, J., Brown, K.K., Colby, T. V, Cordier, J.-F., Flaherty, K.R., Lasky, J. a, et al. (2011). An official ATS/ERS/JRS/ALAT statement: idiopathic pulmonary fibrosis: evidence-based guidelines for diagnosis and management. Am. J. Respir. Crit. Care Med. *183*, 788–824.

Raghu, G., Chen, S.-Y., Yeh, W.-S., Maroni, B., Li, Q., Lee, Y.-C., and Collard, H.R. (2014). Idiopathic pulmonary fibrosis in US Medicare beneficiaries aged 65 years and older: incidence, prevalence, and survival, 2001-11. Lancet. Respir. Med. *2*, 566–572.

Raghu, G., Remy-Jardin, M., Myers, J.L., Richeldi, L., Ryerson, C.J., Lederer, D.J., Behr, J., Cottin, V., Danoff, S.K., Morell, F., et al. (2018). Diagnosis of Idiopathic Pulmonary Fibrosis. An Official ATS/ERS/JRS/ALAT Clinical Practice Guideline. Am. J. Respir. Crit. Care Med. *198*, e44–e68.

Rahimi, R. a, Andrianifahanana, M., Wilkes, M.C., Edens, M., Kottom, T.J., Blenis, J., and Leof, E.B. (2009). Distinct roles for mammalian target of rapamycin complexes in the fibroblast response to transforming growth factor-beta. Cancer Res. *69*, 84–93.

Rathmell, J.C., Fox, C.J., Plas, D.R., Hammerman, P.S., Cinalli, R.M., and Thompson, C.B. (2003). Akt-directed glucose metabolism can prevent Bax conformation change and promote growth factor-independent survival. Mol. Cell. Biol. *23*, 7315–7328.

Ready, N., Karaseva, N.A., Orlov, S. V., Luft, A. V., Popovych, O., Holmlund, J.T., Wood, B.A., and Leopold, L. (2011). Double-Blind, Placebo-Controlled, Randomized Phase 2 Study of the Proapoptotic Agent AT-101 Plus Docetaxel, in Second-Line Non-small Cell Lung Cancer. J. Thorac. Oncol. *6*, 781–785.

Reilkoff, R.A., Bucala, R., and Herzog, E.L. (2011). Fibrocytes: emerging effector cells in chronic inflammation. Nat. Rev. Immunol. *11*, 427–435.

Richeldi, L., du Bois, R.M., Raghu, G., Azuma, A., Brown, K.K., Costabel, U., Cottin, V., Flaherty, K.R., Hansell, D.M., Inoue, Y., et al. (2014). Efficacy and Safety of Nintedanib in Idiopathic Pulmonary Fibrosis. N. Engl. J. Med. 1–12.

Robey, R.B., and Hay, N. (2009). Is Akt the "Warburg kinase"?-Akt-energy metabolism interactions and oncogenesis. Semin. Cancer Biol. *19*, 25–31.

Rodon, J., Dienstmann, R., Serra, V., and Tabernero, J. (2013). Development of PI3K inhibitors: lessons learned from early clinical trials. Nat. Rev. Clin. Oncol. *10*, 143–153.

Ros, S., and Schulze, A. (2013). Balancing glycolytic flux: the role of 6-phosphofructo-2-kinase/fructose 2,6-bisphosphatases in cancer metabolism. Cancer Metab. *1*, 8.

Ryan, G.B., Cliff, W.J., Gabbiani, G., Irlé, C., Montandon, D., Statkov, P.R., and Majno, G. (1974). Myofibroblasts in human granulation tissue. Hum. Pathol. *5*, 55–67.

Salez, F., Gosset, P., Copin, M.C., Lamblin Degros, C., Tonnel, A.B., and Wallaert, B. (1998). Transforming growth factor-beta1 in sarcoidosis. Eur. Respir. J. *12*, 913–919.

Sandbo, N., and Dulin, N. (2011). Actin cytoskeleton in myofibroblast differentiation: ultrastructure defining form and driving function. Transl. Res. *158*, 181–196.

Sarbassov, D.D., Guertin, D.A., Ali, S.M., and Sabatini, D.M. (2005). Phosphorylation and regulation of Akt/PKB by the rictor-mTOR complex. Science *307*, 1098–1101.

Sarbassov, D.D., Ali, S.M., Sengupta, S., Sheen, J.-H., Hsu, P.P., Bagley, A.F., Markhard, A.L., and Sabatini, D.M. (2006). Prolonged rapamycin treatment inhibits mTORC2 assembly and Akt/PKB. Mol. Cell *22*, 159–168.

Sarrazy, V., Koehler, A., Chow, M.L., Zimina, E., Li, C.X., Kato, H., Caldarone, C.A., and Hinz, B. (2014). Integrins αvβ5 and αvβ3 promote latent TGF-β1 activation by human cardiac fibroblast contraction. Cardiovasc. Res. *102*, 407–417.

Sato, N., Takasaka, N., Yoshida, M., Tsubouchi, K., Minagawa, S., Araya, J., Saito, N., Fujita, Y., Kurita, Y., Kobayashi, K., et al. (2016). Metformin attenuates lung fibrosis development via NOX4 suppression. Respir. Res. *17*, 107.

Saxton, R.A., and Sabatini, D.M. (2017). mTOR Signaling in Growth, Metabolism, and Disease. Cell *168*, 960–976.

Sborov, D.W., Haverkos, B.M., and Harris, P.J. (2015). Investigational cancer drugs targeting cell metabolism in clinical development. Expert Opin. Investig. Drugs *24*, 79–94.

Scotton, C.J., and Chambers, R.C. (2007). Molecular targets in pulmonary fibrosis: The myofibroblast in focus. Chest *132*, 1311–1321.

Scotton, C.J., and Chambers, R.C. (2010). Bleomycin revisited: towards a more representative model of IPF? Am. J. Physiol. Cell. Mol. Physiol. *299*, L439–L441.

Scotton, C.J., Hayes, B., Alexander, R., Datta, A., Forty, E.J., Mercer, P.F., Blanchard, A., and Chambers, R.C. (2013). Ex vivo micro-computed tomography analysis of bleomycin-induced lung fibrosis for preclinical drug evaluation. Eur. Respir. J. *42*, 1633–1645.

Selvarajah, B., Azuelos, I., Forty, E., Plate, M., Anastasiou, D., Mercer, P., and Chambers, R. (2016). Metabolic shift during TGF- β-induced collagen synthesis. In 1.5 Diffuse Parenchymal Lung Disease, (European Respiratory Society), p. OA485.

Selvarajah, B., Azuelos, I., Forty, E., Platé, M., Brunori, G., Edwards, L., Blanchard, A., Anastasiou, D., Mercer, P., and Chambers, R. (2017). LSC - 2017 - A critical role for mTOR regulated metabolic reprogramming during TGF-β induced fibroblast collagen synthesis. In Mechanisms of Lung Injury and Repair, (European Respiratory Society), p. OA4436.

Selvarajah, B., Azuelos, I., Platé, M., Guillotin, D., Forty, E.J., Contento, G., Woodcock, H. V., Redding, M., Taylor, A., Brunori, G., et al. (2019). mTORC1 amplifies the ATF4-dependent de novo serine-glycine pathway to supply glycine during TGF-β 1 –induced collagen biosynthesis. Sci. Signal. *12*, eaav3048.

Semenza, G.L. (2010). HIF-1: upstream and downstream of cancer metabolism. Curr. Opin. Genet. Dev. *20*, 51–56.

Semenza, G.L., Jiang, B.H., Leung, S.W., Passantino, R., Concordet, J.P., Maire, P., and Giallongo, A. (1996). Hypoxia response elements in the aldolase A, enolase 1, and lactate dehydrogenase A gene promoters contain essential binding sites for hypoxia-inducible factor 1. J. Biol. Chem. *271*, 32529–32537.

Serini, G., and Gabbiani, G. (1999). Mechanisms of Myofibroblast Activity and Phenotypic Modulation. Exp. Cell Res. *250*, 273–283.

Shaw, R.J., Bardeesy, N., Manning, B.D., Lopez, L., Kosmatka, M., DePinho, R.A., and Cantley, L.C. (2004). The LKB1 tumor suppressor negatively regulates mTOR signaling. Cancer Cell *6*, 91–99.

Shi, L., Pan, H., Liu, Z., Xie, J., and Han, W. (2017). Roles of PFKFB3 in cancer. Signal Transduct. Target. Ther. *2*, 17044.

Shimobayashi, M., and Hall, M.N. (2014). Making new contacts: the mTOR network in metabolism and

signalling crosstalk. Nat. Rev. Mol. Cell Biol. *15*, 155–162.

Shyh-Chang, N., Daley, G.Q., and Cantley, L.C. (2013). Stem cell metabolism in tissue development and aging. Development *140*, 2535–2547.

Sime, P.J., Xing, Z., Graham, F.L., Csaky, K.G., and Gauldie, J. (1997). Adenovector-mediated gene transfer of active transforming growth factor-beta1 induces prolonged severe fibrosis in rat lung. J. Clin. Invest. *100*, 768–776.

Soga, T. (2013). Cancer metabolism: key players in metabolic reprogramming. Cancer Sci. *104*, 275–281.

Soma, Y., and Grotendorst, G.R. (1989). TGF-? stimulates primary human skin fibroblast DNA synthesis via an autocrine production of PDGF-related peptides. J. Cell. Physiol. *140*, 246–253.

Sosulski, M.L., Gongora, R., Danchuk, S., Dong, C., Luo, F., and Sanchez, C.G. (2015). Deregulation of selective autophagy during aging and pulmonary fibrosis: the role of TGFβ1. Aging Cell *14*, 774–783.

Srivastava, S. (2017). The Mitochondrial Basis of Aging and Age-Related Disorders. Genes (Basel). *8*.

Sueblinvong, V., Neujahr, D.C., Mills, S.T., Roser-Page, S., Ritzenthaler, J.D., Guidot, D., Rojas, M., and Roman, J. (2012). Predisposition for disrepair in the aged lung. Am. J. Med. Sci. *344*, 41–51.

Sun, Q., Chen, X., Ma, J., Peng, H., Wang, F., Zha, X., Wang, Y., Jing, Y., Yang, H., Chen, R., et al. (2011). Mammalian target of rapamycin up-regulation of pyruvate kinase isoenzyme type M2 is critical for aerobic glycolysis and tumor growth. Proc. Natl. Acad. Sci. U. S. A. *108*, 4129–4134.

Syed, F., Sherris, D., Paus, R., Varmeh, S., Singh, S., Pandolfi, P.P., and Bayat, A. (2012). Keloid disease can be inhibited by antagonizing excessive mTOR signaling with a novel dual TORC1/2 inhibitor. Am. J. Pathol. *181*, 1642–1658.

Szablewski, L. (2013). Expression of glucose transporters in cancers. Biochim. Biophys. Acta - Rev. Cancer *1835*, 164–169.

Tang, B., Böttinger, E.P., Jakowlew, S.B., Bagnall, K.M., Mariano, J., Anver, M.R., Letterio, J.J., and Wakefield, L.M. (1998). Transforming growth factor-beta1 is a new form of tumor suppressor with true haploid insufficiency. Nat. Med. *4*, 802–807.

Tannahill, G.M., Curtis, A.M., Adamik, J., Palsson-McDermott, E.M., McGettrick, A.F., Goel, G., Frezza, C., Bernard, N.J., Kelly, B., Foley, N.H., et al. (2013). Succinate is an inflammatory signal that induces IL-1β through HIF-1α. Nature *496*, 238–242.

Tanner, L.B., Goglia, A.G., Wei, M.H., Sehgal, T., Parsons, L.R., Park, J.O., White, E., Toettcher, J.E., and Rabinowitz, J.D. (2018). Four Key Steps Control Glycolytic Flux in Mammalian Cells. Cell Syst. *7*, 49–62.e8.

Tashiro, J., Rubio, G.A., Limper, A.H., Williams, K., Elliot, S.J., Ninou, I., Aidinis, V., Tzouvelekis, A., and Glassberg, M.K. (2017). Exploring Animal Models That Resemble Idiopathic Pulmonary Fibrosis. Front. Med. *4*, 118.

Thomas, G. V, Tran, C., Mellinghoff, I.K., Welsbie, D.S., Chan, E., Fueger, B., Czernin, J., and Sawyers, C.L. (2006). Hypoxia-inducible factor determines sensitivity to inhibitors of mTOR in kidney cancer. Nat. Med. *12*, 122–127.

Travis, M.A., and Sheppard, D. (2014). TGF-β Activation and Function in Immunity. Annu. Rev. Immunol. *32*, 51–82.

Travis, W.D., Costabel, U., Hansell, D.M., King, T.E., Lynch, D.A., Nicholson, A.G., Ryerson, C.J., Ryu, J.H., Selman, M., Wells, A.U., et al. (2013). An Official American Thoracic Society/European Respiratory Society Statement: Update of the International Multidisciplinary Classification of the Idiopathic Interstitial Pneumonias. Am. J. Respir. Crit. Care Med. *188*, 733–748.

Tzivion, G., Dobson, M., and Ramakrishnan, G. (2011). FoxO transcription factors; Regulation by AKT and 14-3-3 proteins. Biochim. Biophys. Acta - Mol. Cell Res. *1813*, 1938–1945.

Vancheri, C. (2013). Common pathways in idiopathic pulmonary fibrosis and cancer. Eur. Respir. Rev. *22*, 265–272.

Vancheri, C., Failla, M., Crimi, N., and Raghu, G. (2010). Idiopathic pulmonary fibrosis: a disease with similarities and links to cancer biology. Eur. Respir. J. *35*, 496–504.

Vanhaesebroeck, B., Guillermet-Guibert, J., Graupera, M., and Bilanges, B. (2010). The emerging mechanisms of isoform-specific PI3K signalling. Nat. Rev. Mol. Cell Biol. *11*, 329–341.

Varum, S., Rodrigues, A.S., Moura, M.B., Momcilovic, O., Easley, C.A., Ramalho-Santos, J., Van Houten, B., and Schatten, G. (2011). Energy Metabolism in Human Pluripotent Stem Cells and Their Differentiated Counterparts. PLoS One *6*, e20914.

Vernieri, C., Casola, S., Foiani, M., Pietrantonio, F., Braud, F. de, and Longo, V. (2016). Targeting Cancer Metabolism: Dietary and Pharmacologic Interventions. Cancer Discov. *6*, 1315–1333.

Wagstaff, J.L., Masterton, R.J., Povey, J.F., Smales, C.M., and Howard, M.J. (2013). ^{1}H NMR spectroscopy profiling of metabolic reprogramming of Chinese hamster ovary cells upon a temperature shift during culture. PLoS One *8*, e77195.

Walker, N.M., Belloli, E.A., Stuckey, L., Chan, K.M., Lin, J., Lynch, W., Chang, A., Mazzoni, S.M., Fingar, D.C., and Lama, V.N. (2016). Mechanistic Target of Rapamycin Complex 1 (mTORC1) and mTORC2 as Key Signaling Intermediates in Mesenchymal Cell Activation. J. Biol. Chem. *291*, 6262–6271.

Wang, R., Novick, S.J., Mangum, J.B., Queen, K., Ferrick, D.A., Rogers, G.W., and Stimmel, J.B. (2015). The Acute Extracellular Flux (XF) Assay to Assess Compound Effects on Mitochondrial Function. J. Biomol. Screen. *20*, 422–429.

Wang, Y., Heilig, K., Saunders, T., Minto, A., Deb, D.K., Chang, A., Brosius, F., Monteiro, C., and Heilig, C.W. (2010). Transgenic overexpression of GLUT1 in mouse glomeruli produces renal disease resembling diabetic glomerulosclerosis. Am. J. Physiol. Physiol. *299*, F99–F111.

WARBURG, O. (1956). On the origin of cancer cells. Science *123*, 309–314.

Webb, B.A., Forouhar, F., Szu, F.-E., Seetharaman, J., Tong, L., and Barber, D.L. (2015). Structures of human phosphofructokinase-1 and atomic basis of cancer-associated mutations. Nature *523*, 111–114.

Weinhouse, S. (1976). The Warburg hypothesis fifty years later. Z. Krebsforsch. Klin. Onkol. Cancer Res. Clin. Oncol. *87*, 115–126.

Welcker, M., Orian, A., Jin, J., Grim, J.A., Harper, J.W., Eisenman, R.N., Clurman, B.E., and Clurman, B.E. (2004). The Fbw7 tumor suppressor regulates glycogen synthase kinase 3 phosphorylation-dependent c-Myc protein degradation. Proc. Natl. Acad. Sci. *101*, 9085–9090.

Win, T., Lambrou, T., Hutton, B.F., Kayani, I., Screaton, N.J., Porter, J.C., Maher, T.M., Endozo, R., Shortman, R.I., Lukey, P., et al. (2012). 18F-Fluorodeoxyglucose positron emission tomography pulmonary imaging in idiopathic pulmonary fibrosis is reproducible: implications for future clinical trials. Eur. J. Nucl. Med. Mol. Imaging *39*, 521–528.

Win, T., Thomas, B. a, Lambrou, T., Hutton, B.F., Screaton, N.J., Porter, J.C., Maher, T.M., Endozo, R., Shortman, R.I., Afaq, A., et al. (2014). Areas of normal pulmonary parenchyma on HRCT exhibit increased FDG PET signal in IPF patients. Eur. J. Nucl. Med. Mol. Imaging *41*, 337–342.

Win, T., Screaton, N.J., Porter, J.C., Ganeshan, B., Maher, T.M., Fraioli, F., Endozo, R., Shortman, R.I., Hurrell, L., Holman, B.F., et al. (2018). Pulmonary 18F-FDG uptake helps refine current risk stratification in idiopathic pulmonary fibrosis (IPF). Eur. J. Nucl. Med. Mol. Imaging *45*, 806–815.

Wofford, J.A., Wieman, H.L., Jacobs, S.R., Zhao, Y., and Rathmell, J.C. (2008). IL-7 promotes Glut1 trafficking and glucose uptake via STAT5-mediated activation of Akt to support T-cell survival. Blood *111*, 2101–2111.

Wolf, A., Agnihotri, S., Micallef, J., Mukherjee, J., Sabha, N., Cairns, R., Hawkins, C., and Guha, A. (2011). Hexokinase 2 is a key mediator of aerobic glycolysis and promotes tumor growth in human glioblastoma multiforme. J. Exp. Med. *208*, 313–326.

Wollin, L., Wex, E., Pautsch, A., Schnapp, G., Hostettler, K.E., Stowasser, S., and Kolb, M. (2015). Mode of action of nintedanib in the treatment of idiopathic pulmonary fibrosis. Eur. Respir. J. *45*, 1434–1445.

Woodcock, H. V., Eley, J.D., Guillotin, D., Platé, M., Nanthakumar, C.B., Martufi, M., Peace, S., Joberty, G., Poeckel, D., Good, R.B., et al. (2019). The mTORC1/4E-BP1 axis represents a critical signaling node during fibrogenesis. Nat. Commun. *10*, 6.

Xaubet, A., Marin-Arguedas, A., Lario, S., Ancochea, J., Morell, F., Ruiz-Manzano, J., Rodriguez-Becerra, E., Rodriguez-Arias, J.M., Inigo, P., Sanz, S., et al. (2003). Transforming growth factor-beta1 gene polymorphisms are associated with disease progression in idiopathic pulmonary fibrosis. Am. J. Respir. Crit. Care Med. *168*, 431–435.

Xie, N., Tan, Z., Banerjee, S., Cui, H., Ge, J., Liu, R.-M.M., Bernard, K., Thannickal, V.J., and Liu, G. (2015). Glycolytic reprogramming in myofibroblast differentiation and lung fibrosis. Am. J. Respir. Crit. Care Med. *192*, 1462–1474.

Yamamoto, N., Ueda, M., Sato, T., Kawasaki, K., Sawada, K., Kawabata, K., and Ashida, H. (2011). Measurement of Glucose Uptake in Cultured Cells. In Current Protocols in Pharmacology, (Hoboken, NJ, USA: John Wiley & Sons, Inc.), p. 12.14.1-12.14.22.

Yoon, Y.-S., Lee, J.-H., Hwang, S.-C., Choi, K.S., and Yoon, G. (2005). TGF β1 induces prolonged mitochondrial ROS generation through decreased complex IV activity with senescent arrest in Mv1Lu cells. Oncogene *24*, 1895–1903.

Yu, G., Tzouvelekis, A., Wang, R., Herazo-Maya, J.D., Ibarra, G.H., Srivastava, A., de Castro, J.P.W., DeIuliis, G., Ahangari, F., Woolard, T., et al. (2017). Thyroid hormone inhibits lung fibrosis in mice by improving epithelial mitochondrial function. Nat. Med. *24*, 39–49.

Zank, D.C., Bueno, M., Mora, A.L., and Rojas, M. (2018). Idiopathic Pulmonary Fibrosis: Aging, Mitochondrial Dysfunction, and Cellular Bioenergetics. Front. Med. *5*, 10.

Zeisberg, M., and Kalluri, R. (2004). The role of epithelial-to-mesenchymal transition in renal fibrosis. J. Mol. Med. *82*, 175–181.

Zha, X., Wang, F., Wang, Y., He, S., Jing, Y., Wu, X., and Zhang, H. (2011). Lactate dehydrogenase B is critical for hyperactive mTOR-mediated tumorigenesis. Cancer Res. *71*, 13–18.

Zhang, Y.E. (2009). Non-Smad pathways in TGF-beta signaling. Cell Res. *19*, 128–139.

Zhang, Y.E. (2017). Non-Smad Signaling Pathways of the TGF-β Family. Cold Spring Harb. Perspect. Biol. *9*, a022129.

Zhang, D., Li, J., Wang, F., Hu, J., Wang, S., and Sun, Y. (2014). 2-Deoxy-D-glucose targeting of glucose metabolism in cancer cells as a potential therapy. Cancer Lett. *355*, 176–183.

Zhang, J., Xu, P., Wang, Y., Wang, M., Li, H., Lin, S., Mao, C., Wang, B., Song, X., and Lv, C. (2015). Astaxanthin

prevents pulmonary fibrosis by promoting myofibroblast apoptosis dependent on Drp1-mediated mitochondrial fission. J. Cell. Mol. Med. *19*, 2215–2231.

Zhang, W., Patil, S., Chauhan, B., Guo, S., Powell, D.R., Le, J., Klotsas, A., Matika, R., Xiao, X., Franks, R., et al. (2006). FoxO1 Regulates Multiple Metabolic Pathways in the Liver. J. Biol. Chem. *281*, 10105–10117.

Zhao, Y., Butler, E.B., and Tan, M. (2013). Targeting cellular metabolism to improve cancer therapeutics. Cell Death Dis. *4*, e532–e532.

Zhao, Y.D., Yin, L., Archer, S., Lu, C., Zhao, G., Yao, Y., Wu, L., Hsin, M., Waddell, T.K., Keshavjee, S., et al. (2017). Metabolic heterogeneity of idiopathic pulmonary fibrosis: a metabolomic study. BMJ Open Respir. Res. *4*, e000183.

Zhong, H., Chiles, K., Feldser, D., Laughner, E., Hanrahan, C., Georgescu, M.M., Simons, J.W., and Semenza, G.L. (2000). Modulation of hypoxia-inducible factor 1alpha expression by the epidermal growth factor/phosphatidylinositol 3-kinase/PTEN/AKT/FRAP pathway in human prostate cancer cells: implications for tumor angiogenesis and therapeutics. Cancer Res. *60*, 1541–1545.

Zhu, A., Lee, D., and Shim, H. (2011). Metabolic positron emission tomography imaging in cancer detection and therapy response. Semin. Oncol. *38*, 55–69.

Zi, Z., Chapnick, D.A., and Liu, X. (2012). Dynamics of TGF-β/Smad signaling. FEBS Lett. *586*, 1921–1928.

Zundel, W., Schindler, C., Haas-Kogan, D., Koong, A., Kaper, F., Chen, E., Gottschalk, A.R., Ryan, H.E., Johnson, R.S., Jefferson, A.B., et al. (2000). Loss of PTEN facilitates HIF-1-mediated gene expression. Genes Dev. *14*, 391–396.

7. Publications

7.1. Article published

Selvarajah B.*, **Azuelos I.***, Platé M., Guillotin D., Forty E. J., Contento G., Woodcock H. V., Redding M., Taylor A., Brunori G., Durrenberger P. F., Ronzoni R., Blanchard A. D., Mercer P. F., Anastasiou D., and Chambers R. C. 2019. mTORC1 amplifies the ATF4-dependent de novo serine-glycine pathway to supply glycine during TGF-β 1 –induced collagen biosynthesis. Sci. Signal. 12: eaav3048.

*=Authors contributed equally to this work

7.2. Article submitted/ in preparation

Forty E., **Azuelos I**, Durrenberger PF, Selvarajah B, Kalber T, Gendron T, Blanchard AD, Vitulli G, Barrett J, Anastasiou D, Mercer PF and Chambers RC, Understanding the role of aerobic glycolysis in pulmonary fibrosis, in preparation (2018)

7.3. Published Abstracts

Azuelos, I., Selvarajah, B., Platé, M., Woodcock H.W., Taylor A., Brunori G., Blanchard A., Mercer, P., and Chambers, R. (2018). LSC – 2018 - mTOR regulates TGFß-induced collagen synthesis via increased glycine biosynthesis. In Pulmonary fibrosis: from models to patients, (European Respiratory Society, Paris, France), p. PA986.

Selvarajah, B., **Azuelos, I.**, Forty, E., Platé, M., Brunori, G., Edwards, L., Blanchard, A., Anastasiou, D., Mercer, P., and Chambers, R. (2017). LSC - 2017 - A critical role for mTOR regulated metabolic reprogramming during TGF-β induced fibroblast collagen synthesis. In Mechanisms of Lung Injury and Repair, (European Respiratory Society, Milan, Italy), p. OA4436.

Forty, E., **Azuelos, I.**, Kalber, T., Gendron, T., Zaw-Thin, M., Vitulli, G., Barrett, J., Anastasiou, D., Mercer, P., Blanchard, A., et al. (2017). LSC - 2017 - Targeting glucose metabolism in experimental lung injury and fibrosis. In Mechanisms of Lung Injury and Repair, (European Respiratory Society, Milan, Italy), p. PA3470.

Azuelos, I., Selvarajah, B., Forty, E., Platé, M., Anastasiou, D., Mercer, P., and Chambers, R. (2016). Glucose Uptake in TGFβ-Induced Fibroblast Differentiation, (American Thoracic Society, San Francisco, USA), A2413.

Selvarajah, B., **Azuelos, I.**, Forty, E., Plate, M., Anastasiou, D., Mercer, P., and Chambers, R. (2016). Metabolic shift during TGF- β-induced collagen synthesis. In 1.5 Diffuse Parenchymal Lung Disease, (European Respiratory Society, London, UK), p. OA485.

7.4. Oral Presentations

mTOR regulates TGFß-induced collagen synthesis via increased glycine biosynthesis, Lung Science Conference (LSC) (accepted with travel bursary), Estoril, Portugal, March 2018

A critical role for mTOR-regulated metabolic reprogramming during TGFβ-induced fibroblast collagen synthesis. European Respiratory Society (ERS) presentation, Milan, Italy, September 2017

mTOR regulates glucose metabolism during TGFβ-Induced fibroblast to myofibroblast differentiation, conference presentation, International Colloquium on Lung and Airway Fibrosis, Dublin, Ireland, September 2016

Metabolic reprogramming in TGFβ-induced fibroblast differentiation, GlaxoSmithKline CRAFT meeting (Creative Advances in Fibrosis Therapeutics), Stevenage, UK, July 2015